TU Delft

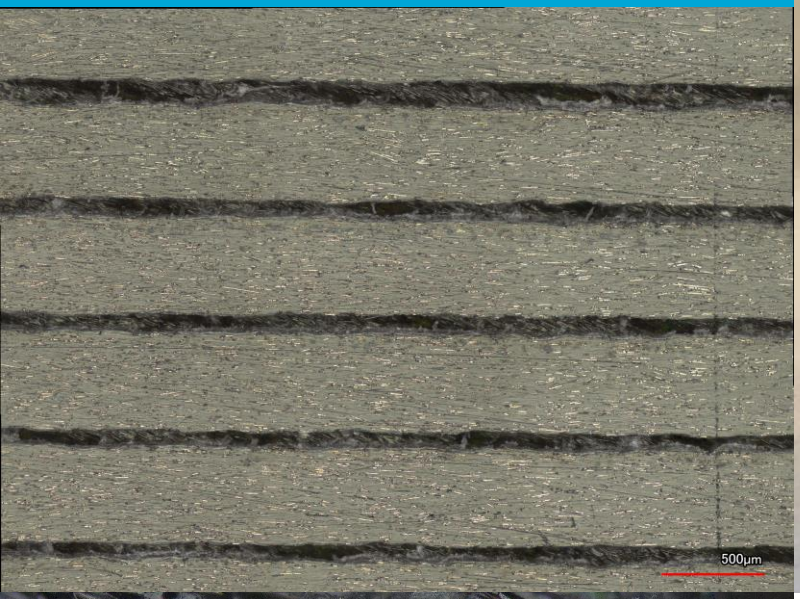

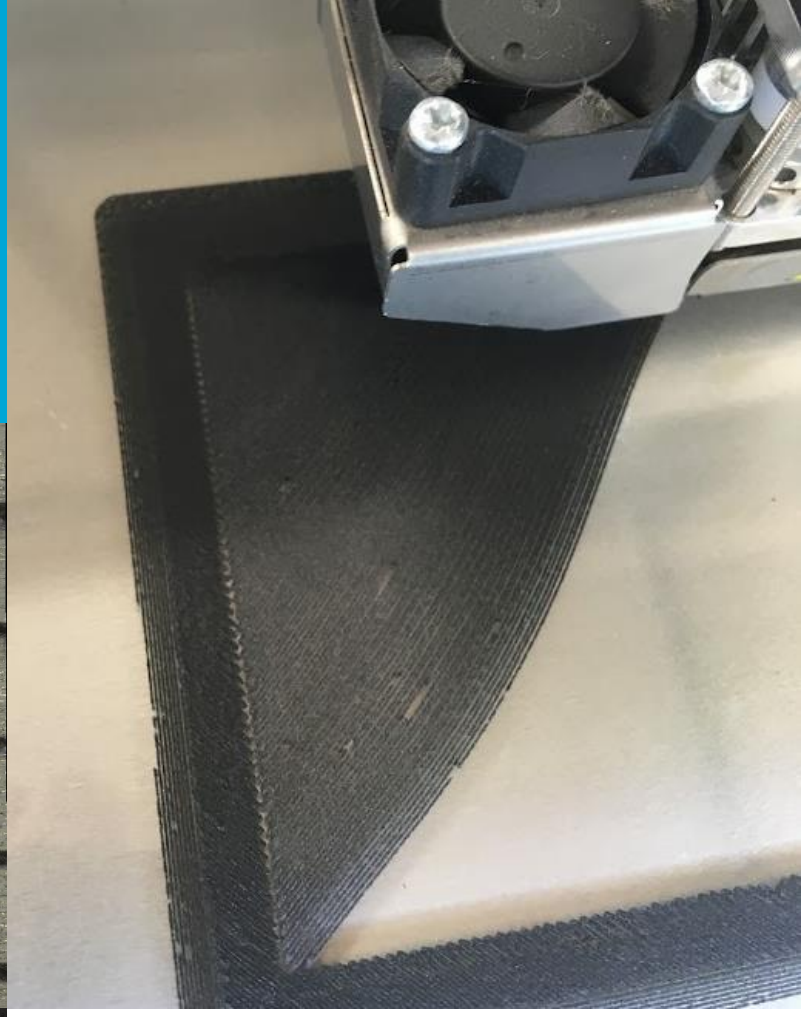

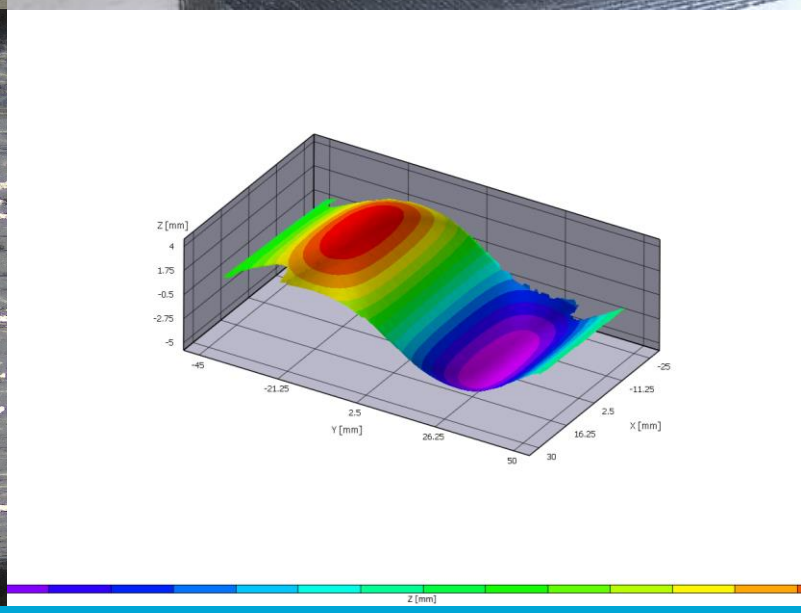

BUCKLING PERFORMANCE IMPROVEMENT IN 3D PRITNED VARIABLE STIFFNESS COMPOSITE LAMIANTES

Master of Science Thesis

Ranjan Gaur

BUCKLING PERFORMANCE IMPROVEMENT IN 3D PRINTED VARIABLE STIFFNESS COMPOSITE LAMINATES

by

Ranjan Gaur

in partial fulfilment of the requirements for the degree of

Master of Science

in Aerospace Engineering

at the Delft University of Technology.

Student number	5108719
Supervisors	Dr. Kunal Masania
	Dr. ir. Daniël Peeters
Project committee	Prof. Clemens Dransfeld
	Dr. Ir. John-Allan Pascoe

TU Delft Delft University of Technology

"Good times become good memories, but bad times make good Lessons."

- Uncle Iroh

Acknowledgments

This report is mosaic.

Mosaics needs a vision. Unlike a jigsaw puzzle where pieces fit in an order as they are supposed to, a mosaic must be sought and delivered to its final form. To me, this mosaic was only made possible by supervisors Daniël and Kunal. It was my privilege to work with and learn from you both. I will forever be grateful.

Mosaics are made whole with different pieces coming together. To me, these were my research group – my colleagues. It was an absolute delight working along with some of the most talented individuals (and Kevin) I have had the pleasure of meeting. Thanks to Caroline and Vinay for all your help, and Chiara, Berend, Nick, Lars, Silvan and the entire team at NematX whom I worked the closest with. And Muhamad, Satya and Sungi for making the research group as awesome as it is. As hard it is hard for me to say nice things about Kevin, I can agree it was ok working with him. I jest, thanks a bunch for making long days at the lab better. And of course, Alexander, Dave, and Victor for all the help around the lab.

Mosaics are held together in place. To me, these were my friends. Friends I've made, and friends I had. Deepika, Tanvi, Reddhi, Likhitha, Arshdeep and Karthik, thanks for making this place home. Irene, Joan, Ameya, Huub, Ninad and Srini, thanks for betting on me when I wouldn't. Gisela for all the cat memes. And Palak, well, I wouldn't know how to thank you. Anukrati, Nishita, Rhythm, Abhilash, Aditya, Aditya, Ankur, Taher, the Heggz, and DC - my mains, my constants. And of course, my family, without whom I wouldn't be where I am, and I wouldn't get where I want to.

This report is a mosaic, and it's my favourite one.

Ranjan Gaur

June 2022

Abstract

Over the past decades, fibre-reinforced composite structures have been increasingly adopted into mainstream manufacturing over conventional metals owing to their higher performance attributes, such as superior strength-to-weight ratios. Composite structures offer the unique advantage of tailoring reinforcements in correspondence with design load cases. This allows for more efficient and better performing structures.

Traditionally for composite laminate structures, the design space and freedom were vastly influenced by the accumulated experience in design and certification, as well as available flexibility in manufacturing processes; the available degree of freedom in aligning fibres dictated the design freedom available. With the advent of advanced processes such as automated fibre placement (AFP), reinforced tows can now be placed with more freedom and accuracy; even allowing for tows to be steered during deposition. These are called variable stiffness composite laminates. Fibre directionality within these laminates can be tailored to achieve an optimal load redistribution, thereby increasing its structural performance.

Novel additive manufacturing such as Fused Deposition Modelling (FDM) allow for more complex geometries to be manufacturable in a variety of materials. Such a process can allow more design space and freedom in existing optimization frameworks for designing variable stiffness laminates. Many reinforced thermoplastic materials can be processed using FDM. Short fibre reinforced materials are very readily available and can be used on all commercially available FDM platforms with minimal changes.

This research culminates the three key aspects in engineering – design, material, and process. First, a suitable design framework is chosen, which in combination with added the design freedom by virtue of a novel process such as FDM, is used to design laminates optimized for buckling performance. Additional design freedom is afforded to the optimization framework by means of relaxing the manufacturability constraint – which restricts the maximum allowable curvature of each individual path within the laminate. Secondly, these laminates are manufactured using short fibre reinforced thermoplastic material, for which the shear-induced alignment of the material is analysed to predict the effective mechanical properties under the parameters used for printing the laminates. Lastly, to validate the effect of additional design space on the effective performance of these laminates, a suitable experimental protocol is devised and used. For the optimized laminates, two cases for maximum allowable steering curvature are considered – one low and one high, and an effective quasi-isotropic laminate is used as a benchmark for comparison. Finally, all the laminates are tested under compression and analysed. The increase in buckling performance of optimized laminates corresponding to increase in allowable steering is verified, as well as insights are drawn from the processing and experimentation to suggest future recommendations.

Contents

List of Figures

List of tables

1. Introduction

1.1. Origins and chronology

The disposition of constitutive elements in any structure contributes to its structural characteristics and performance as equally as the inherent strengths of each individual component. Often, two or more materials are 'combined', or more literally, used in conjunction to enhance collective performance [1]. These are termed as composite materials. Unlike in mixtures or solutions, constitutive elements in general retain their original composition in a composite.

Composite materials have been known to be used by humankind for a long time. Earliest engineering examples are the buildings made with the wattle and daub technique, over 6000 years ago, where lattices made of woven wood were daubed using clay [2]. Many other examples are seen over history, such as straw reinforced mud bricks and composite bows made using wood, bone, and sinew [3].

In the modern technical era, many synthetic materials were developed, and such composited combinations were explored. Reinforced plastics, in particular, attracted a lot engineering interest. In the 1930s, fibreglass was developed at Owen Cornings [3] primarily as a reinforcing material, which was stiff and strong yet very light-weight, while du Pont developed the first suitable resins to be used as the dispersion media for these fibres. In the early 1950s, carbon fibres were synthesized and since have been used extensively owing to their high strength-to-weight ratio. Since their introduction, fibre reinforced plastics have attracted most attention from the aviation industry - the simpler abstraction here being that lighter aircraft were more efficient to fly. Strength performance combined with lightweight constructions are of key importance in the aerospace industry, and over the past decades, the composite composition of commercial aircraft by structural weight has seen a significant increase, shown in Figure 1

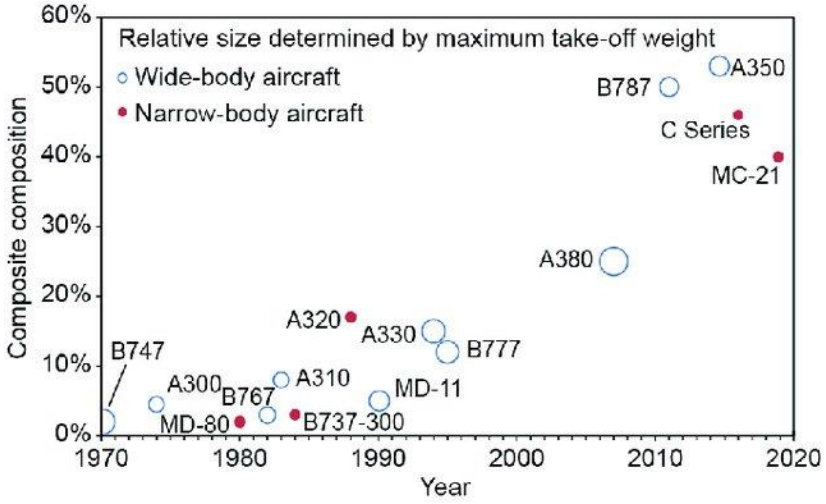

Figure 1 – Composition of composites in a commercial aircraft by structural weight shows an increasing trend in use of composites over the five decades [4]

Over the past millennia of human technological advancements, composite materials have played an important role. Rudimentary constructions made with naturally available materials such as bone and wood evolved into more complex systems made with synthetic materials. Presently, and going forward, the need for more efficient lightweight structural materials gets more acute, given the reliance on conventional sources of energy being used more commonly. Typically, engineering advancements have relied on an expanding technological inventory of materials and process. However, the need to shift towards more sustainable manufacturing and recycling practices necessitates better design, manufacturing processes as well as material selection strategies.

A major portion of the global manufacturing of reinforced plastics is done with the use of thermoset resins – resins that irreversibly harden when cured, and thus, cannot be recovered or recycled. In comparison, thermoplastic resins can be remoulded and given new form by thermal processing. In 2019, about 61% of the global composites manufacturing was done with thermoset resins, as compared to 39% which used thermoplastics [5]. The recycling of thermoset fibre reinforced plastics is also very energy intensive. Usually, the thermoset resin is burnt off by pyrolysis or by solvolysis, and the fibre reinforcements are retrieved for further use. However, these processes are very energy intensive and results in substantial greenhouse gas emissions. A large portion of composite waste also finds its way into landfills, which is also not very desirable. These concerns have inspired a shift towards thermoplastic resins as suitable matrices for engineering applications. Such parts can be remoulded with relative ease. Further, thermoplastics can be thermally joined, which eliminated the need for mechanical fastening or adhesive bonding. This, coupled with a steady rise of automation in manufacturing processes, makes it possible to design and manufacture more complex geometries with lesser parts needing assembly later.

1.2. What next?

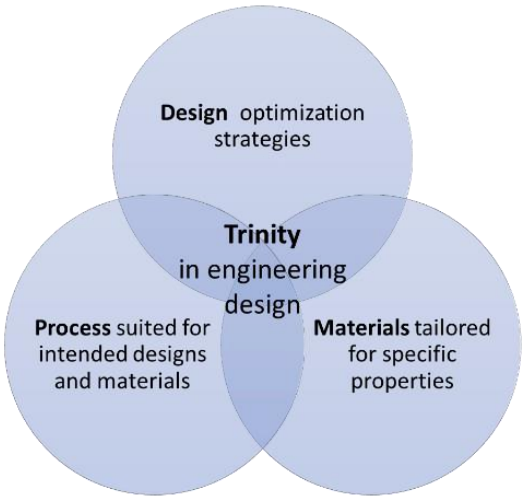

Figure 2 – The concept of 'Trinity' in engineering design, comprising of concurrent focus on design, process and materials

With the advent of novel methods of manufacturing and inventive computational frameworks, increasing focus is now being given to developing materials, optimization

strategies and manufacturing processes. Efficiency of aircraft in lieu of the climate impact and recyclability of composites are also areas of great concern; most conventional fibre reinforced plastics, typically made in thermoset resins, are not easily recyclable and need energy intensive processing to be recycled into short fibre composites.

The subsequent review aims to address the 'trinity' in engineering design - a confluence of approaches towards design, materials, and processing. This takes into consideration the inter-relatedness of each individual discipline.

For instance, it is impossible to extract the true potential of a design optimization strategy unless the manufacturing process can adequately process the material used as desired. Material performance is also directly related to the compatibility with the process. Thus, progressive design and optimization strategies must be developed while keeping in mind tailored materials with specific characteristics, to be used with novel yet relevant manufacturing techniques. A holistic approach towards additive manufacturing of optimized laminates using reinforced polymers is explored as a potential area of enquiry, thereby accommodating intricate and organic designs which cannot be manufactured easily or at all using conventional processes.

2. Review of literature

2.1. Fibre reinforced composites, an introduction:

Fibre-reinforced composites (FRCs) are vastly employed in the aerospace sector, owing to their high strength-to-weight and stiffness-to-weight ratios. FRC laminates are generally constructed additively; by stacking multiple plies of reinforcing fibres and subsequent curing into net shape in a rigid matrix, such as epoxy or phenolic resins. A typical FRP laminate can be seen in Figure 3. FRCs help exploit the power of anisotropy in engineering design; with material used in predetermined orientations, based on requirements imposed by structural applications of the system.

Most routinely used manufacturing processes for FRC laminates, such as hand layup, resin transfer moulding and autoclave curing of pre-impregnated sheets, use fibre reinforcements in the form of sheets or plies, which have pre-aligned reinforcing fibres. Traditionally, these fibre orientations were restricted to cardinal orientations such as 0, 45, -45 and 90 degrees, owning to the ease and simplicity in design, manufacturing, and certification; these are commonly used now, too. Fibre angles are varied along the thickness of the laminate per ply, to achieve the best possible design for a particular loading scenario. The design of laminates is done while considering good design practices [6], such as symmetric and balanced architecture (i.e., for every + θ ply there should be a – θ ply of the same material and thickness in the laminate), at least 10% of the plies in a laminate must have fibres in each principal direction - 0, 45, -45, and 90 degrees.

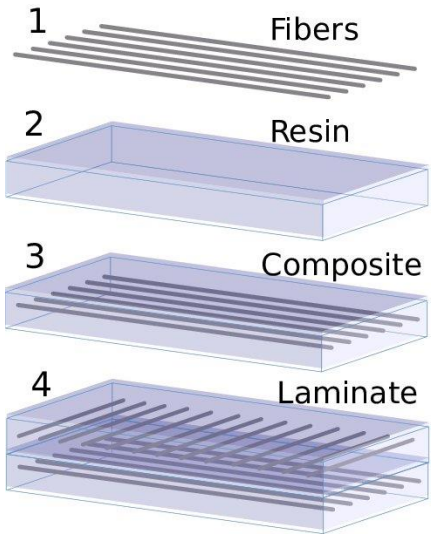

Figure 3 – Schematic of construction of a laminate, made up many individual laminae [7]

Variations in orientation of ply sequences and fibre angles allow for exploiting the inherent anisotropy of reinforcing fibres to yield a very efficient composite laminate. However, owing to the associated complexity in manufacturing, traditional design approaches were limited to straight fibre orientations and cardinal fibre angles within a stacking sequence of plies.

Over the past decades, composite materials have found increasing favour within the engineering industry. Since their first use, considerable focus has been given to automation

in the manufacturing processes as well. With the advent of more sophisticated automated processes, engineers could explore more complex designs, or 'non-conventional' laminates. Sophisticated automated technologies also offer the possibility of 'steering' fibre tows during deposition. For constant fibre angles, the stiffness of the laminates is also constant, whereas steered fibres allow for stiffness properties to be varied over the structures. Thus, such laminates are called variable stiffness laminates (Figure 4). Steering of fibres allows engineers to explore more efficient designs, as more design space is available compared to that in a classical stacking sequence design approach. Thus, such an approach for tailoring reinforcement directionality allows for designing laminates with improved mechanical performance as compared to conventional laminate designs.

Figure 4 – Fibre tows being steered during deposition using AFP process [8]

2.2. Advanced manufacturing processes

Advanced, automated processes allow for hierarchical arrangement of material, allowing designers to explore more efficient material architectures. Some commonly used processes are reviewed in this section.

2.2.1. Automated Fibre Placement (AFP)

Automated fibre placement is an advanced method of manufacturing composites, where tows of pre-impregnated fibres are deposited on a substrate through a dispenser mounted on a robotic arm or gantry. A schematic of the process is shown in Figure 5.

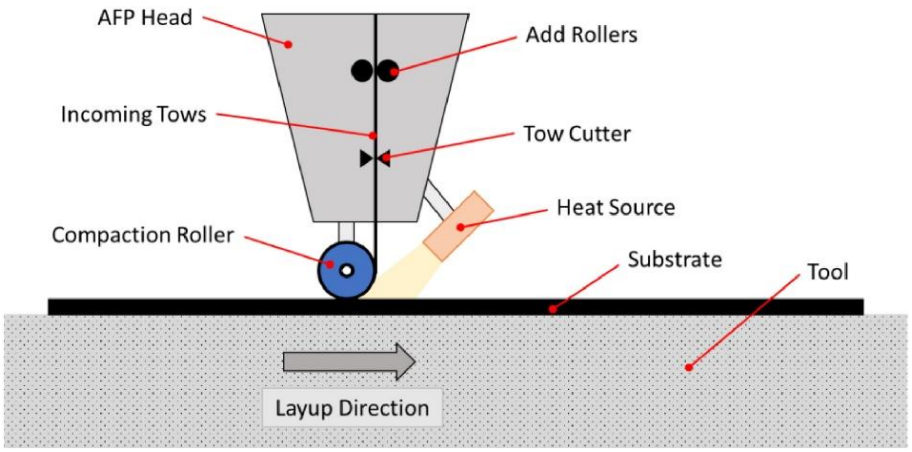

Figure 5 – Schematic representation of Automated Fibre Placement process [9]

AFP allows for high rates of material deposition as well as enables high degree of precision even on complex geometries. With AFP, fibre tows can also be steered during deposition, although the width of the tows dictate the amount of steering possible realistically without inducing defects. The in-plane waviness in deposited fibre tows and the induced defects along the inner boundary can be seen in Figure 6.

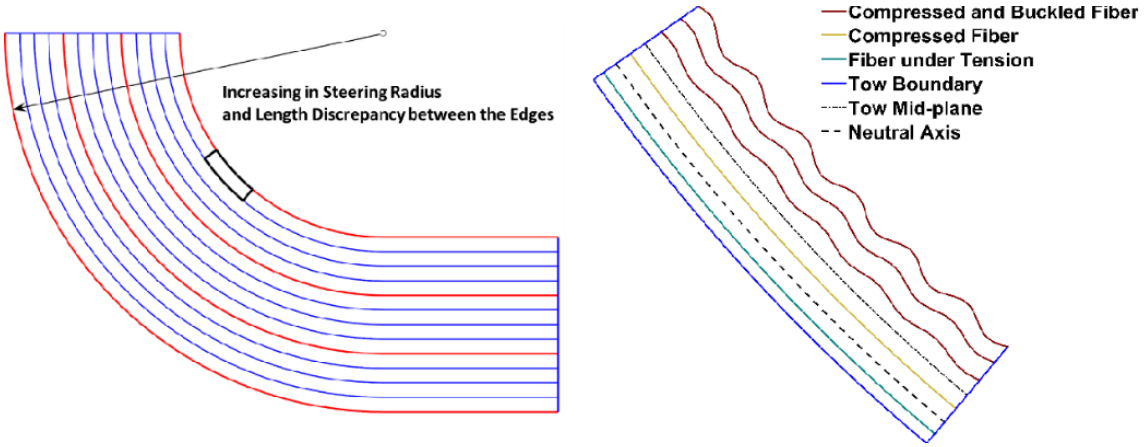

Figure 6 - (L) Schematic representation of three courses (red boundaries) laid down using AFP, (R) Idealized model of in-plane waviness in the highlighted region [10]*, showing buckled fibres in the interior region of the curved tows*

During deposition of steered tows using AFP, steering induced gaps and overlaps and overlaps are seen [11], [12]. This occurs as steered tows will always converge or diverge from each other. The problem of gaps and overlaps can be seen in Figure 10 (a) and Figure 10 (b) respectively - as the head for AFP turns along the reference tow path, subsequent tows in the direction of shift exhibit gaps or overlaps along the curvature. To counter the issue over gaps and overlaps in VSLs manufactured using AFP, two main strategies are used – tow overlaps and tow dropping. In the tow overlap strategy, seen in Figure 7 (a), the deposited fibre tows are allowed to overlap each other, and the localised thickness build-ups act as integral stiffeners within the laminates [13]. In the tow drop strategy (Figure 7 (b)), the deposited tows are cut or 'dropped' before overlapping each other, leading to a

constant thickness structure. However, this approach results in wedge-shaped zones with no fibres.

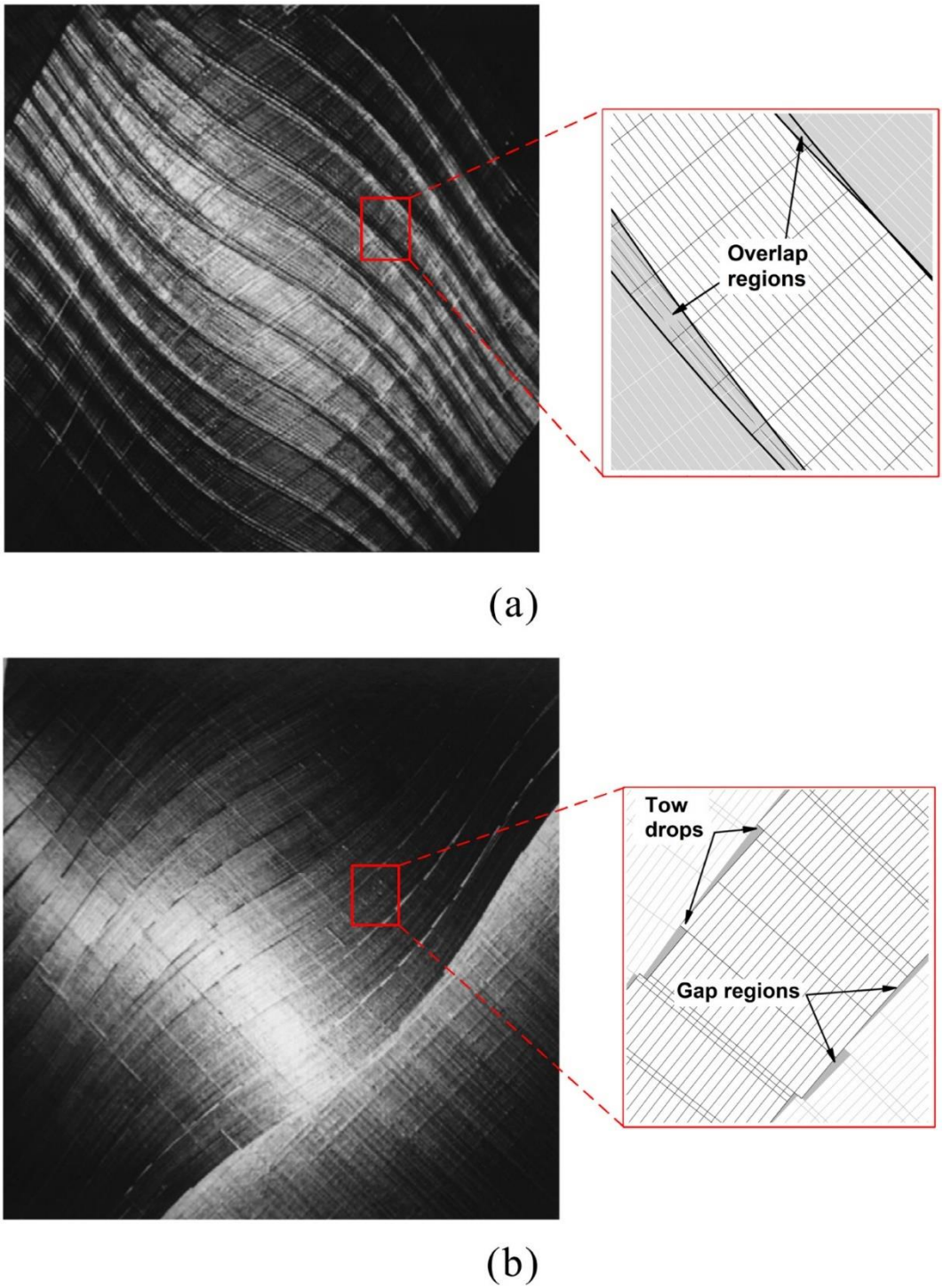

Figure 7 - Laminates manufactured by AFP using (a) overlap strategy, and (b) tow drop strategy [14], [15]*, showing overlaps and gap regions in respective laminates*

2.2.2. Continuous Tow Shearing (CTS)

Continuous tow shearing allows for turning semi-impregnated fibre tows which can avoid the gap and overlap defects as seen in AFP. Fibres are sheared instead of being turned; this

is by using the compaction shoe to hold the deposited fibre in place as the head moves in the shifting direction. The deformation mechanism and its comparison vis-à-vis AFP is highlighted in Figure 8, while the process schematic is seen in Figure 9.

The maximum change in angle possible using CTS are limited by the maximum shear angle. During CTS, the steering of the tow results in localised thickness changes, as seen in Figure 8(b). CTS is also slower than AFP in terms of processing time.

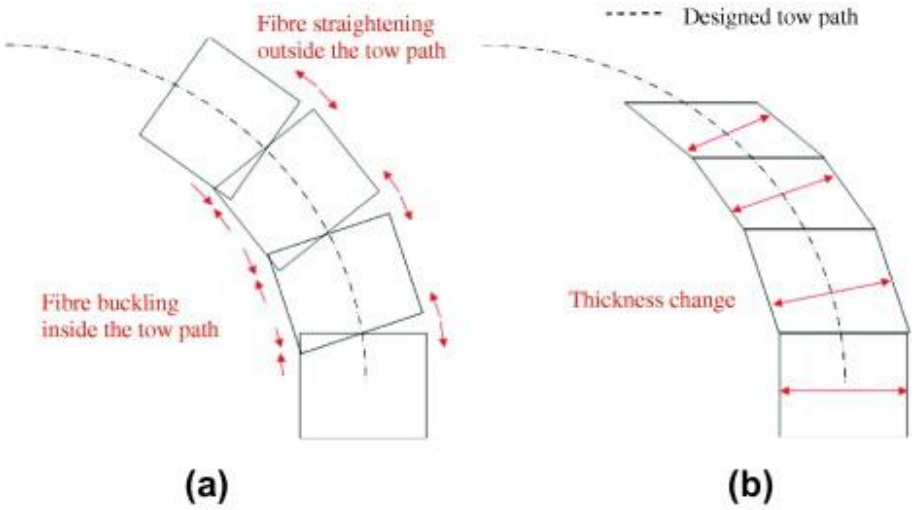

Figure 8 – Comparison of tow deformation in (a) Automated Fibre Placement, and (b) Continuous Tow Shearing, [11]

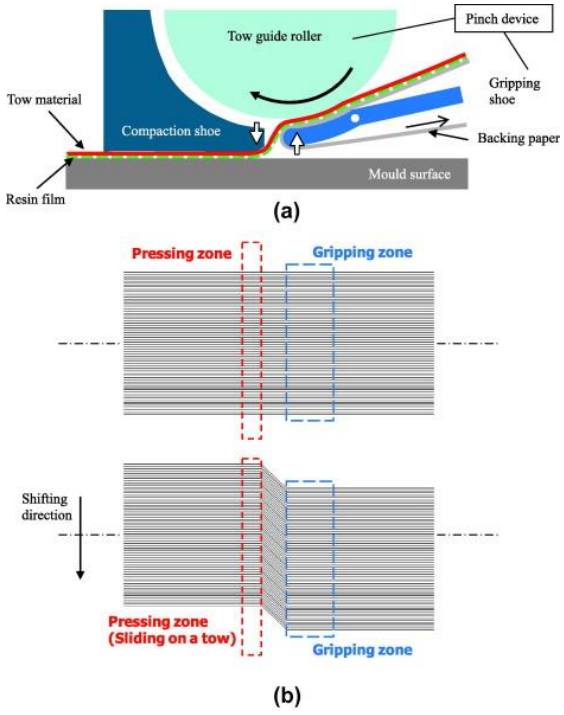

Figure 9 – (a) Compaction shoe and pinch device of a CTS head (sideview), and (b) relative movement of the compaction shoe, pinch device and deformed tow material (top view), [11]

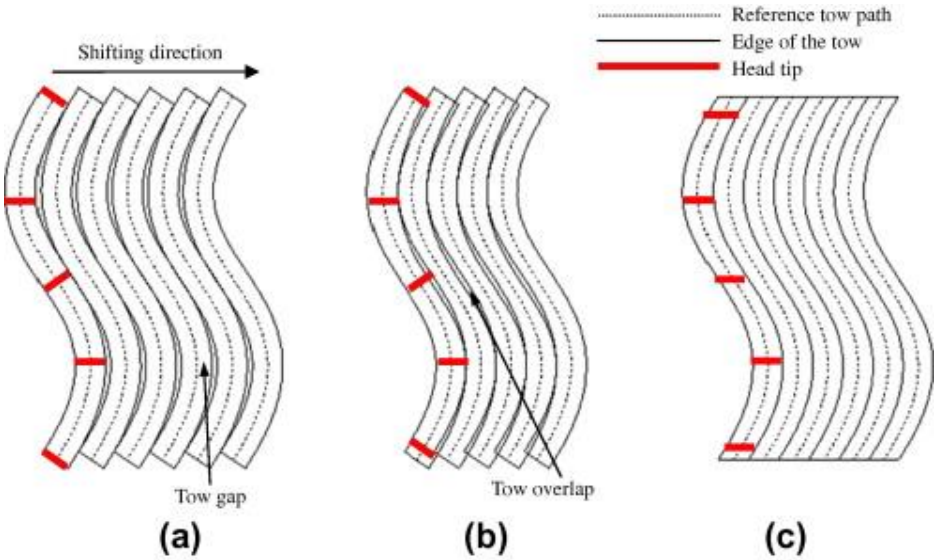

Figure 10 – Tow and head travel comparisons with (a) conventional AFP (tow gap), (b) conventional AFP (tow overlap), and (c) CTS, [11]

2.2.3. Randomly Oriented Strands (ROS) Composites

Continuous fibre composites manufactured using conventional methods are generally limited with respect to part geometry and complexity; simpler geometries and lesser features are preferred. On the other end of the spectrum, short fibre composites are easily injection moulded to a high degree of part complexity, but the mechanical properties obtained are far lower. Randomly oriented strand (ROS) composites are in the middle of this performance spectrum, as the lengths of reinforcements are between those seen in short and continuous fibre composites. The trend between processability and performance of ROS composites can be seen in Figure 11 (a). ROS composite parts are obtained by using chopped strands of unidirectional pre-impregnated tapes, which are bulk moulded into net shape, as can be seen in Figure 11 (b).

The use of prepreg tapes ensure a high fibre volume percentage, which in turn yields better mechanical properties. While it is possible to manufacture parts with intricate features and even varying thicknesses, parts produced do not have sufficiently high mechanical properties for aerospace applications [16].

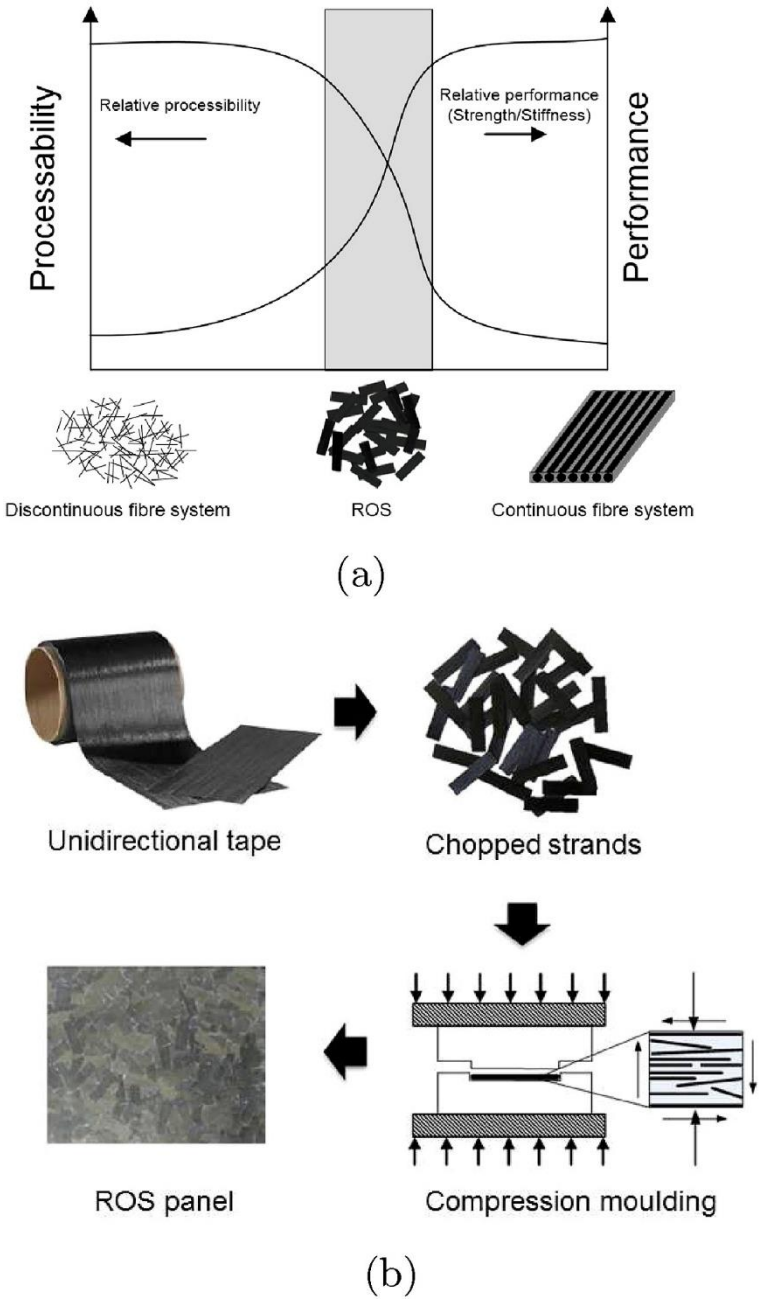

Figure 11 – (a) Comparison and relative trends between processability and performance of different composite material systems, and (b) Schematic overview of the manufacturing cycle for ROS panels [17]

2.2.4. Fibre Patch placement (FPP)

Fibre patch placement is another advanced process where small unit patches of a material are applied on a mould robotically [18]. As the patches are discontinuous, it allows for a more complex part to be produced than AFP. Fibre cut-off wastage is also considerably low in this process. Such a complex assembly of discrete patches allows for local variations in the

laminate, and this can be used to produce a highly tailored anisotropic design; however, due to numerous discontinuities along the patch edges, complex stress distributions occur [19].

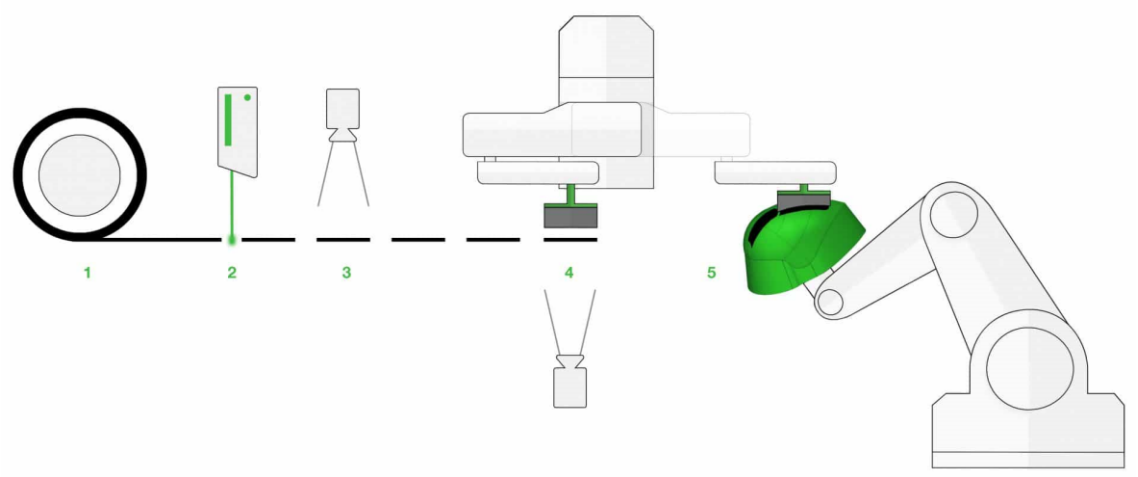

Figure 12 – Process schematic for Fibre Patch Placement: (1) Feed fibre tape, (2) Cut fibre tape into patches, (3) Inspect fibre patch quality, (4) Pick up patch, check patch position, (5) Position patch on 3D preforming tool, [20]

2.2.5. Tailored Fibre Placement (TFP)

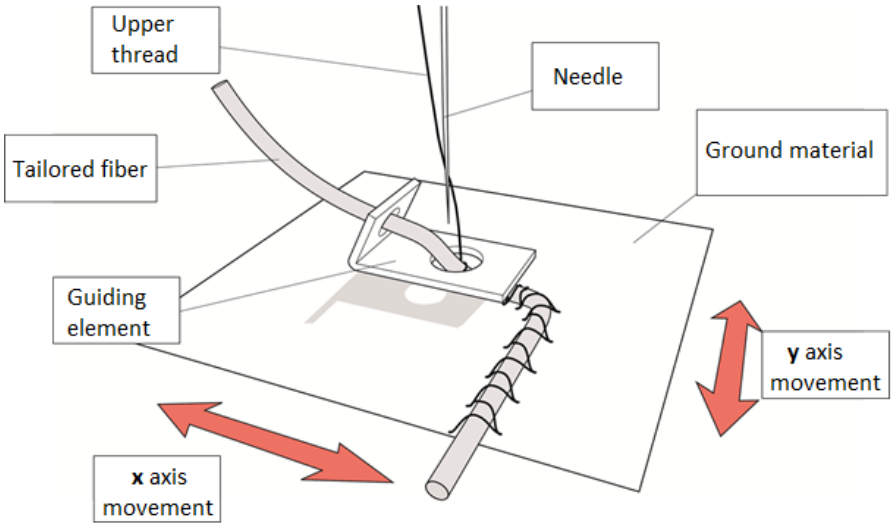

Figure 13 - Process schematic of Tailored Fibre Placement [21]

Tailored fibre placement (TFP) is based on the workings of an embroidery machinery, wherein reinforcements are tailored on to a base material. This process can be used to manufacture dry fibre preforms, that can be later impregnated with resin transfer moulding. The process deposits a guided pattern of the reinforcing fibre material, which is stitched into place by zig-zag cross-stitches. This process can be used to create complex preforms with minimal wastage of material, as well as allows for stitching of a continuous fibre over an extended length. This process can also be used to manufacture hybrid preforms made from multiple fibres.

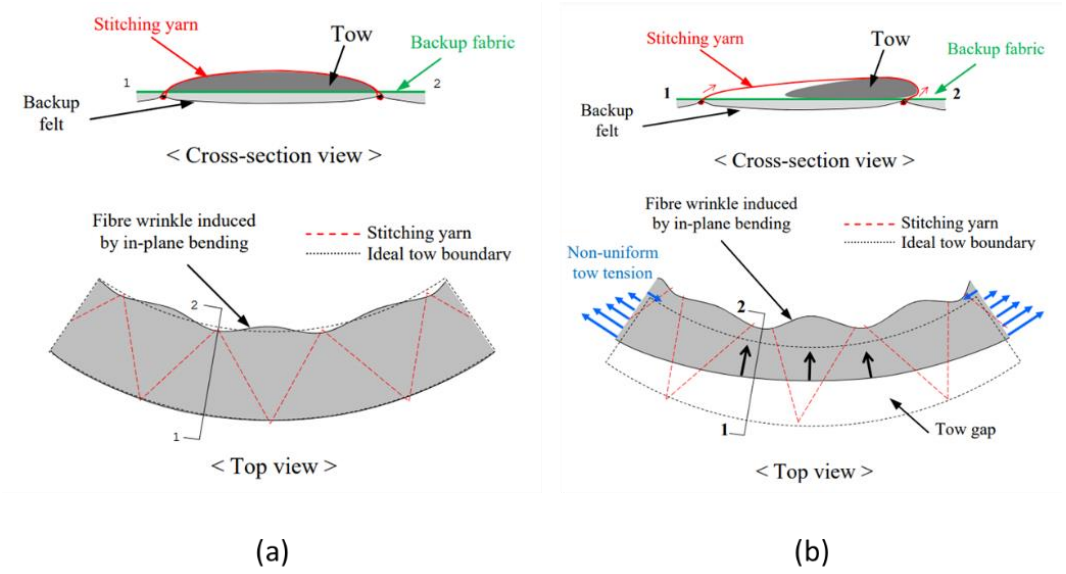

Figure 14 - (a) ideal tow deformation during TFP, and (b) real tow deformation during TFP [22]

However, TFP is also susceptible to localised buckling of tows. This is better elaborated in Figure 14 (a) and (b). The local deformations due to in-plane bending give rise to local buckling on fibre tows even in the ideal case, whereas the real deformation of the tow is much more complex.

2.2.6. 3D printing (3DP)

3D printing, also colloquially referred to as Additive Manufacturing (AM), is an umbrella term describing a wide range of processes with fundamentally additive approach towards material deposition. Using 3D printing, a plethora of materials can be processed, such as plastics, plastics with reinforcements and even metals. Since material deposition in 3D printing is gradual and successive, it also allows for the generation of complex geometries with intricate features with minimal assembly need.

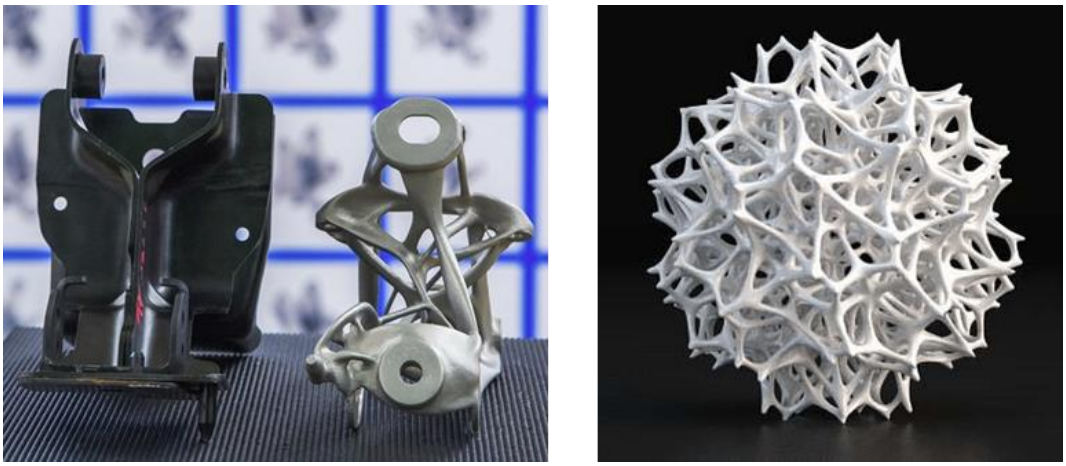

Figure 15 – (a) Generatively designed seat bracket by GE and Autodesk [23]*, and (b) intricate feature-rich geometry possible only by AM* [24]

Figure 15 (a) shows lighter and stronger seat bracket, developed by General Motors and Autodesk using generative design [23]. Such parts are difficult, sometimes even impossible to manufacture using conventional processes (e.g., subtractive processes such as machining or turning). For example, parts with internal features like seen in Figure 15 (b) cannot be machined as a single part, but are possible to make using 3D printing [24].

Although it has seen a substantial boom in research and commercial interest, AM as a technology has been around for a few decades. William Masters is credited with the first patent in 3D printing. On July 2nd, 1984, he filed a patent for his Computer Automated Manufacturing Process and System. This was the first of his three patents which are regarded as to have laid the foundation of modern 3D printing systems. Notable pioneering contributions can be seen summarized in Table 1. With most original patents dating back to the 1980s, the turn of the millennium saw most of these expire, inciting a surge of research and commercial interest in these technologies. Now, many of these technologies have attained a high degree of maturity.

Table 1. Pioneering patents in Additive Manufacturing

Patent holder	**Process**	**Patent details**
William Masters	Ballistic Particle Manufacturing (Direct Jetting)	US 4665492, July 1984 [25]
	Fused Filament Fabrication	US 5134569, June 1989 [26]
	3D printing using pin array	US 5546313, Sept 1994 [27]
Chuck Hull	Stereolithography	US 4575330, Aug 1984 [28]
Carl Deckard	Selective Laser Sintering	US 4,938,816, Oct 1986 [29]
S. Scott Crump	Fused Deposition Modelling	US 5121329, June 1989 [30]
Eli Sachs	Binder Jetting	US 5204055, June 1998 [31]

Key processes under the hypernym 3D Printing are noted in Table 2, along with the materials typically processed [32]:

Table 2. 3D Printing technologies with their main input materials.

Technology	**Sample Materials**
Material Jetting	Photopolymers, silver, wax
Powder Bed Fusion	Aluminium, ceramic, cobalt, gold, inconel, nickel, polymer, silicate, steel, titanium
Binder Jetting	Aluminium, bronze, ceramics, foundry sand, gypsum, inconel, stainless steel
Stereolithography (Vat photopolymerization)	Polymers, composites, ceramics

Technology	Sample Materials
Sheet Lamination	Carbon fibre, copper, fiberglass, aramid, stainless steel, titanium
Material Extrusion	Polymers, composites, fiberglass, aramid, metal, nylon, biomaterials
Directed Energy Deposition	Aluminium, copper, inconel, magnesium, nickel, steel, titanium, zirconium

Material extrusion:

Material extrusion is better known as fused deposition modelling (FDM), or fused filament fabrication (FFF). It is the most popular AM technique, due to its widespread use by industry as well as hobbyists, enthusiasts, and students. Most desktop FDM printers are very easy to install and use, and do not require extensive set ups. Ease of operation and various open-source projects within the community ensure widespread adoption and penetration of this technology.

Thermoplastic material, typically in the form of a filament, is fed to a moving extruder head, which heats the material, and the melt is deposited as desired. These extruder heads are typically mounted on gantry or a robot head, which control the degrees of freedom. Most common FDM printers have 3 degrees of freedom, but more sophisticated industrial and/or research setups may have up to 6 degrees of freedom.

FDM also supports a very wide range of materials. Pure thermoplastics such as PLA, ABS and PETG are more extensively used. However, reinforced thermoplastics (continuous and short fibre) can also be 3D printed using this process.

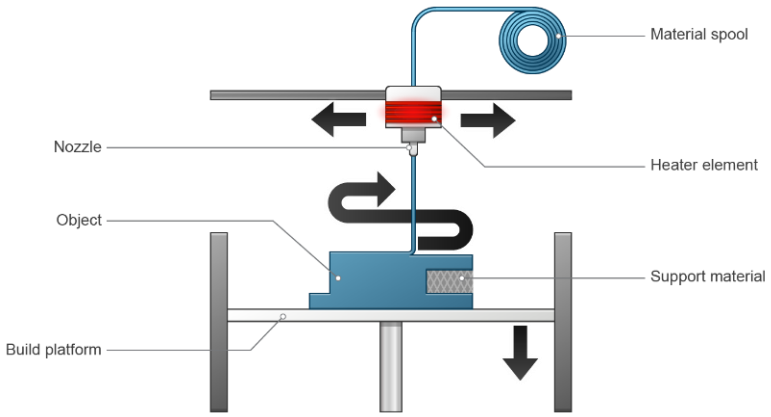

Figure 16 – Process schematic for Fused Deposition Modelling [33]

2.3. Design optimization frameworks

Advances in manufacturing processes have been complemented by extensive research towards designing better structures. Anisotropy is a powerful tool in an engineer's arsenal – with intelligent use of material in required areas, directions, and configurations, we get

efficient structures with respect to both material usage and performance. Such intelligent hierarchical material architecture is often seen in nature, which has been the inspiration for a lot of research in structural optimization frameworks. This section takes a closer look at the approach towards such optimization strategies and frameworks.

2.3.1. Optimizing fibre directionality

Composite laminates with a constant fibre angle along each of its plies have a constant stiffness. With processes such as AFP or CTS, one could orient the fibre tows in a curvilinear path, giving rise to a laminate with a varying stiffness. Such varying stiffness laminates have been explored in greater detail over the years.

The first investigation in varying stiffness laminates was by Chang et al. [34], who investigated the enhancement in notched strength by comparing drilled and moulded-in holes in a CFRP panel. The increase in performance was attributed to increased fibre volume concentration around the holes and continuity in fibres within the panel. Later, the research and investigations by Hyer and Lee [35], [36] evaluated buckling performance of a plate with a circular hole. These works demonstrated the improvement in performance of the panel by maintaining the continuity in fibre reinforcements along effective load paths – which were in essence defined as the path from point of load application to the point of reaction out of the structure. Fibres aligned in the principal stress direction is another approach taken for manufacturable designs. Crothers et al. [37] found reduced stress concentrations and weight savings for the tailored fibre placement method, although manufacturability with AFP was not possible.

Investigations in such steered fibre laminates have always encountered the problem of employing manufacturability constraints. Linearly varying fibre angles have been proposed as a solution [38]–[41] to this problem in many works over the years to ensure manufacturability. For linearly varying fibre angles, all fibre paths are parallel to each other in one direction, while changing in the other direction according to the relation [41]:

$$\theta(x) = \theta_0 + (\theta_1 + \theta_0)\frac{|x|}{d}$$

Here, θ_0 is the angle in the middle, θ_1 is the angle on the side at a length *d* from the middle. This is represented in Figure 17.

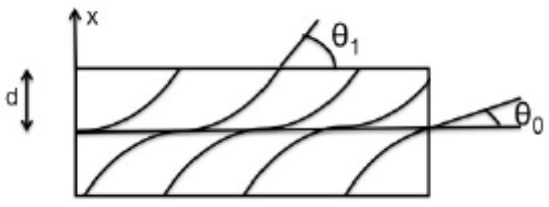

Figure 17 - Graphical representation of linearly varying fibre angles [42]

However, the problem of gaps or overlaps in the deposited tows, as discussed in the earlier sections, is seen still, yet, increase in buckling performance under compression and shear

was noted by Jegley et al. [14], [43]. Continuous tow shearing as a technique for using shear deformation characteristic of dry fibre tows to minimize process induced defects, such as wrinkling, was presented by Kim et al. [11]. However, CTS causes an increase in local thickness proportional to the steering, which influences the structural behaviour of the manufactured laminate.

Some of the widely accepted strategies for optimization of variable stiffness laminates are discussed and compared in detail by Ghiasi et al. [44] for parameters such as robustness and simplicity. One strategy discussed was the multi-level optimization approach, where the optimization problem is broken into smaller work packages and solved iteratively in different steps. Building on this approach, a robust multi-level optimization framework consisting of gradient based algorithms was proposed by Ijsselmuiden [45]. The framework followed a three-step design procedure: first, an optimal laminate stiffness and thickness distribution was determined; second, optimal fibre angle distribution was computed with respect to the imposed manufacturability constraints for steering radii; third, this fibre angle distribution was converted to continuous fibre paths to be used for manufacturing. This framework was furthered improved upon by Peeters [42].

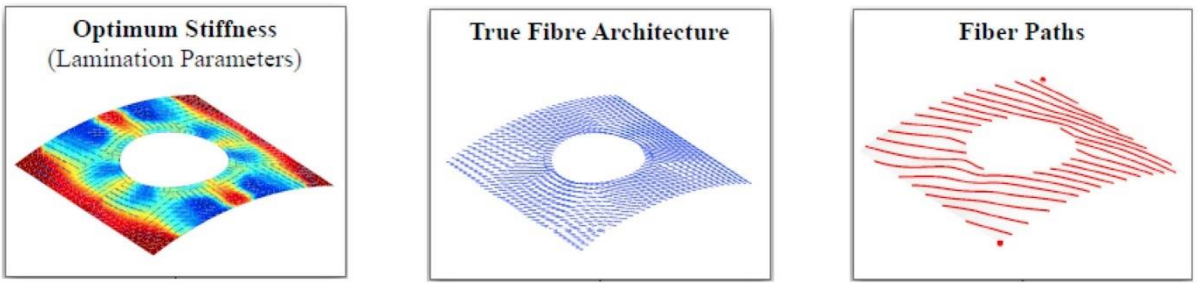

Figure 18 - Schematic overview of three-step optimisation approach [46]

Here, the first step of the framework was extended in scope to incorporate topology optimization concurrently, and step two was extended in scope to perform fibre angle optimization while keeping manufacturability intact.

2.3.2. Optimizing topology

Apart from tailoring directionality of fibres with respect to load paths or principal stresses, another approach is to optimize the material architecture for a body is to design a multi-scale structure. Such multi-scale architectures are seen in nature, e.g., in bone and bamboo. Topology optimization is the computational design method used for generating such structures with maximized performance within given specifications. In topology optimization, the structural design problem is formulated as optimizing material distribution within a discretized domain.

Research by Bendsøe and Kikuchi [47] is considered the formative work in this area. It characterized the equivalent mechanical properties of a material model with infinitely small square cells with rectangular holes. Optimized structures comprise of spatially varying geometric patterns spanning multiple length scales. However, due to restrictions posed by the manufacturing approaches at the time, focus moved towards a mono-scale approach,

wherein the distribution of homogeneous solid isotropic material was optimized. Some important work in this regard was carried out by Xie and Steven (evolutionary procedures) [48], Wang et al. (level set method) [49], and Sigmund [50].

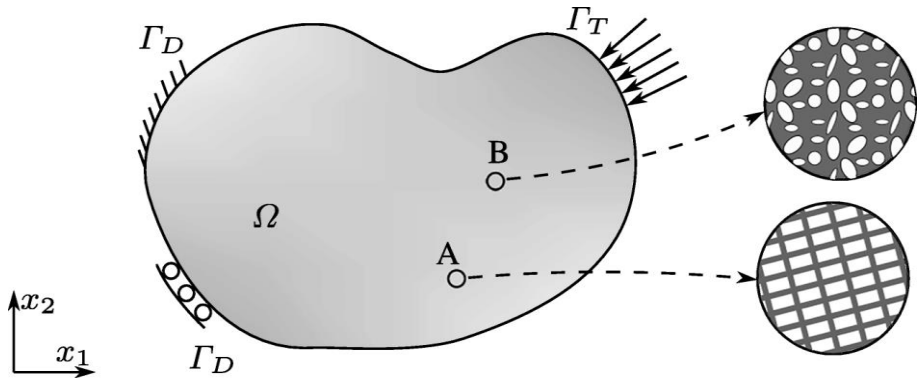

Figure 19 - A multi-scale structure with distinct local microstructures [51]

With the advent of more sophisticated manufacturing techniques such as additive manufacturing, interest, and enquiry in the field of multi-scale structures has seen a resurgence. A multi-scale structure is shown in Figure 19. Here, points A and B represent distinct points on the macroscale structure with corresponding repetition of a local microstructure.

A detailed review of the state of the art for multi-scale topology optimization is presented by Wu et al. [51].

2.4. Review of materials

Reinforced composites are typically manufactured using fibres such as carbon fibres, glass fibres, aramid, etc., in different types of matrix materials such as epoxies and phenolic resins. These materials are available and used in various forms depending upon the process employed for manufacturing. For the scope of this review, literature pertaining to additive manufacturing of composites using FDM is considered. A broader overview of fibre reinforced composites by Waghmare et al. [52] is referred to the interested reader.

Commercially available FDM printers can print with a wide variety of materials like polylactide (PLA), acrylonitrile butadiene styrene (ABS), polyethylene terephthalate glycol (PETG) and nylon to name a few. However, reported mechanical properties for products printed purely with these materials are not very high [54]. To improve mechanical performance, reinforcements such as particles or fibres are added to the polymer. Both discontinuous and continuous fibre reinforced feedstock is commercially available today. A detailed review of the state of the art by Li et al. [53] is referred to as the state of the art for highlighting relative performance between different additive manufacturing techniques.

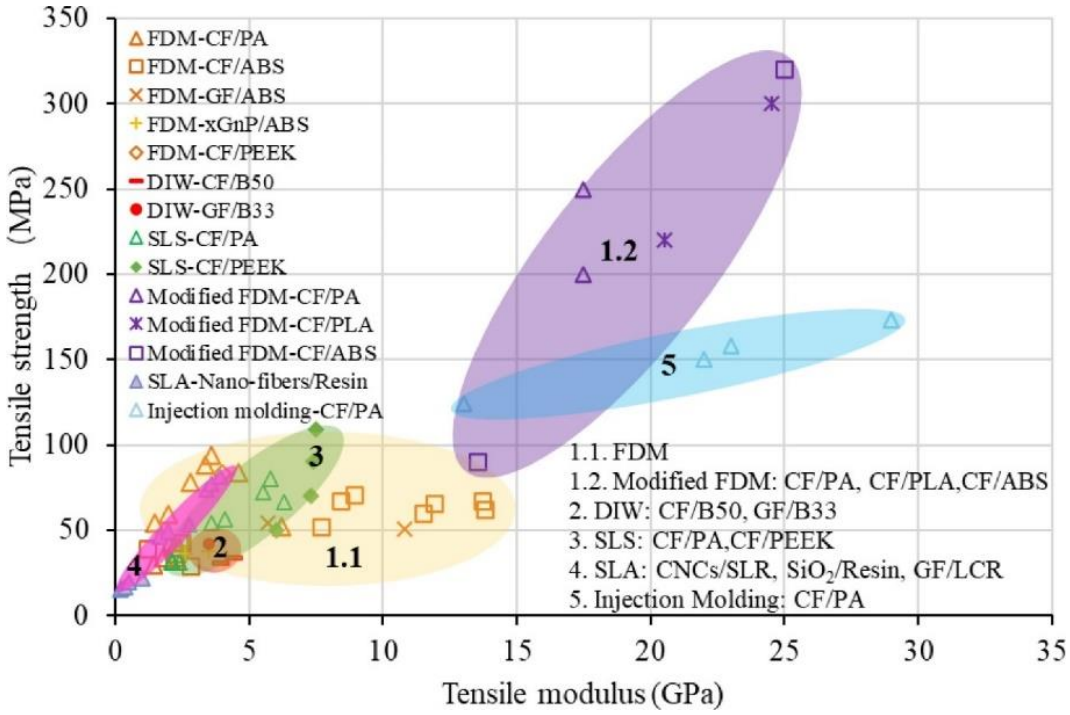

Figure 20 - Relative performance of parts manufactured using different additive manufacturing processes [53]

Regions 1.1 and 1.2 in Figure 20 represent the performance of discontinuous fibre reinforced composites manufactured using FDM method and modified FDM method, which are overall better in comparison to the other processes. The 'High Performance Discontinuous Fibre' (HPDF) method proposed by Yu et al. [55] includes a consolidation step when mixing and extruding the filament, which results in significant improvement in properties.

Literature pertaining to implementation of such materials and FDM printing is also reviewed as helpful process benchmarks can be set for use in this research. The work of Shafighafard et. al [56] is found to be very compelling in its approach. This work uses a commercially available short fibre reinforced polymer material and reports on the anisotropy developed by virtue of the printing process itself. The printed material is further analysed and the theoretical performance of the material in lieu of the induced anisotropy is calculated.

3. Thesis definition

3.1. Research gap

Based on the reviewed literature, certain areas of potential improvement are identified for further scientific inquiry.

At the outset, some observations are made:

- Currently, AFP is one of the most mature automated technologies for manufacturing high performance composites. Designs can either be manufactured with gaps or overlaps only. Further, local buckling of tows due to in-plane deformation restricts the maximum curvature possible with AFP
- As an alternative CTS can account for the gap and overlap problem seen in AFP, but it is a very slow process and encounters localised thickness build-ups. TFP is, too, seen as an alternative, but also encounters process induced defects in the deposited tows.
- Existing design frameworks must employ manufacturability constraints surrounding the limitations of the process. These constraints restrict the design freedom available to the optimization framework.
- Reinforced plastics used with AFP and CTS are tailored for specific designs and recycling is thus a concern. The fibres retrieved from end-of-life parts often end up as chopped fibres to be used as reinforcements for moulding-based processes, which means that recycled parts can only be used for decreasingly stronger composite parts.
- Other processes like ROS and FPP do not exploit continuity in reinforcements used.

Key aspects encompassing the trinity in engineering – design, material, and process – will be addressed during the course of the research.

Approach towards design

Considering the works reviewed so far, the optimization framework designed for AFP put forward by Peeters [42] is very interesting as it considers both laminate and topology optimisation. For this work, only laminate optimization is focused upon. The design space available to the framework is restricted by a manufacturability constraint which restricts the maximum allowable curvature in each ‘course’ fibre path. In theory, for a higher allowable steering, the same framework can compute more optimized architectures. With a suitable process, these constraints could be varied/relaxed and translated easily to a different, more suitable manufacturing process. For the purpose of this work, buckling optimization of laminates is considered as the design case.

Approach towards manufacturing

FDM can be considered very similar to AFP, as they both involve material to be deposited onto a substrate by means of a robot-controlled head. Compared to AFP, FDM also allows for a much higher degree of steering freedom – as FDM deposits material in the melt form,

by controlling feed rate and print speed, very sharp steering radii can be achieved. Moreover, the problems with gaps and overlaps will still need to be overcome; this can be approached by exploring ways to vary the width of material deposition during printing.

Approach towards materials

FDM also allows for use of commercially available feedstock with reinforcements. As this is a preliminary inquiry into a broader investigation into using additive manufacturing of high-performance composites, as an initial step readily available short fibre reinforced material can be used. These materials, owing to the small size of reinforcements, can be easily used for manufacturing without major changes to desktop FDM machines. Further, for such commercially available materials, user forums and crowd sourced knowledge are readily accessible for fine tuning and troubleshooting the manufacturing process.

3.2. Research proposal

To summarise, the proposed research project aims to adapt a suitable optimization framework (design) for use with conventional FDM printers (process), to be used to print fibre reinforced polymers (material) into optimized laminates. This comprehensive approach would allow to demonstrate improvements possible in laminate design and manufacturing owing to use of more advanced processes and materials.

The main goals of this research can be categorized in two major aspects, wherein certain sub-questions will be answered.

I. Adapting and employing an optimization framework for FDM printing of laminates:
   a. *Generating usable g-codes for computed design specimens*
   b. *Varying material deposition to address gaps and overlaps between material deposition courses.*

II. Experimentally validating performance improvement, if any:
   a. *Printing specimens within a range of varying design freedom*
   b. *Validating performance of different specimens experimentally*

The research questions can be summarised as follows:

I. What are the effective mechanical properties of the material due shear-induced alignment of the short-fibre reinforcements?
II. Can existing design frameworks be employed with additional design freedom to generate better designs, and
III. If yes, can the relative performance of these designs be validated experimentally?

The main research objective, therefore, is summarized as –

Experimental validation of buckling performance improvement in optimized variable stiffness composite laminates by varying allowable manufacturing constraints.

3.3. Research roadmap

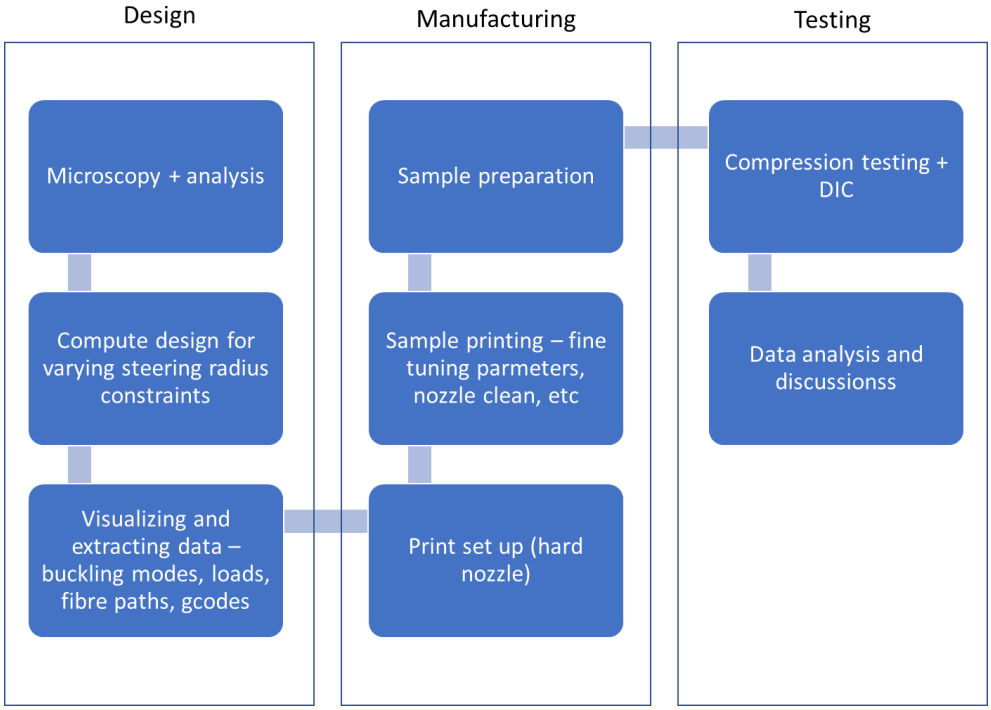

Figure 21 – Planned roadmap of salient project milestones during the course of research

The approach towards the thesis research is summarized in Figure 21. Broadly categorized as:

Design:

1. Evaluating the material used, by means of performing microscopic analysis to predict the theoretical performance of the material.
2. Using the design framework to compute optimal design paths. The effect of relaxing steering constraints in the design framework will be evaluated between a low allowable steering curvature and a high allowable steering curvature, and a QI layup will be used as a reference/control.

Manufacturing:

1. Setting up the FDM printer for manufacturing design specimens, as well as fine tuning the parameters for smooth and interrupted printing
2. Determining the experimental protocol and set up to be employed for experimental validation.

Testing:

1. Performing experiments and recording data, followed by post-processing and reporting results
2. Drawing insights and making recommendations for future research.

4. Methodology: Implementation and experimental protocol

4.1. Material selection and characterization

4.1.1. Selection and printing parameters

The first step in this research was material selection. Currently, a variety of reinforced printing feedstock is available commercially. Based on availability and ease of use, Colorfabb™XT-CF20 was chosen. This is a PETG matrix material reinforced with short carbon fibres (~100 um) up to 20% of its volume. PETG has great self-adhesion as well as higher mechanical properties than PLA, which is more commonly used as a FDM feedstock material. Further, XT CF20 is commonly used in the maker community, and thus, a decent amount of user-based information could be sourced for reference.

Firstly, ideal printing parameters for this material were evaluated. The recommended printing parameters prescribed by the manufacturer were used as a starting point and further fine-tuned by means of trial and error. It was observed that the first layer adhesion was critical for printing with this material, hence an adhesive spray is highly recommended, along with extremely slow first layer print speed. Once the first layer is successful, the print speeds can be ramped up significantly, up to the values provided by the manufacturer. The best results were observed with the parameters described in Table 3, which are tabulated in the column 'Recommended':

Table 3 - Evaluated and recommended printing parameters

Parameter	**From manufacturer**	**Recommended by this thesis**
Print speed – first layer	40 – 70 mm/s	10 mm/s
Print speed – rest	40 – 70 mm/s	~25 mm/s (<30 mm/s till ~6 layers, 40 mm/s or more subsequently)
Bed temperature – first layer	60 – 70 °C	75 °C
Bed temperature – rest	60 – 70 °C	70 °C overall
Printing temperature	240 – 260 °C	250 °C (Factoring PTFE degradation) *
Retraction	6.5 mm + 25 mm/s	4 mm + 40 mm/s (Up to 2 mm if needed)

*PTFE is known to rapidly degrade over 260°C. While most commercial printers use accurate thermistors to regulate hotend temperatures, a ± 3 - 5°C fluctuation can be expected. To avoid cases where the hotend temperature would increase over 260°C over the print

duration of multiple samples, the extrusion temperature was set at 250°C to avoid any problems.

4.1.2. Material characterization

Colorfabb™XT-CF20 is a commercially available short-fibre filled PETG thermoplastic material, no less than 20% fibres by volume, as specified by the manufacturer. However, since the short-fibre reinforcements in the material are discontinuous, the elastic moduli of the material must be appropriately evaluated. From the properties specified by the manufacturer and reviewed literature, the properties of the material and reinforcement known are tabulated in Table 4. Further, during printing, the 2.85 mm feedstock is forced through a small orifice (0.4mm nozzle) under pressure, during which shear induced alignment of short fibres is expected. The distribution and orientation of the reinforcement media must be assessed to a. demonstrate this effect, and b. calculate the effective mechanical strength of the material with respect to the printing parameters used.

Table 4 - Fibre and matrix properties of the short fibre reinforced material, Colorfabb™XT-CF20 [56]

E_m (GPa) E modulus, matrix	**ν_m** Poisson's ratio, matrix	**E_f (GPa)** E modulus, fibre	**ν_f** Poisson's ratio, fibre	**V_f** Fibre volume fraction	**l/d** Aspect ratio of fibres
1.8	0.3	190	0.2	0.2	8

Small unidirectional coupons were printed with parameters defined in Table 3 and polished for optical microscopy with progressively fine grit sandpapers (400, 800, 1200, 2000 and 3200). The printed courses were observed under a microscope and a MATLAB® script was used to evaluate the fibre angle distribution in the images by using Image Processing Toolbox from MATLAB® [57]. An indicative representation of the same is seen in Figure 22. A region of multiple courses was assessed, raw image of the same is supplemented in Appendix A. Alignment of fibres in the direction of print can be clearly seen in these images. In total 2110 fibres were identified in the samples. The angle distribution histogram of the short fibres in the specimen is seen in Figure 23.

There are many mathematical formulations for heterogeneous inclusions dispersed in a medium. The process induced directionality in the short fibre reinforcements and their effect to the overall mechanical performance are modelled on these formulations. To quantify this effect, we use the fibre angle distribution in the observed samples to approximate a Representative Volume Element (RVE). The unit RVE is used for homogenization of effective mechanical properties. The effective orthotropic moduli for the RVE are calculated and used in the design of laminates. Based on reviewed literature the Advani-Tucker homogenisation model is implemented in this research [58], [59].

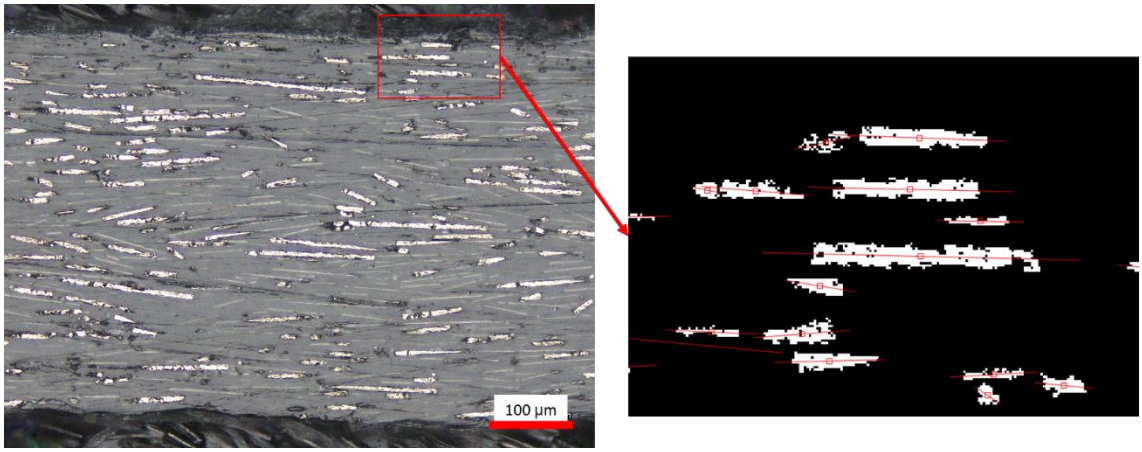

Figure 22 - Angle distribution of short-fibre reinforcements from image processing of optical microscopy images of polished printed unidirectional coupons

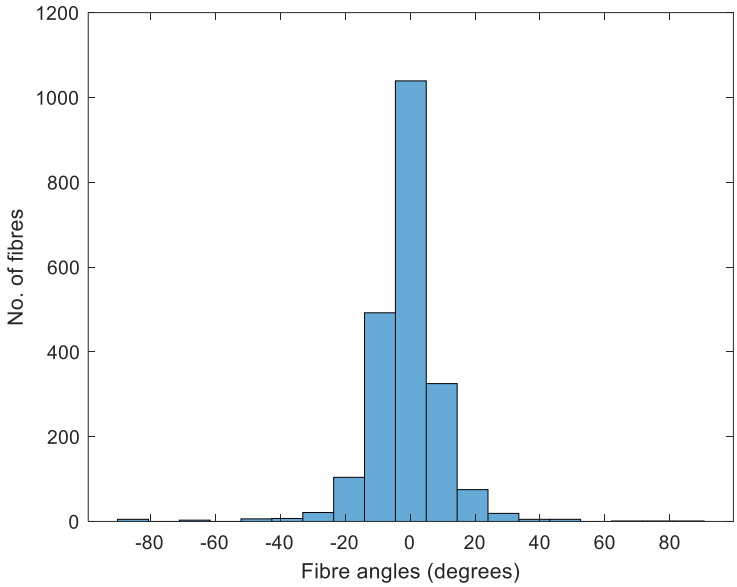

Figure 23 - Angle distribution of fibres identified in the optical microscopy sample (N = 2110)

To evaluate the mechanical performance, the angle distribution observed by image analysis was used to evaluate the second order Advani-Tucker fibre orientation tensor [58]. In this model, the filament orientation of each discrete fibre is represented as a unit vector $\mathbf{p} = < cos(\theta), sin(\theta), 0 >$. The second order tensor is calculated using the relation:

$$a = \int_{-\frac{\pi}{2}}^{-\frac{\pi}{2}} p_i p_j \Psi(\theta)\, d\theta$$

Here $\Psi(\theta)$ is the probability density distribution function of the fibres. For simplicity, the relation was approximated as a summation of each discrete fibre orientation as:

$$a_{ij} = \int_{-\frac{\pi}{2}}^{-\frac{\pi}{2}} p_i p_j \Psi(\theta)\, d\theta \approx \frac{1}{N} \sum_{n=1}^{N} p_i^n p_j^n$$

An open-source python package fiberpy [60] for analysis of fibre reinforced composites was used for calculating the fourth order tensor and effective elastic tensor. Using the Advani-Tucker hybrid closure model [58], [59], a fourth order tensor was further calculated. The Mori-Tanaka formulation is then used to evaluate the orthotropic moduli of the homogenized RVE. The calculated orthotropic moduli calculated are highlighted in Table 5.

Table 5 - Calculated values of orthotropic moduli of material used

E_1	7.58 GPa
E_2	2.61 GPa
G_{12}	1.04 GPa
v_{12}	0.35

Additional microscopy images are supplement in Appendix A.

4.1.3. Printing setup

A standard Ultimaker 2+ was used to prepare samples. As the feedstock material used was known to be abrasive to the stock brass nozzles, a hardened steel nozzle of diameter 0.4 mm was used on the stock hotend of the printer. PETG as a material is also known to stick to the nozzle itself during printing, and during printing it was observed that these blobs of material would harden over time and deposit on the specimen mid-print, thereby causing defects in the specimen. To address this, a rather low-tech solution was employed - a manual 'nozzle wipe' step was added at the end of each layer where the nozzle was programmed to return to the front of the print bed and wipe itself over a brass nozzle. The setup is seen in Figure 24.

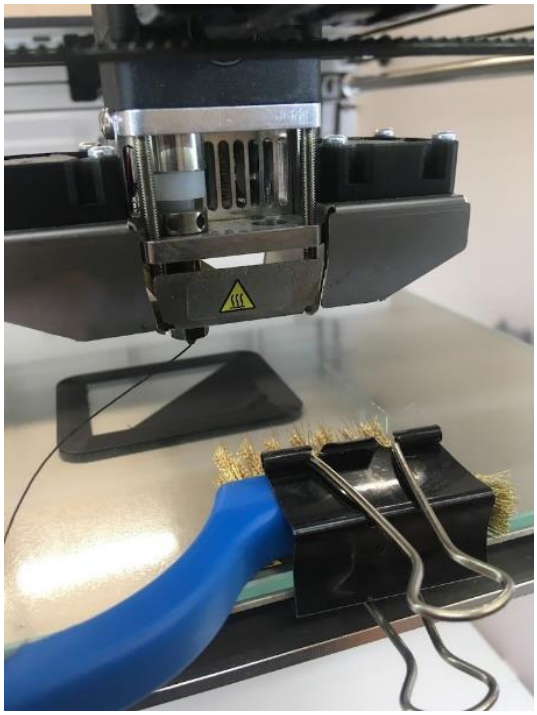

Figure 24 - Printing setup: Stock Ultimaker 2+ with hardened steel nozzle and brass brush for nozzle wipe

4.2. Specimen design

The three-step optimization framework developed by Peeters is chosen as the design optimization framework for this research. This framework allows for optimizing both fibre angles and densities during optimisation, but for the scope of this research, only fibre angle optimization is performed. The solution procedure of the optimization algorithm can be seen in the flowchart in Figure 25. A multi-level approximation is used in combination with the method of successive approximations. In the first level, optimal stiffness distribution is approximated in terms of the lamination parameters. On the second level, a fibre angle distribution is approximated, to which a suitable manufacturing constraint is applied (in the case of this research, the local element-wise steering is constrained to an upper bound). The second level sub-problem of fibre angle optimization is then solved using a predictor-corrector interior point method. Once the solution of the level two problem is obtained, the stiffness distribution parameters at level one are updated, and level two approximation is updated. This is repeated till the optimum fibre angle distribution is found. A more elaborate explanation regarding problem formulation and damping functions can be found in Peeters et al. [61], [62].

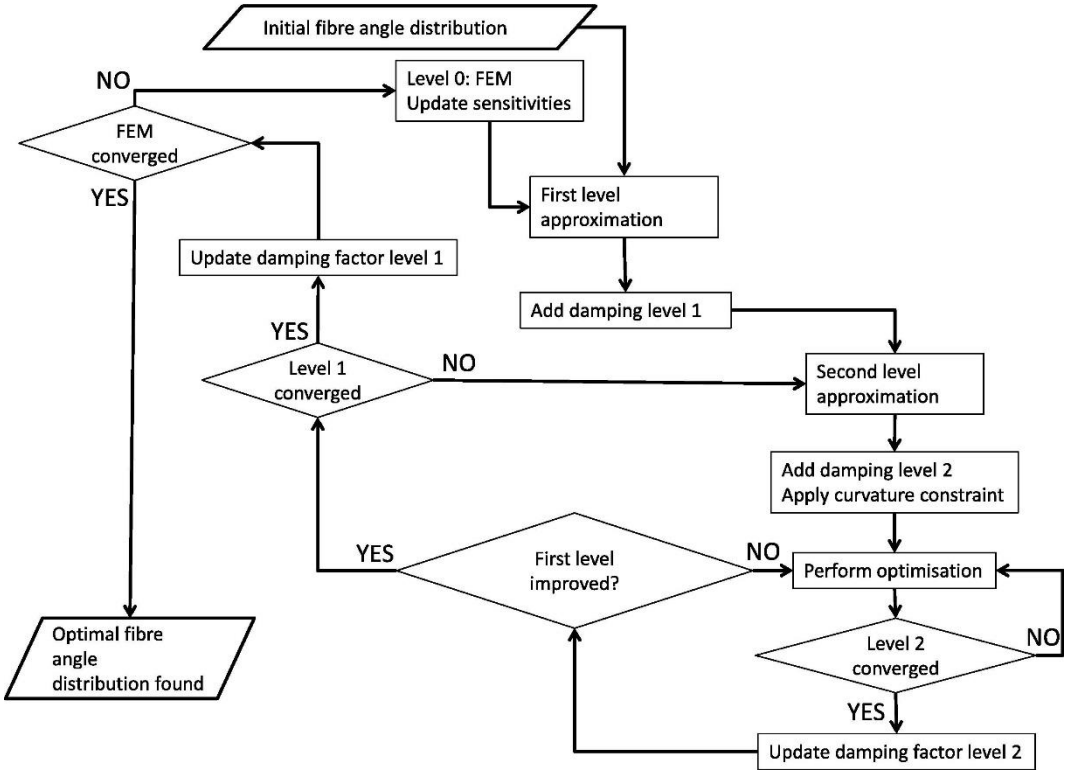

Figure 25 – Flowchart detailing the solution procedure of the multi-level optimization framework used [61]

For this research, fibre angle optimization for buckling performance is performed, while the stiffness is constrained, meaning the stiffness of the laminate is kept constant or close to that of a QI laminate. A QI laminate is defined as one for which the lamination parameters are all zero, and no layup is specified. Further, stability of laminates in the post-buckling

regime has been shown to be linked to stiffness [63], therefore, a constrain on stiffness is favourable. To study the effect that steering has on the performance of the laminate, the maximum allowable steering during the optimization is varied. During compression, the steered fibres in a VSL will favourably redistribute the load towards the supported edges, away from the middle region of the laminate, where the buckling waves usually occur.

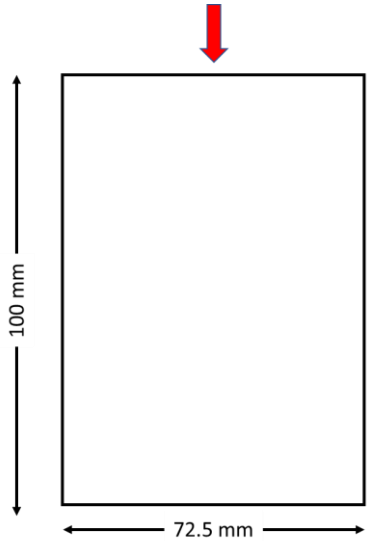

Figure 26 – Design space and loading direction applied during optimization

A design space of size 100 mm x 72.5 mm is considered for optimization, whose dimensions are defined based on available experimental setup (explained further in Chapter 4.3). Out-of-plane movement of all edges are constrained ($u_z = 0$), and a uniaxial compressive load is acted upon the laminate. Indicative design space and load applied during optimization can be seen in Figure 26.

The corresponding MATLAB® solver itself offers visualization options to plot and observe the optimal fibre paths computed for the given design case. The raw data obtained from the script was in the form of a point cloud for each course laid out in a ply. This raw data is then used as a basis for generating the G-codes. Further, the predicted buckling modes can also be computed and visualized from the eigen vectors calculated in the solver, as seen in Figure 27.

To evaluate the performance improvements seen by increasing the design space available to the optimization framework, the steering constraint imposed is relaxed and subsequently optimized designs must be validated experimentally. For this research, we aim to evaluate the increase in buckling performance of optimized laminates under uniaxial compression, while the stiffness of the laminate is constrained. Two cases of allowable steering curvatures are chosen for this purpose on either end – one low and one high, and both these are compared against an equivalent QI layup.

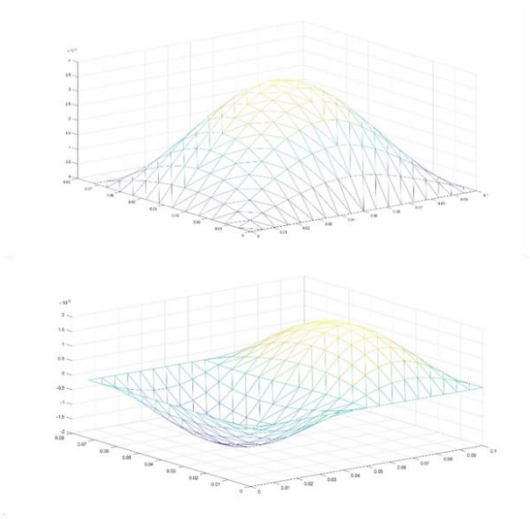

Figure 27 - One and two half wave buckling modes seen as visualized from optimization framework

From the optimization framework, the relative performance of each design vis-à-vis the allowable steering curvature normalized with respect to QI design are shown in Table 6.

Table 6 - Buckling performance predictions vis-à-vis maximum allowable steering curvature, normalized with respect to QI laminate

Layup	**Steering curvature (m^{-1})**	**Buckling Load 1**	**Buckling Load 2**
QI	-	1	1
R10	10	1.203	1.203
R100	100	1.385	1.396

The calculated values of buckling loads are tabulated in Table 7.

Table 7 - Calculated values of buckling loads

Layup	**Buckling load 1 (N)**	**Buckling load 2 (N)**
QI	2939.19	
R10	3535.65	3535.65
R100	4069.77	4102.72

Another script developed internally at Shaping Matter Lab, TU Delft, was used to generate the machine instruction, or the G-codes, for the actual manufacturing of the samples. This script, written in MATLAB®, uses the 'farthest point seeding for placement of streamlines' strategy proposed by Mebarki et al. [64]. This strategy uses Delaunay Triangulation to generate streamlines. In this method, one streamline is plotted at a time, and each subsequent streamline is placed farthest away from the previous one, thereby favouring the longest streamlines possible. This 'course' data, i.e., the coordinate data of each streamline is stored. The distance between each streamline can be varied and set as the 'bandwidth'. To accommodate for the problem of gaps and overlaps between two curved courses, the script also run another triangulation for each coordinate point to evaluate the distance

between the neighbouring streamline, and this distance data is used to calculate localised variations in extrusion.

Effect of bandwidth

The maximum spacing between two streamlines is dictated by a specified parameter, 'bandwidth'. This parameter dictates the extent to which the streamlines are spaced, and therefore the amount of variation in extrusion rates needed to compensate for the gaps between the streamlines. Here, we look at the visualizations for these width variations and compare them to observed variations in the samples.

The open-source tool gCodeViewer [65] offers an option to visualize print widths against a scale of mm of material extruded per mm. The material extrusion is denoted as the length l of a cylinder whose diameter is the filament diameter (2.85 mm). As the height of the print (0.15 mm) remains constant throughout, the material deposited is a cuboid, for which we can calculate effective widths 'w' printed per 1 mm length:

$$\pi \times \frac{2.85^2}{4} \times l = 1\,mm \times 0.15\,mm \times w$$

Where, *l* is the amount of feedstock material extruded in mm. A range of widths *w* corresponding to effective lengths *l* is shown in Table 8. In the subsequent visualizations, effective widths for the minimum and maximum extrusions seen in the legend are shown as Min_{data} and Max_{data}. However, visually it is also seen that predominantly occurring values are not necessarily the minimum/maximum values, and hence, a maximum value based on visual assessment is also calculated for reference, shown as Max_{visual}. We consider a general rule of thumb that maximum allowable extrusion width for printing is to be kept under twice the nozzle diameter, in our case 2 x 0.4 mm = 0.8 mm. From Table 8, we can see that this rule of thumb is in effect till extrusion values a little over 17.5 µm.

Table 8 - Effective widths extruded per mm move for different extrusion lenghts of feedstock material

Extruded length (µm)	Effective width per mm
5.0	0.213
7.5	0.319
10.0	0.425
12.5	0.532
15.0	0.638
17.5	0.744
20.0	0.851
22.5	0.957
25.0	1.063

The width variations for the series R10 are visualized in Figure 28. We see that the variations in width are minimal as the curvature between courses is consistent. Except for some small streamlines (seen in red, e.g., top left corner), the extrusions widths are well under our expected threshold of 0.8 mm. This is also corroborated by visual inspection of samples

under an optical microscope, as seen in Figure 29; widths at four different points are measured and highlighted, and all values seen are under 0.5 mm. The approximate region of images taken is highlighted in the dotted box in Figure 28. This region shows extrusions of ~0.425 mm (from legend, Table 8).

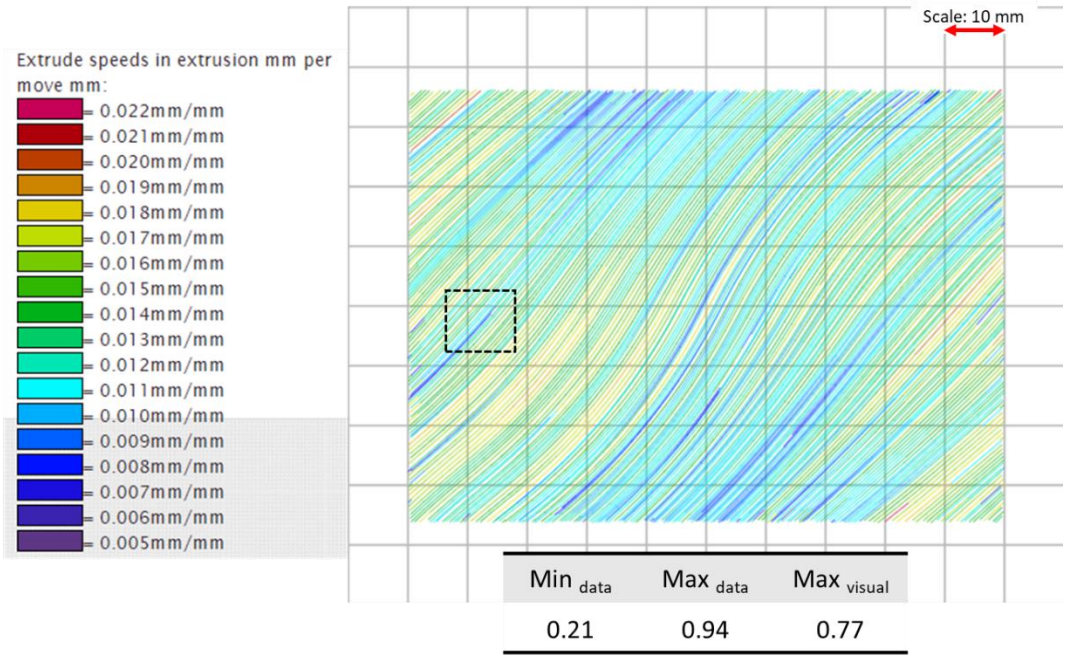

Figure 28 - Width variation visualisation for R10 series (dotted box shows approximate area for optical images)

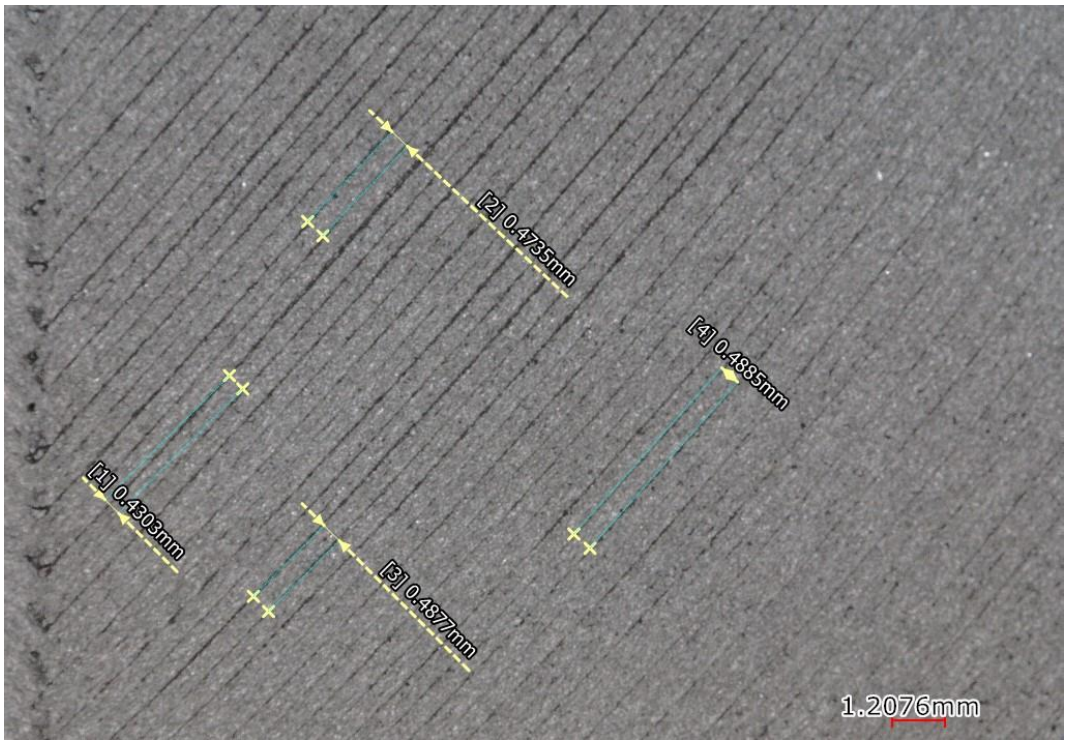

Figure 29 - Width variations in R10 series as seen in the highlighted region from width visualization (Figure 28)

However, for the series high curvature layup series R100 and R100N, the effect of bandwidth selection was more pronounced. Figure 30 (a) and (b) show the visualization of widths in the series R100 and R100N respectively, which correspondingly are specimens with coarser and finer bandwidths. For comparison, the specimens were also compared under a microscope and stark differences in printed widths was observed. The approximate area is highlighted in a red dotted box in Figure 30 (a) and (b).

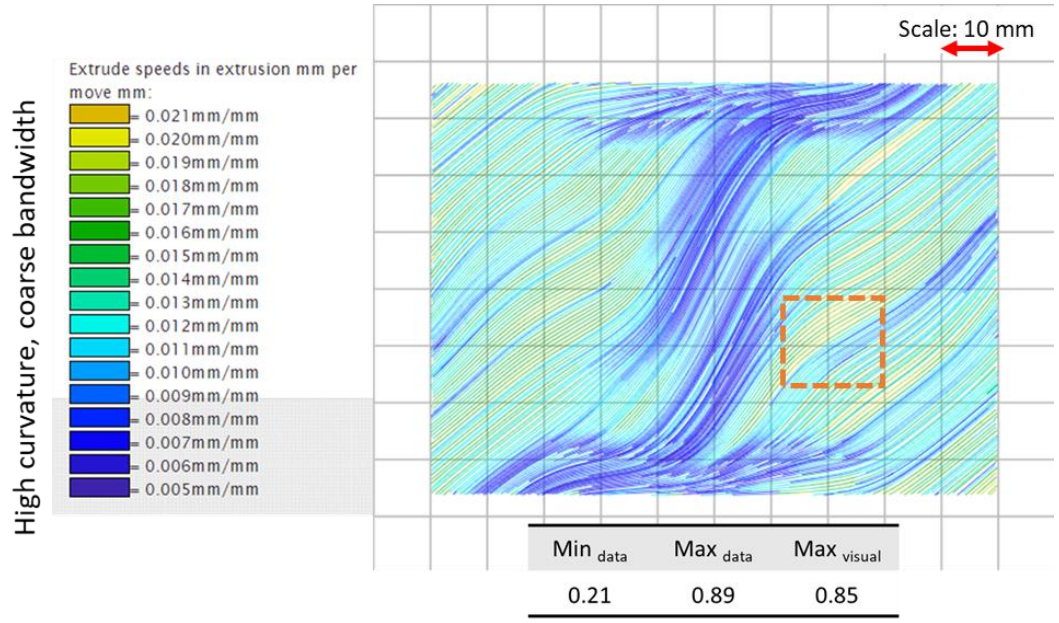

(a)

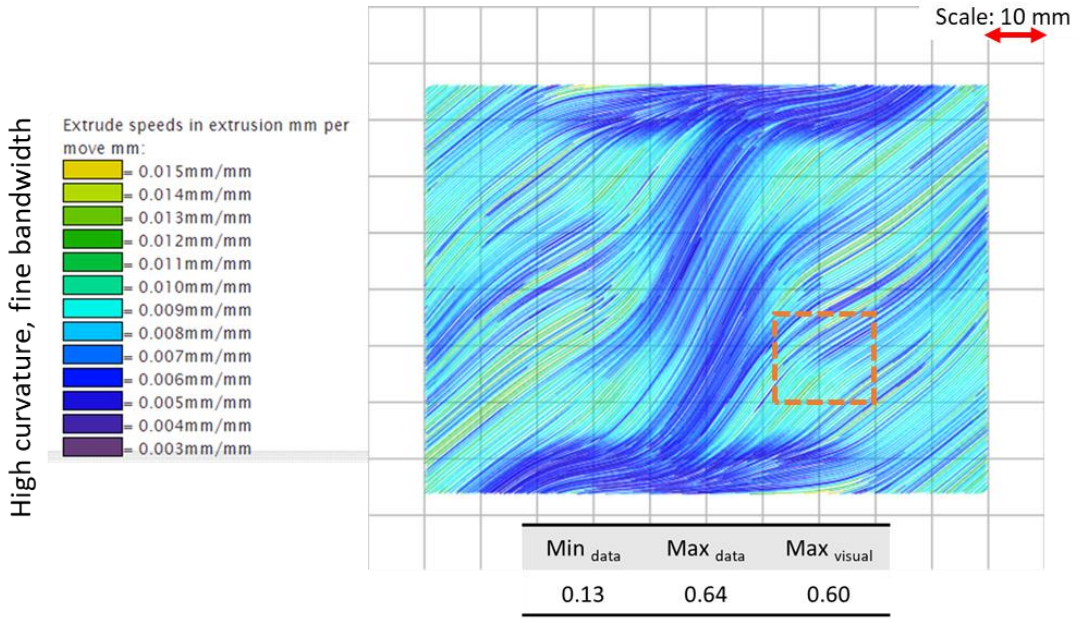

(b)

Figure 30 - Width variation visualisation for high curvature layup series – (a) series R100, (b) series R100N

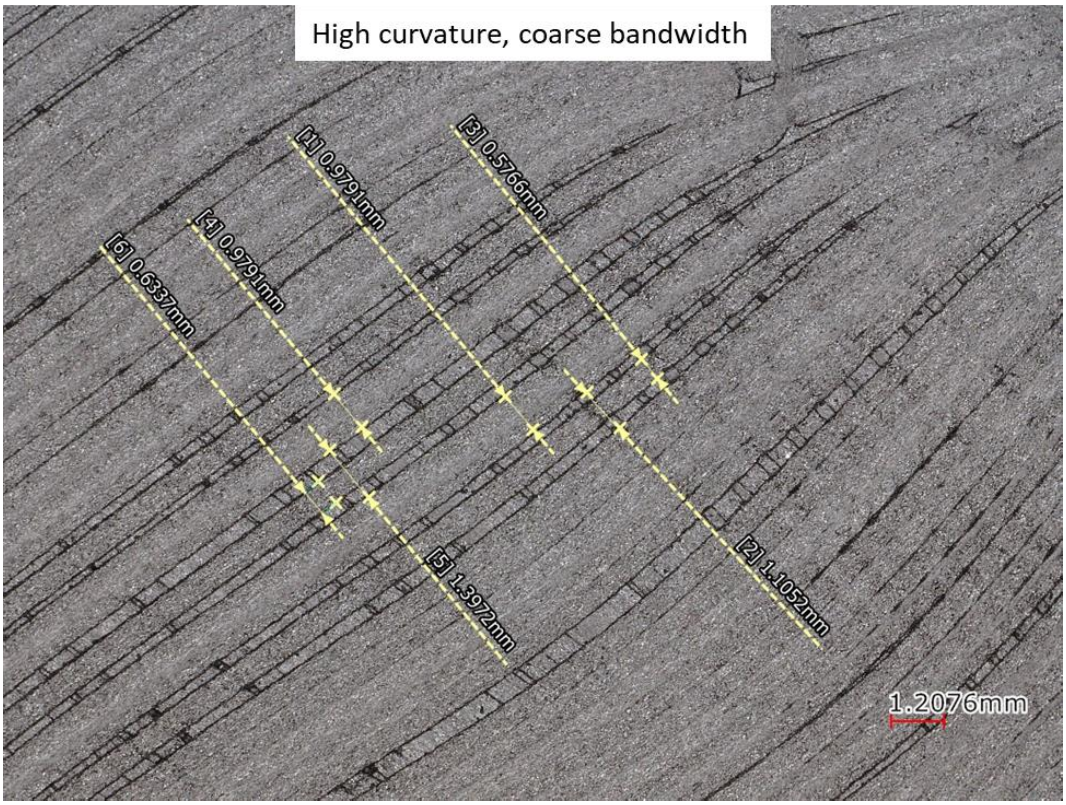

(a)

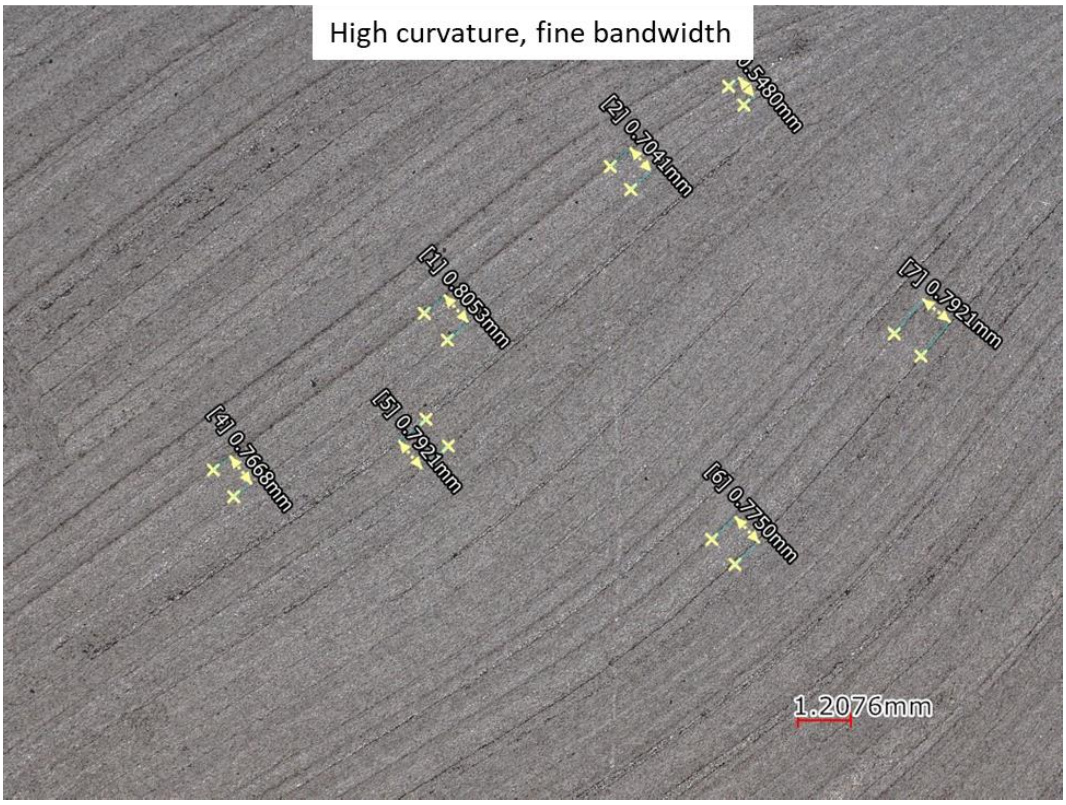

(b)

Figure 31- Width variations in regions highlighted in Figure 30 for specimens with (a) coarse bandwidth and (b) fine bandwidth

It is clear that the specimen with a finer bandwidth shows much more consistent extrusions and very little gaps between each course of material deposition. This is also reflected in the recorded weights of each specimen printer (discussed subsequently).

For validation, 4 specimen series were selected with 3 samples in each series. Salient highlights for these are:

- **QI laminate:** In the optimization framework, no specific QI layup is defined. A QI layup is considered as one with all lamination parameters as zero.
  For practical purposes, a balanced and symmetric layup is needed. Angular increment between each layer is defined as = 180°/n for n = 8 plies. Thus, we get an increment of 22.5°. Therefore, the layup chosen is: **[0 22.5 45 67.5 90 112.5 135 157.5] s**
  For this layup, the expected buckling load is calculated using a FEM software 'Kolibri'. Corresponding buckling load calculated is **2991.57 N**, which is close to the calculated value from table 5.
- **R10:** Steering curvature set at 10 m-1
- **R100:** Steering constraint set at 100 m^{-1}, bandwidth set at 1 mm
- **R100N:** Steering constraint set at 100 m^{-1}, bandwidth set at 0.75 mm

Nomenclature referred in the subsequent sections is with the format "Series_SerialNo." The averaged thicknesses (measured at 4 different locations each) and weights of the printed specimens are tabulated in Table 9Table 10 and Table 10, respectively.

Table 9 - Averaged thicknesses of printed specimens, in mm

Series / Specimen	Thickness in mm			
	QI	R10	R100	R100N
1	2.70	2.68	2.47	2.71
2	2.65	2.68	2.63	2.74
3	2.46	2.65	2.58	2.61

Table 10 - Recorded weights for printed specimens, in grams

Series / Specimen	Weight in g			
	QI	R10	R100	R100N
1	26.38	28.83	26.97	27.49
2	26.65	29.35	26.45	28.87
3	27.17	27.82	24.26	31.49*

*Specimen R100N_3 (Figure 32) was observed to carry a sizeable defect on the uppermost layer during printing. However,

- The defect was only on the outermost layer, and
- The courses apart from the region of the defect, no other 'courses' were affected,

hence, this sample was still tested as a part of the specimen series R100N.

As we see from the recorded weights and the width variation data, the series R100 is less dense and exhibits more porosity visually. Therefore, series R100 is skipped from detailed discussions.

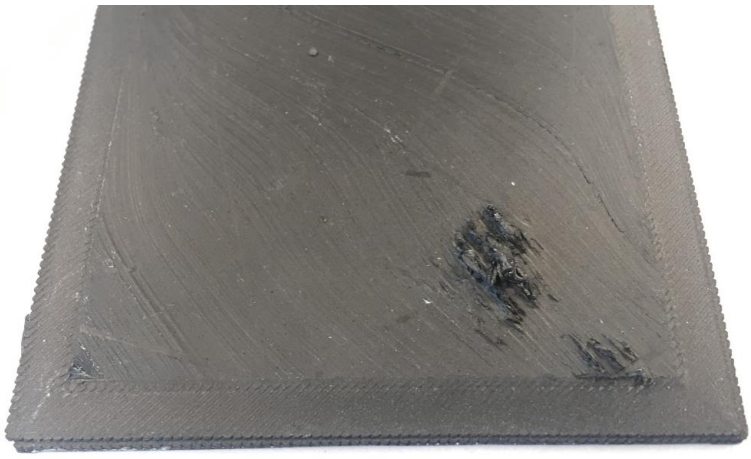

Figure 32 - Defect seen in the top surface of specimen R100N_3

4.3. Experimental protocol and setup

To evaluate the buckling performance of each design specimen set under uniaxial compression, a suitable experimental protocol and setup were devised.

The chosen dimensions of the specimen were influenced by the available compression testing fixture available. The boundary conditions for all the edges were approximated closer to simply supported, which was used as an input in the optimization framework. The available fixture allowed for a maximum uniaxial compression up to 4 mm, but for the sake of safety, the allowed compression was limited to 3.5 mm during the actual tests.

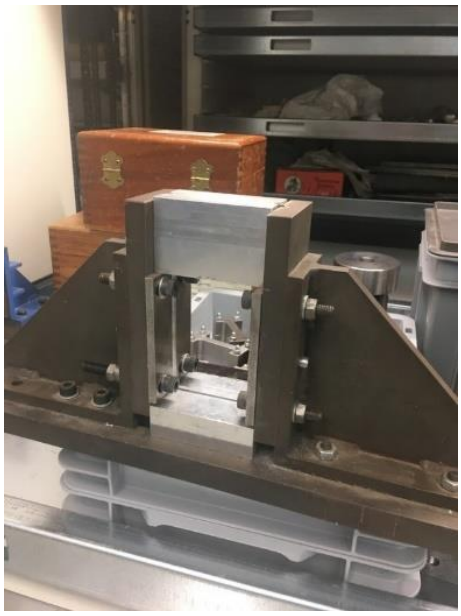

Figure 33 - Fixture used for compression tests of laminates

The dimensions of the samples needed to be accounted for use with the fixture. Essentially, the computed design needed a perimeter to be able to be mounted properly in the fixture. This was chosen as an approach as if not, some area of the optimized laminate would be 'outside' the loading area. To avoid this to happen, especially in laminates with layers where near-straight fibre orientations are seen, an excess frame was manually added, which accounted for the dimensions such that all the design specimen area was loaded during testing. The schematic representation of the same is seen in Figure 35, and the measure distances are highlighted in Table 11.

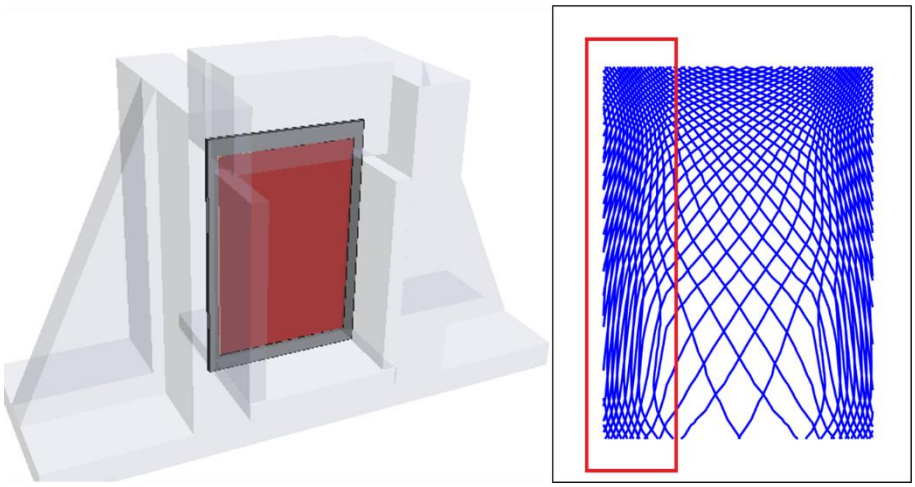

Figure 34 - Schematic representation of excess required for mounting of specimen in fixture, (L) specimen in red + excess region needed for mounting in gray, and (R) approximate area of the design space needed to be compensated for in excess

The added frame shows a weld-line between the frame and the specimen. Indicative representation is shown in Figure 35.

Table 11 - Specimen dimensions and excesses measured for the test fixture

(in mm)	Length	Width	Thickness
Specimen	100	72.5	2.4
Specimens + excess	112	84	2.4

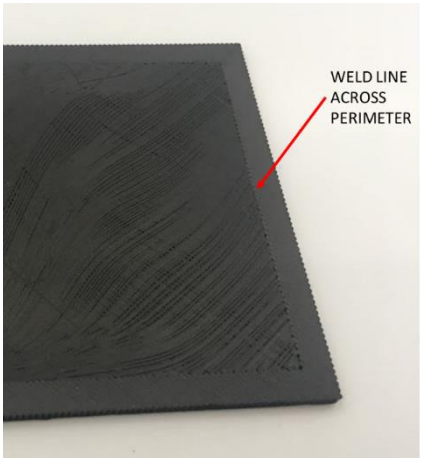

Figure 35 - Weld-line along the periphery of R100 specimen (coarse bandwidth)

To evaluate the out-of-plane deflections, a stereo DIC system was used to record data at intervals of 0.5 seconds. The compression fixture was setup on a Zwick 10 kN test bench, and speed-based loading of 2 mm/min was used to load the specimen. All the specimens were painted with a speckle pattern for DIC analysis. The setup used is seen in Figure 36.

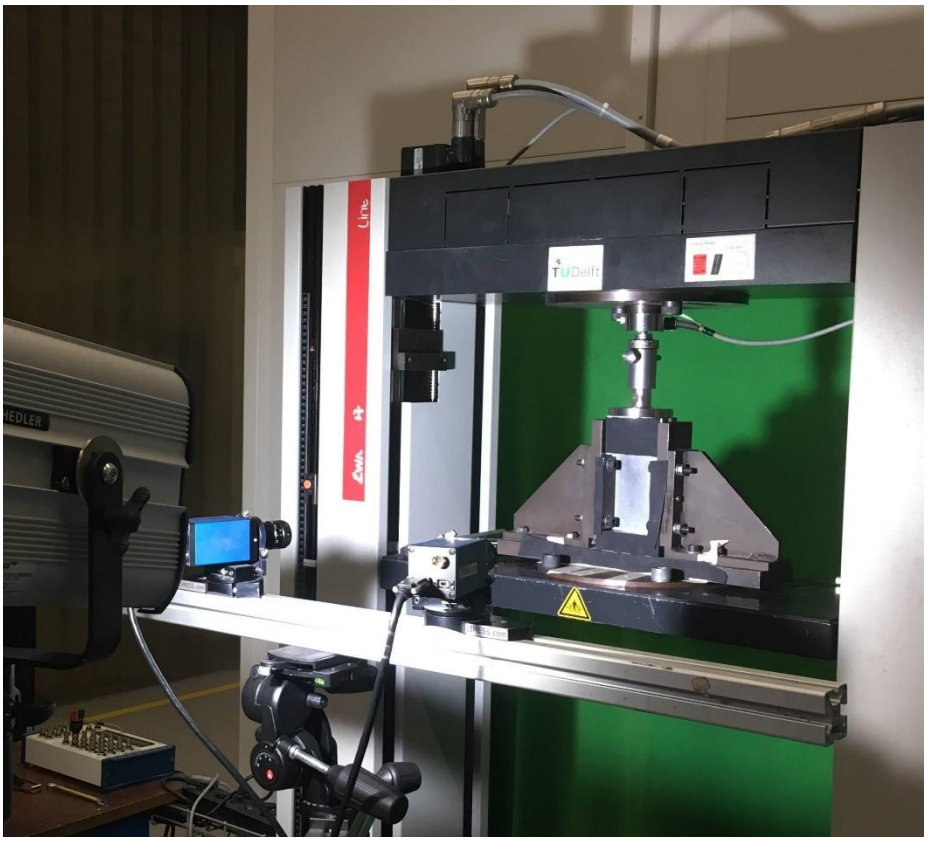

Figure 36 - Test setup used for compression tests shows stereo camera DIC system, light source and compression fixture mounted on test bench.

5. Results and discussions

A total of 3 samples per specimen set, i.e., 12 samples were printed and tested according to the specifications and protocol specified in the earlier chapter. From the optimization framework, expected performance of each sample set are tabulated below. The expected performances are tabulated in Table 12.

Table 12 - Expected performances of optimized laminates

Layup	Buckling load 1 (N)	Buckling load 2 (N)
QI	2991.57	
R10	3535.65	3535.65
R100	4069.77	4102.72

During the experiments, two sets of data were recorded – load vs axial displacement data recorded on the test bench, and the out-of-plane displacements recorded by the DIC system. First, the load-displacement data is observed and discussed.

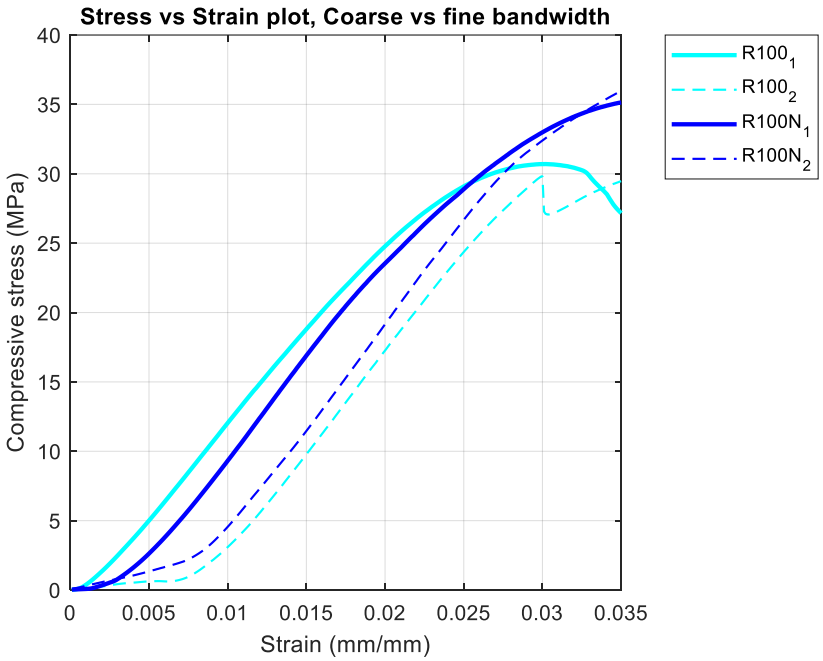

Figure 37 - Compressive stress vs strain for series R100 and R100N

The plot in Figure 37 shows the load bearing performance between the specimens printed with the high allowable steering curvature but different bandwidths. The specimens printed with a fine bandwidth (where the distance between two streamlines was set closer to each other), series R100N_x, performed better under compression and exhibited higher load bearing than the ones printed with a coarser bandwidth (series R100_x). The gaps, seen visually on the specimens themselves, were also more pronounced and hence, this specimen set printed at a coarser bandwidth is not considered for further discussion.

The best performing specimens from the series QI_x, R10_x and R100N_x are shown in Figure 38.

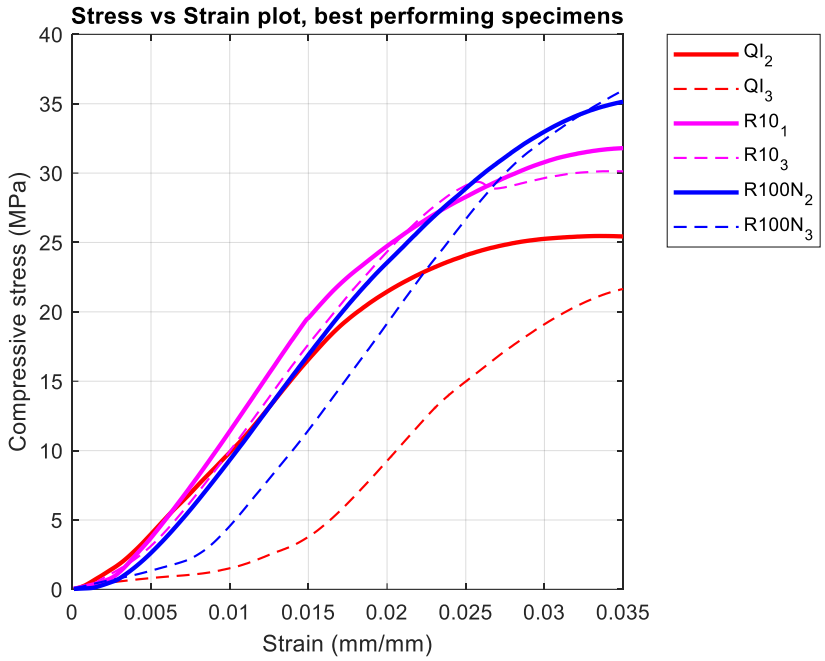

Figure 38 - Compressive stress vs strain for series QI, R10, R100N

From Figure 38, it is seen that the increase in allowable steering curvature in a series corresponds to an increase in compressive load taken by the respective specimen set. Higher allowable curvatures exhibit more maximum compressive load at the maximum allowable deformation possible during the experiments.

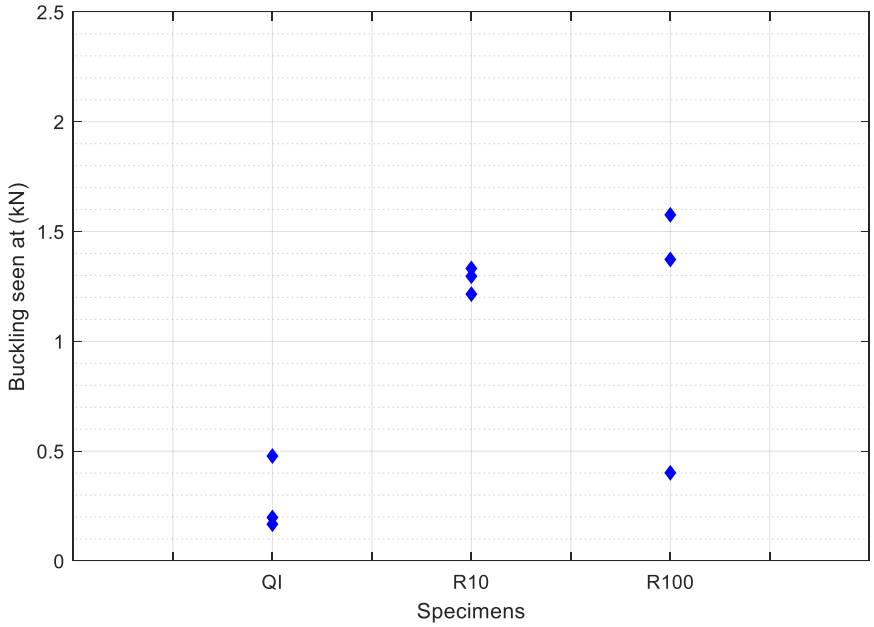

Figure 39 - Loads at which buckling was observed for respective speciemn series

As the specimens were optimized for buckling, we take a deeper look at the out-of-plane displacements and analyse the failures observed in the samples. For the sake of conciseness, the best three specimens from each series are discussed here. Additional data for each sample tested during experimentation is supplemented in Appendices B and C.

DIC data recorded during each test was used to calculate the out of plane displacements over the course of the test. The change in out-of-plane displacements of each specimen was monitored visually, and the load at which onset of buckling waves were seen was recorded. Salient results, as observed by postprocessing DIC data are highlighted in the Table 13.

Table 13 - Data recorded during compression test of specimens

Specimen	**Weight (g)**	**Expected buckling at (N)**	**First buckling mode seen at (N)**	**Second buckling mode seen at (N)**	**Load at end of test (N)**
QI_1	26.38	2991.57	197.8	2329.0	3688.9
QI_2	26.65		167.3	1515.2	4143.1
QI_3	27.17		**477.6**	2156.0	4517.1
R10_1	28.83	3535.65	1215.1	5365.4	5830.5
R10_2	29.35		**1332.1**	2944.4	4994.8
R10_3	27.82		1296.5	3656.4	6089.6
R100N_1	27.49	4069.77	401.3	4282.0	5492.5
R100N_2	28.87		1372.7	--	6956.9
R100N_3	31.49*		**1576.2**	--	6871.1

The end of the test is dictated by the maximum travel set during the test as limited by the physical dimensions of the fixture used. The onset of buckling in the best performing specimens in series QI, R10 and R100N are shown in Figure 40, Figure 42 and Figure 44 respectively.

Some observations are made here, which are discussed subsequently.

- Specimen QI_3 fails at value over twice the load for the other two specimens in the series.
- Specimen R100N_1 shows a much lower load than the other two specimens in the series.
- Specimen R100N_3 shows some surface irregularity in the speckle pattern in the upper half, and these spots duly considered while monitoring the deflections seen during the onset of buckling.
- All specimens continued to get loaded after onset of buckling. Maximum loads at the end of the test (forced stop at 3.5 mm axial compression) were in seen increasingly higher in the series with higher allowable steering (R100N > R10 > QI)

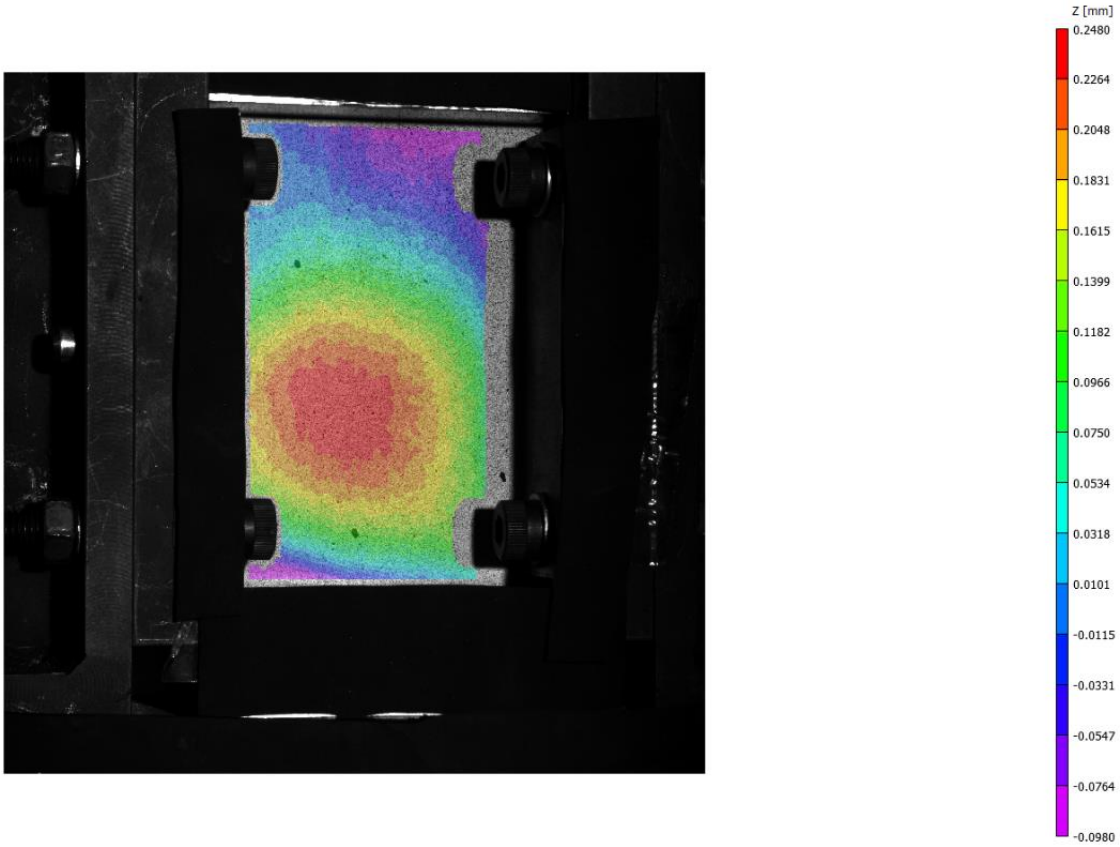

Figure 40 - Onset of buckling, QI specimen no. 3 at 447.6 N

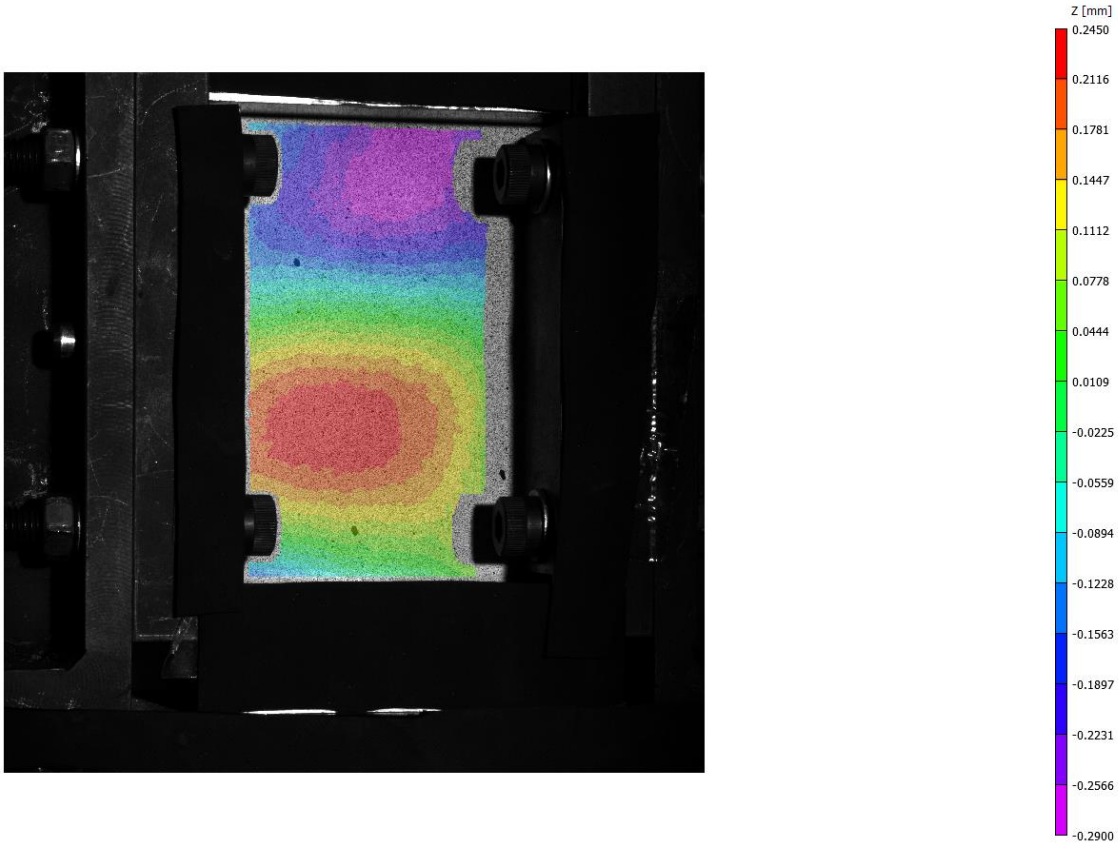

Figure 41 - Onset of mode change in QI specimen 3 at 2156.0 N

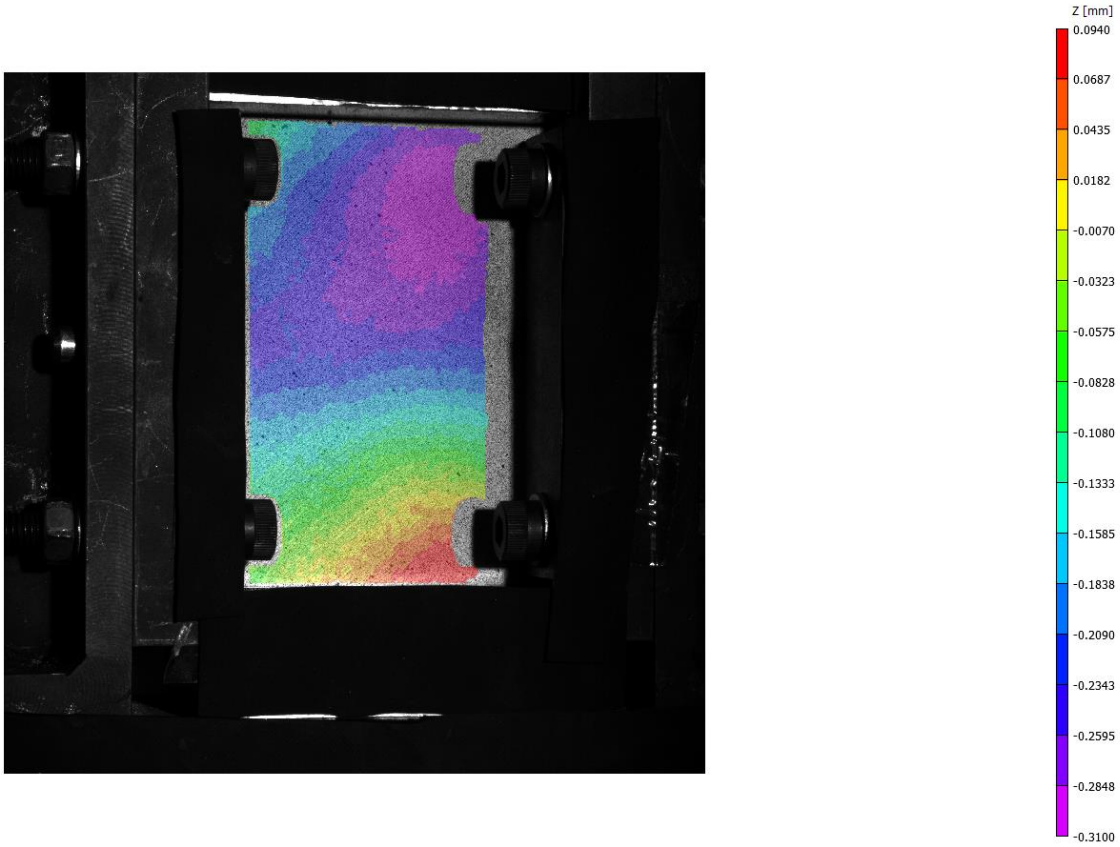

Figure 42 – Onset of buckling, R10 specimen no. 2 at 1332.1 N

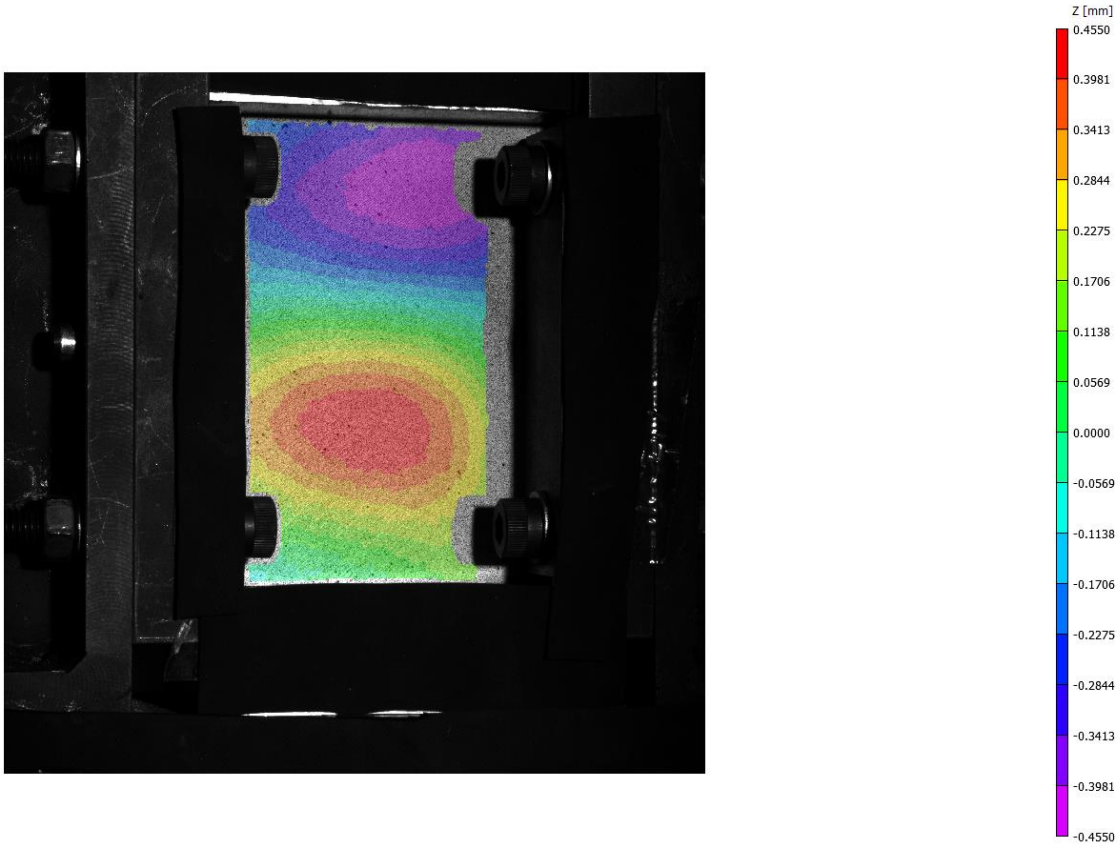

Figure 43 - Onset of mode change in R10 specimen 2 at 2944.4 N

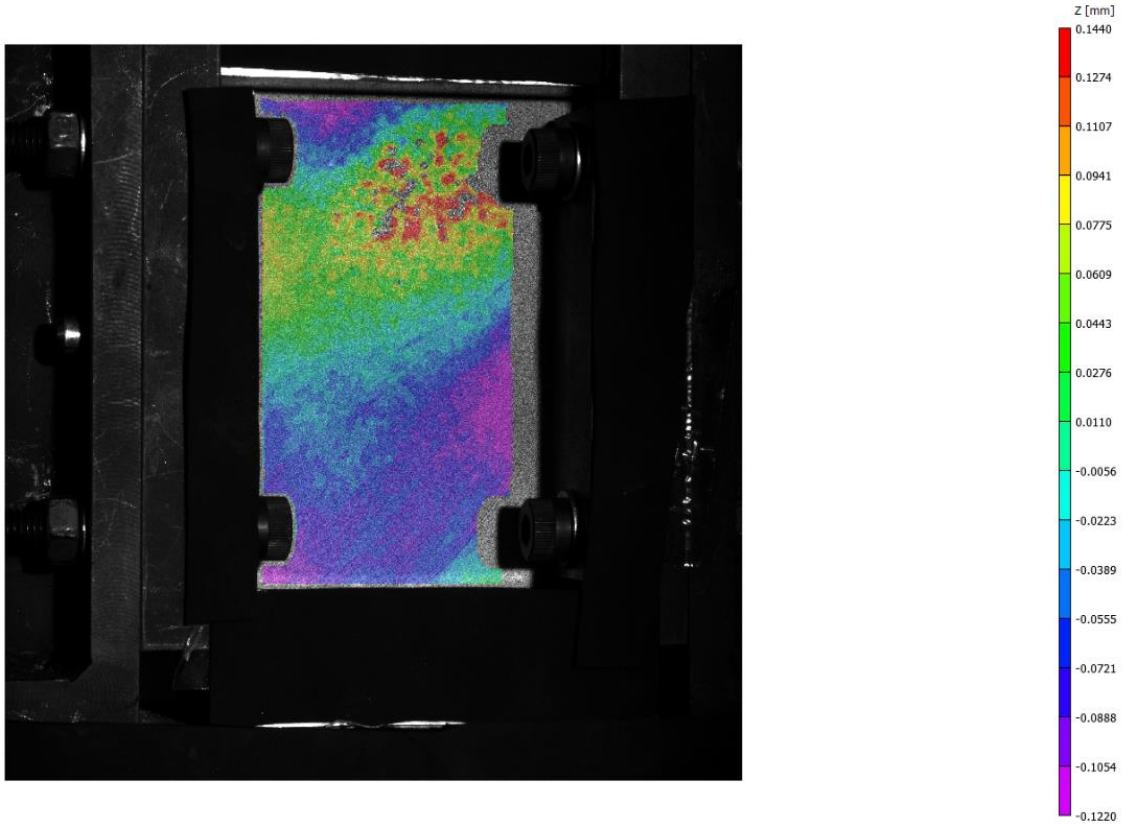

Figure 44 - Onset of buckling, R100N specimen no 3 at 1576.2 N

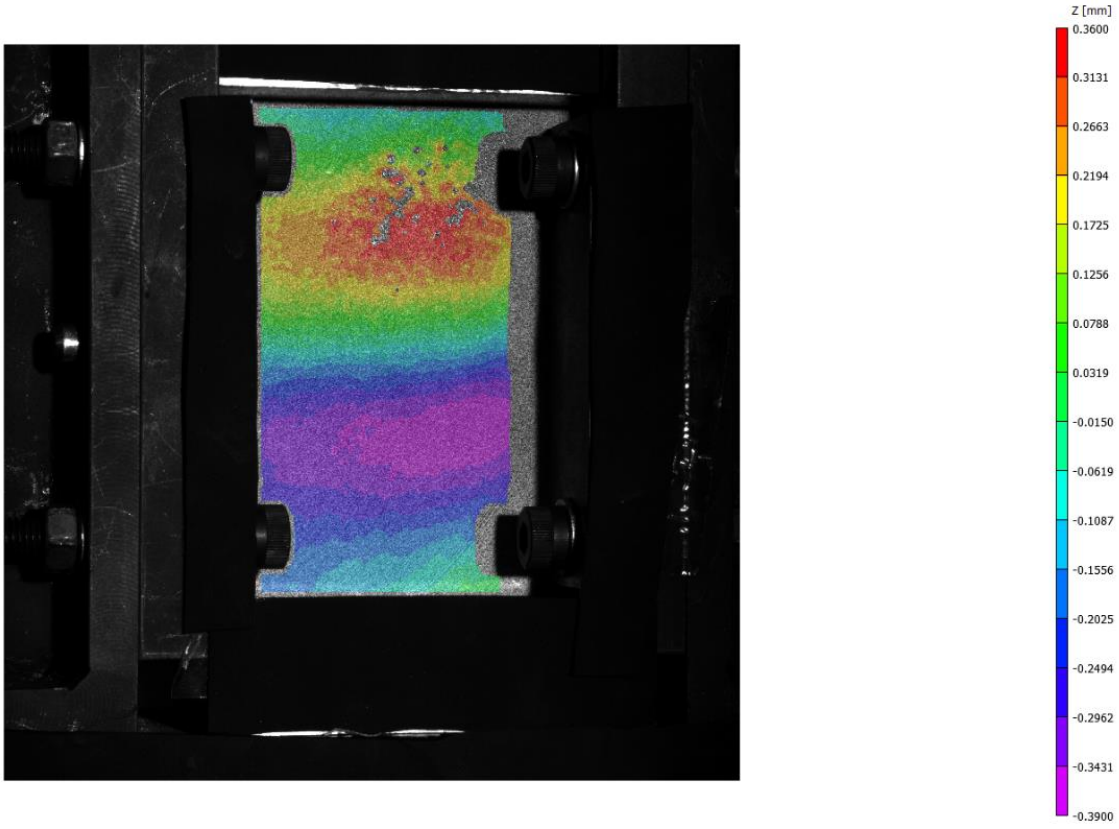

Figure 45 - Buckling mode seen at end of test for R100N specimen 3 at 6871.1 N (no mode change seen)

At the outset, it was noted that all specimens exhibited buckling. Further, the expected trend in allowable curvature and buckling failure loads was seen consistent in both the calculated and experimentally observed data. Lastly, for the series R100N, a mode change in buckling was not seen till the maximum allowable travel of the fixture.

However, a considerable knockdown is seen between the theoretically predicted and experimentally verified values at which buckling occurs. Some insights are drawn and highlighted:

Manufacturing induced defects.

- Weight related discussions

A general correlation between weight of a specimen and the buckling load is seen in the Table 13. For the QI series, two out of three specimens weigh under 27 grams, and these two specimens buckle at almost half the load of the specimen QI_3. Similar trend is seen in the series R100N – R100N_1 weighing the least of three (with the obvious consideration that R100N_3 does not have the most accurate weight representation) also buckles at a much lower value.

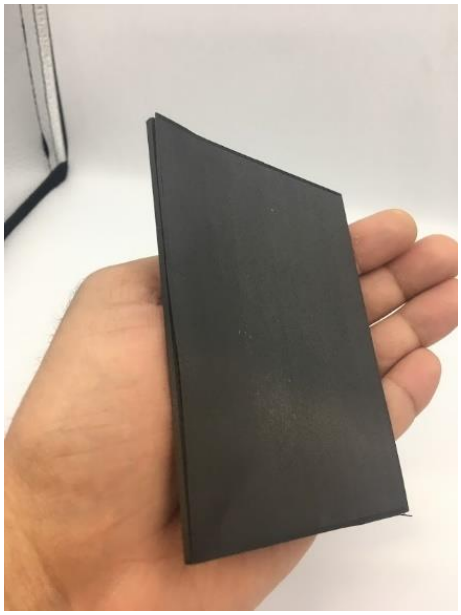

Figure 46 - Poor interlayer adhesion seen in QI specimens (trial specimen)

It should also be noted that only the optimized laminates were printed with the excess frame. This might be a contributing factor for both additional weight in the steered specimens as well as additional interlayer adhesion. QI laminates, printed with an edge boundary, showed signs of poor interlayer adhesion during print trials and testing (Figure 46).

Lastly, for specimen R100N_3, the defect (seen in Figure 32) could also have acted as a discontinuity, forcing for load distribution into other continuous streamlines, especially the longer ones along the diagonal. As the damage was limited to only external layer, the effect of the defect is considered tangible yet not very pronounced.

- Non-extrusion moves

3D printed specimens are susceptible for process induced defects such as porosity. These can be caused by thermal hysteresis on the hotend, and since the extrusion rates for each course printed were constantly varying, material inertia would also be a factor in variations of the actual amount of material deposited during printing. Secondly, the G-code generation algorithm results in jumps over the courses deposited in each layer, as the courses are printed longest to shortest. These non-extrusion/travel moves can be seen in Figure 47.

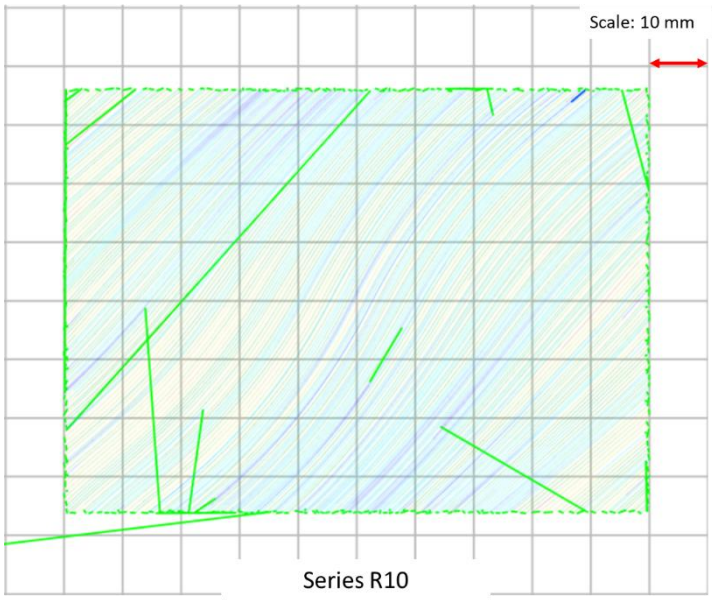

(a)

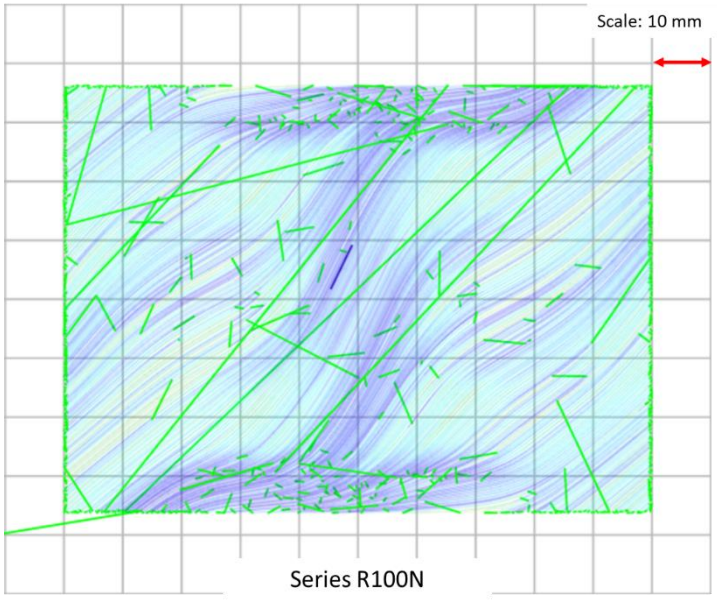

(b)

Figure 47 - Non-extrusion travel moves (in green) seen in series (a) R10 and (b) R100N show difference in number of moves required in respective series

The algorithm does use Z-hopping (upward and downward movement of the extruder to avoid laterally movements over deposited material), however, these spots do cause localised material gaps and excesses when the extruder lifts and comes down, respectively.

More non-extrusion moves are needed per lamina for the series R100N as compared to R10, as the streamlines are denser and more curved. Therefore, this induces a high chance of porosity variations within the series R100N and R10, and that would explain the consistent performance of the specimens in the latter.

Loading induced defects

The mounting and loading of each sample involved actions such as tightening/loosening the mounting frame bolts. Inconsistencies in loading and deviations from design specified boundary conditions, as a result, may also have been caused due to human error.

Design-choice induced defects

The onset of out-of-plane deflections was routinely seen along the weld-line between the 'excess' added to the plate. Since this was a very specific and known discontinuity along the periphery of the specimen, it could have acted as a local defect prompting earlier failure than the buckling load of the laminate. However, the QI plate, which had no such discontinuity, also failed at a much lower load than predicted, hence further enquiry with variations in design choice must be carried out to verify.

6. Conclusions and recommendations

6.1. Conclusions

Three main research questions were posed as a part of the proposal for this thesis, outlined in section 3.2. Each question is now addressed, and certain conclusions are presented based on the observations and interpretations made over the course of the thesis project.

I. What are the effective mechanical properties of the material due shear-induced alignment of the short-fibre reinforcements?

Printing parameters such as extrusion temperature and print speed vastly influence the material being printed, especially ones with heterogenous reinforcement media. Extrusion temperature varies the viscosity of the melt, and thus affects the effective shear-induced alignment of the short fibre reinforcements in the material used in this research. For the chosen printing parameters, unidirectional specimens were observed under optical microscopes and image analysis was used to characterize the effective alignment of short fibres. A high degree of order was seen in the alignment (Figure 22). The short fibres in the printed samples showed a high degree of alignment due to shear interaction of melt in the printer nozzle under pressure. This alignment orientation data was then used to calculate effective mechanical properties of the material, which was further used to calculate the mechanical performance of the designed laminates

II. Can existing design frameworks be employed with additional design freedom to generate better designs?

For this research, the work of Peeters [42] was chosen as the framework based on which further work was carried out. A manufacturability constraint imposed as a part of the optimization algorithm was found ideal to be adapted for FDM with minimal changes to the framework itself. The data generated from this framework was further used to generate machine instruction for FDM printers. Here, choice of design parameters and their corresponding impact on manufacturability was also identified, and two different cases for the same overall design (R100 vs R100N) were manufactured for further enquiry.

III. If yes, can the relative performance of these designs be validated experimentally?

Finally, the hypothesis that increasing the design freedom afforded to the optimization framework would yield better mechanical performance was put to test. An experimental protocol was designed to validate the performance of the specimens against their computed performance. As hypothesized, an increase in performance was seen in the manufactured specimens. However, a considerable knockdown from calculated performance was also observed, and possible reasons like manufacturing defects, process induced inconsistencies (weld-line along the periphery of sample, non-extrusion/travel moves) were highlighted and discussed.

6.2. Recommendations

Based on the insights drawn not only from the experimental data recorded, but also experiences gained during the process of the research, certain recommendations are made for further enquiry. These are yet again identified in all three key aspects of engineering – design, material, and process.

Design improvements

The research was aimed at evaluating improvements in performance of laminates by means of increasing design space available. Further research is recommended for exploring the effects of including topology optimization within the design as well.

Secondly the design choice made to add an 'excess' frame for mounting purposes gave rise to weld lines along the periphery of the specimen. This region was recurringly seen as the area of out-of-plane deflection onset. It is recommended that subsequent experimental specimens be generated with modifying boundary conditions within the design space itself, or, add extra material in a more 'organic' fashion to the specimen itself, to eliminate this weld-line periphery. The effects of such a change in design choices should be corroborated experimentally for comparison and future use.

Further, the problem of non-extrusion, travel moves discussed earlier can be eliminated in one way by ordering the print courses once the course lines are printed. This, however, requires substantial computational expenses and necessitates a detailed enquiry to accommodate very complex path geometries as well.

Lastly, there is scope of improvement in the mounting fixture. The top block of the mounting fixture restricts the max. travel possible during the test. Different construction ideas can be tested to approximate the loading conditions while allowing for more travel possible.

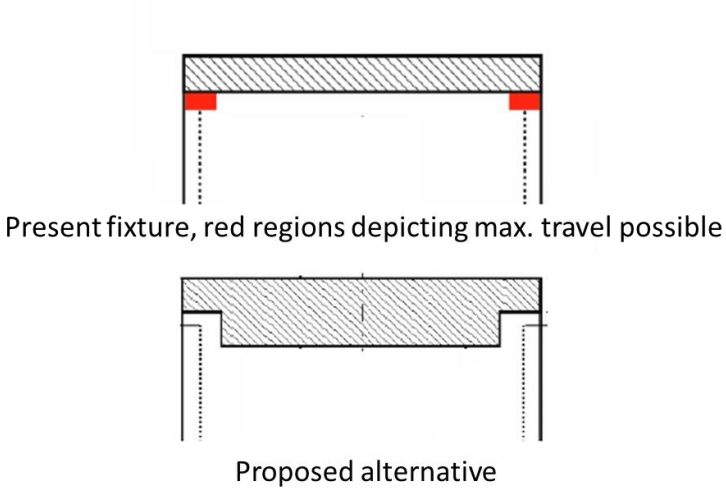

Figure 48 - Maximum permissible travel of fixture seen in red (top), and propsed alternative of fixture design (bottom) which could allow for higher deformation

Process improvements

Commercially available FDM printer was used with minimal modification (nozzle changed for using abrasive feedstock) for manufacturing specimens. Bed levelling is identified as an important stop in the process flow itself – crucial not only for dimensional accuracy of the specimens, but also greatly affects the bed adhesion and thus printing as well. For a stock UM2+, a bed levelling sensor can be mounted and installed for improvements and repeatability.

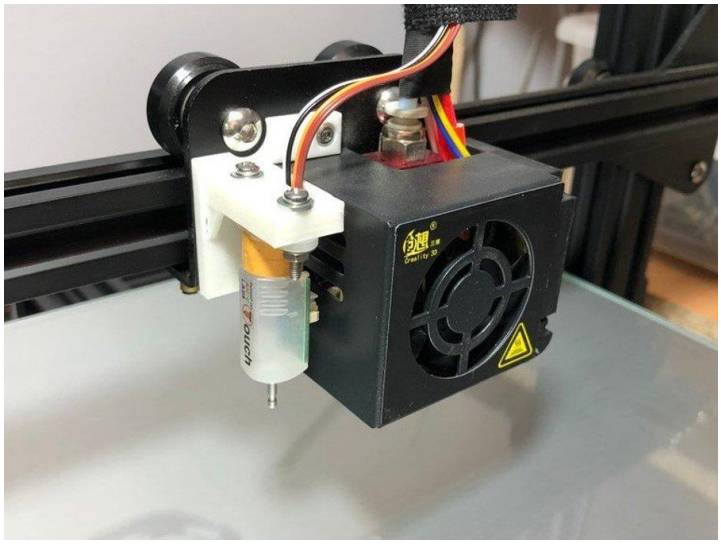

Figure 49 - BLTouch z-level sensor for bed-level correction

Swapping the Bowden tube extruder to a direct drive is also recommended. This allows for better control of and a wider array of feedstock material. Direct drive extruders also allow for more reliable material control during extrusion and retraction.

Gharehpapagh et al. [66] also explored the effect on bead width if a constant cross-section nozzle with a rectangular profile is turned entirely, instead of having intricate mechanisms within the nozzle. To demonstrate this, they printed multiple polygons and found that the effective width being laid down varies linearly with the angle at which the rectangular cross-section is kept at with respect to the direction of travel.

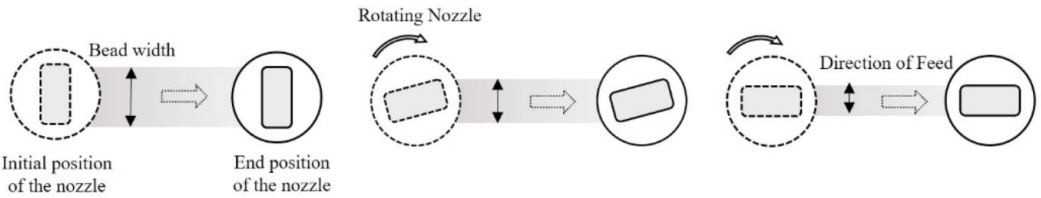

Figure 50 - Rectangular cross-section nozzle travel with respect to travel direction [66]

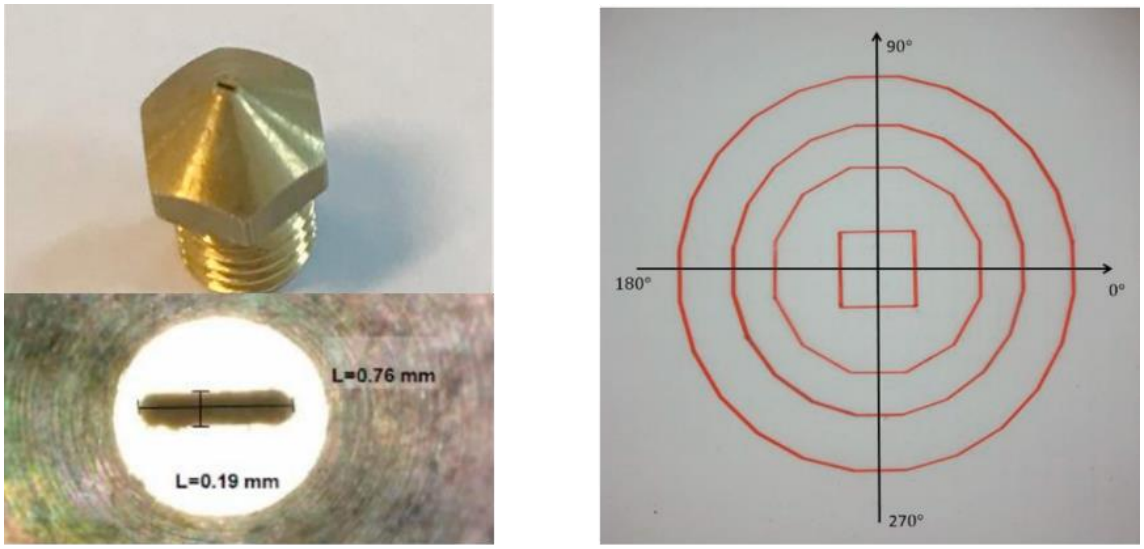

Figure 51 - (a) Close up of nozzle, and (b) printed multi-sided polygons, [66]

Löffler et al. [67] explored this concept further - by implementing the rotational degree of freedom on the nozzle. This was done as a compromise between level of detail and reduction in print time. This work is a proof-of-concept to demonstrate large volume of material flow while varying width by rotation of nozzle enables reduction of print time at the cost of print resolution. This approach could further be incorporated to for continuously varying widths during material deposition.

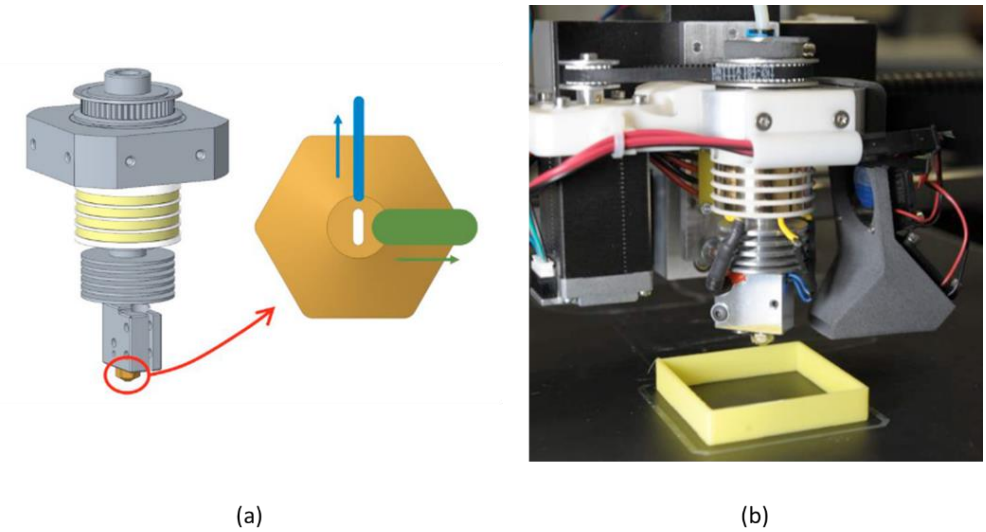

Figure 52 - Rotating nozzle (a) concept, and (b) in action [67]

Material

As a step forward in this research in terms of material used, continuous reinforcements are proposed as a major improvement to a similar approach. Commercially available FDM printers can print with a wide variety of materials like polylactide (PLA), acrylonitrile

butadiene styrene (ABS), polyethylene terephthalate glycol (PETG) and nylon to name a few. A detailed review of the state of the art by Dickson et al. [68] is recommended for the interested reader. Zhuo et al. [69] discuss certain limitations in the process, such a poor fibre wetting and impregnation, susceptibility to voids and low fibre volume fractions. Inherent heterogeneity in reinforced feedstock poses additional challenges to recycling.

Gantenbein et al. [70] discuss a different approach towards reinforced polymers for FDM. A liquid crystal polymer (aromatic co-polyester having monomers p-hydroxybenzoic acid and 2-hydroxy-6-naphthoic acid) with highly ordered molecular domains are used to exploit the shaping freedom offered by FDM. Owing to the mechanics of FDM, the ordered domains of the liquid crystal polymer (LCP) self-assemble, thereby giving rise to anisotropy inherent to the material being deposited. Figure 53 describes this in greater detail.

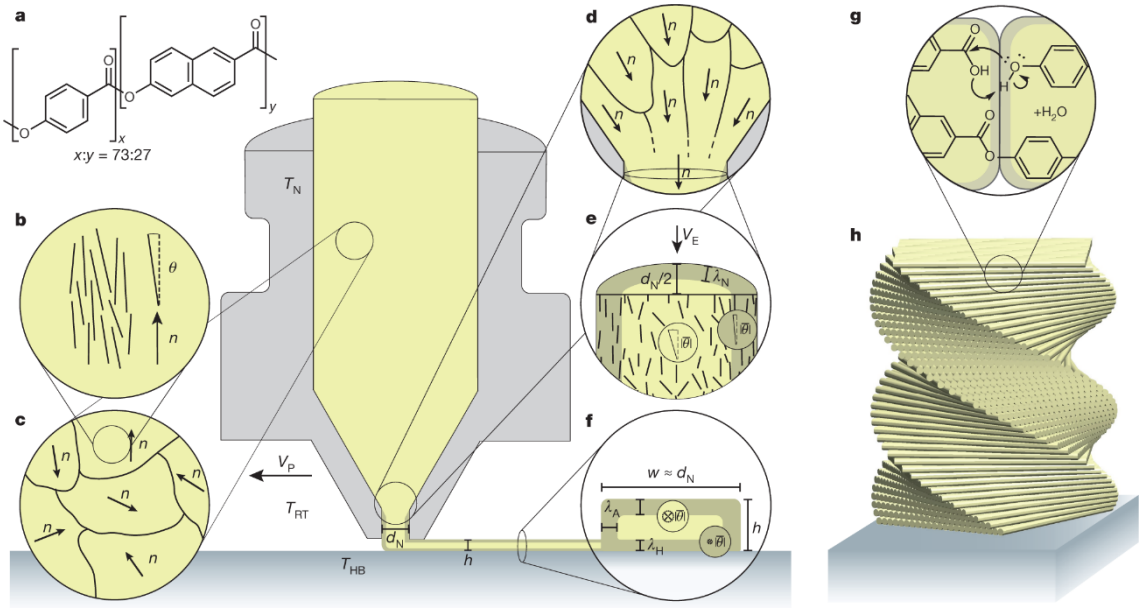

Figure 53 - Hierarchical self-assembly of liquid crystal polymers by FDM [70]

In Figure 53, points highlighted (a) to (c) show the nematic domains with randomly oriented directors which form quasi-isotropic bulk of the polymer melt. Each nematic domain contains short chains of monomers misaligned with the director **n** by a certain angle **θ**. Point (d) shows the extrusion causing the directors to self-align in the direction of extrusion. Further as is seen in (e) and (f), the other domains cool faster and freeze in the ordered orientation, whereas the inner domains relax, giving rise to a core-shell architecture. (g) and (h) show annealing promotes the crosslinking of chain ends and enhances stress transfer between filaments.

The core-shell architecture is seen in the scanning electron microscopy image of the fibre (Fig. 47). Gantenbein et al. report a maximum elastic modulus of 34 GPa and a maximum of strength of 800 MPa for horizontally printed filaments. Furthermore, and very importantly, the material would be fully recoverable and recyclable, eliminating the need to retrieve any heterogenous reinforcements, ensuring a sustainable alternative to conventional reinforced

printing filaments. It should also be noted that not just the end-of-life, but overall carbon-footprint of the material in such a comparison is much lower for the liquid crystal polymer.

Figure 54 - SEM image of tensile-tested filament specimen [70]

Appendices

Appendix A – Microscopy images from specimens

Fibre alignment seen along the skin of filament strand extruded at layer height of 0.15 mm:

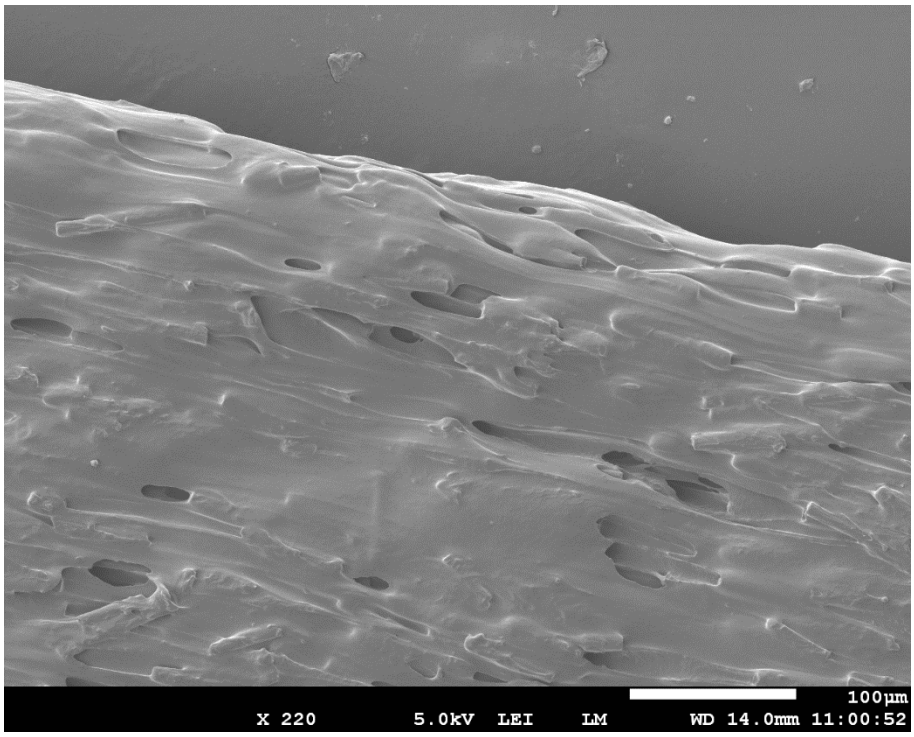

Cross section of freely extruded material showing perpendicular short fibres along the cross-section:

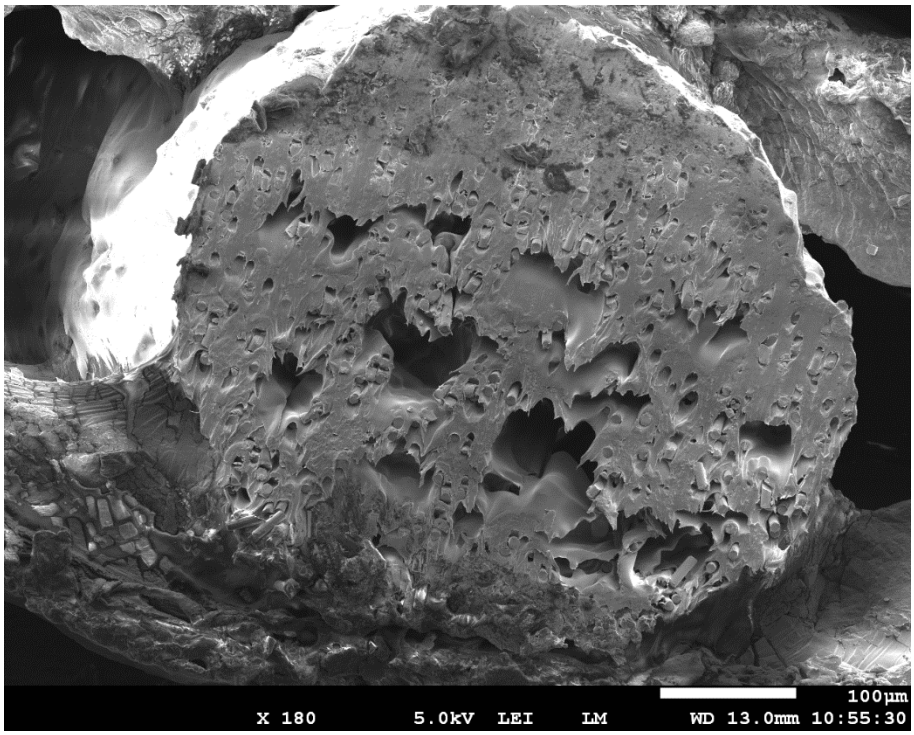

Unidirectional specimen observed under optical microscope (multiple courses):

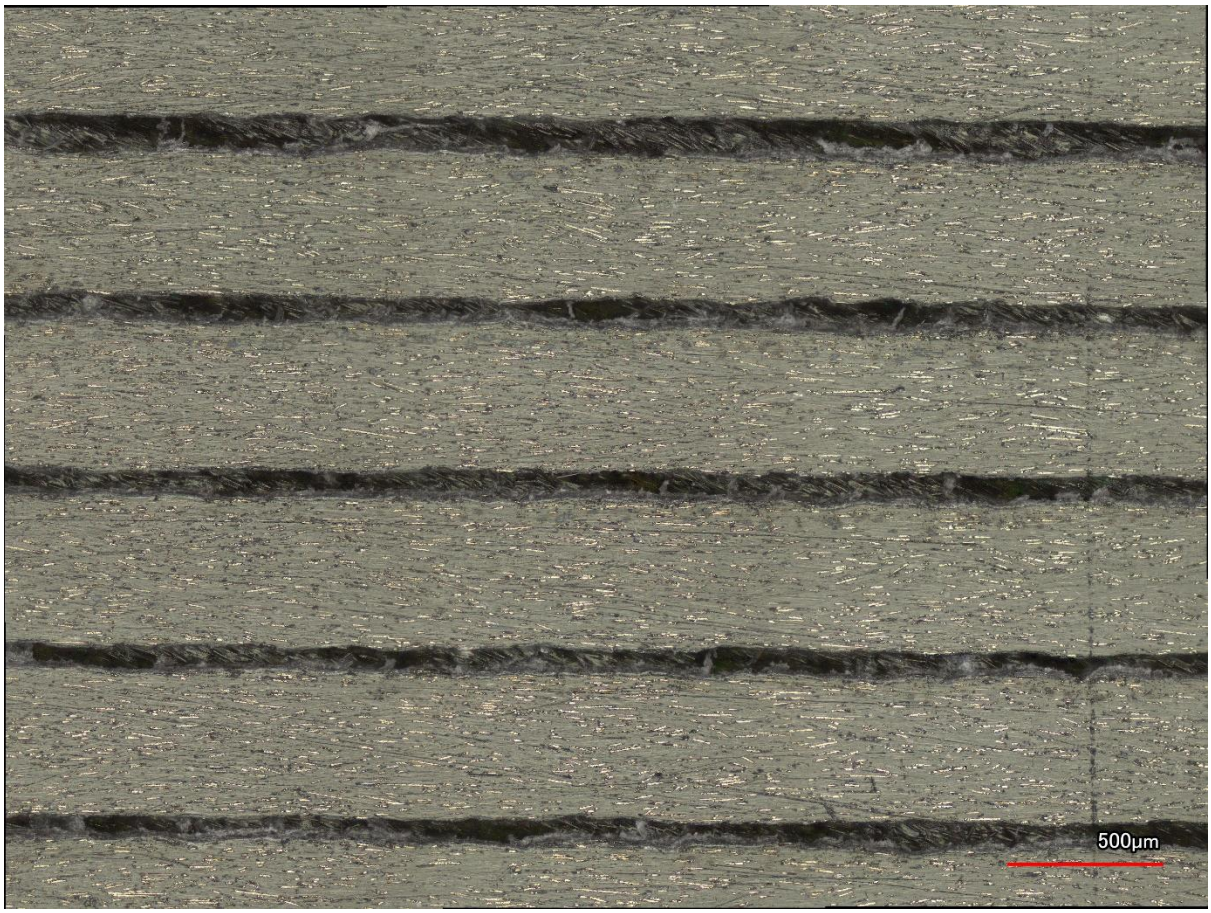

Appendix B – Stress vs Strain plots for each specimen

Plots of engineering stresses vs strains for each of specimen series tested

Series QI:

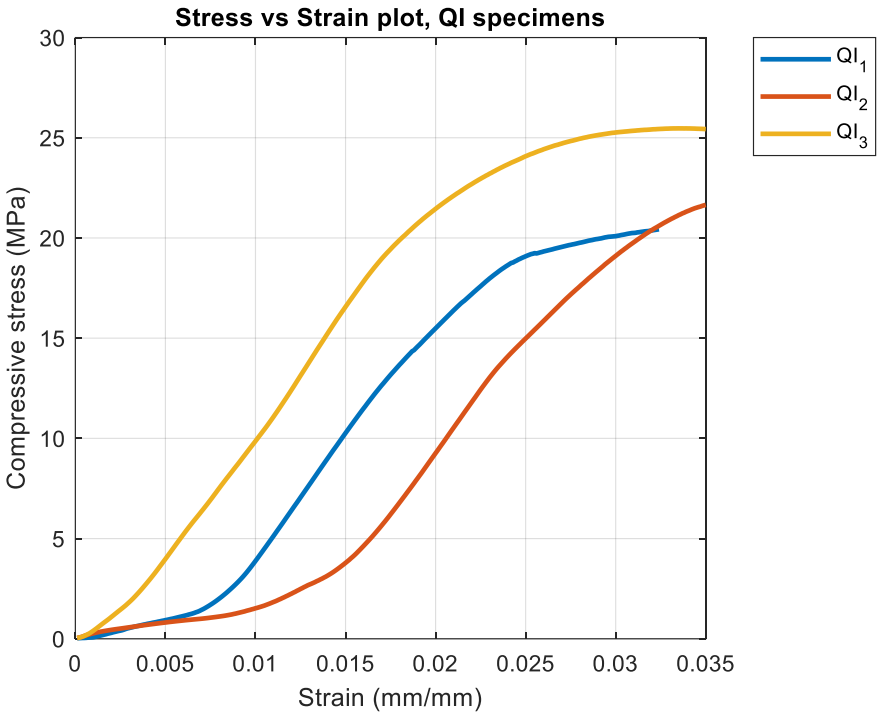

Series R10:

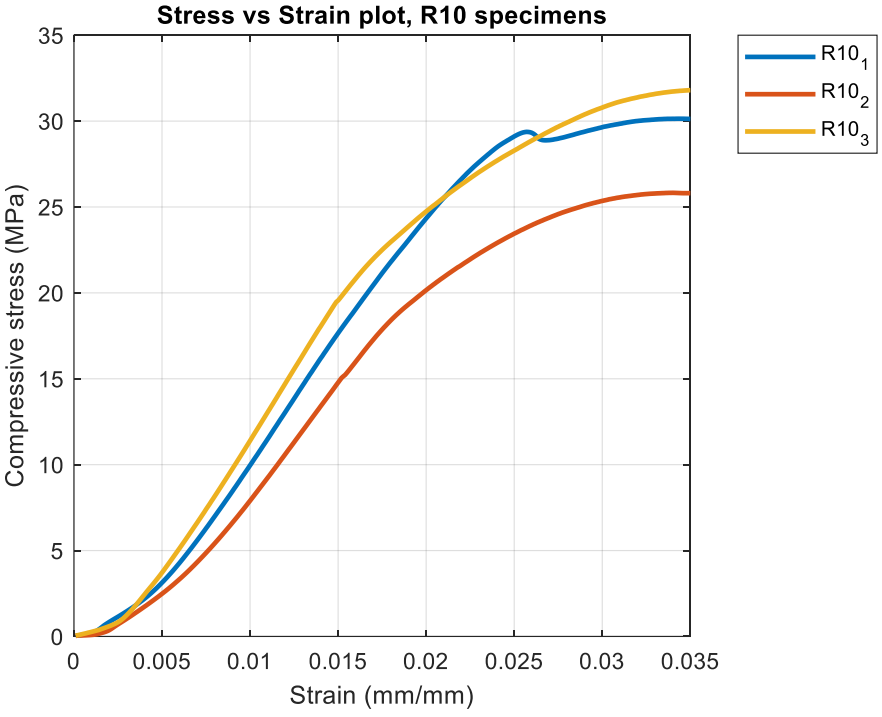

Series R100

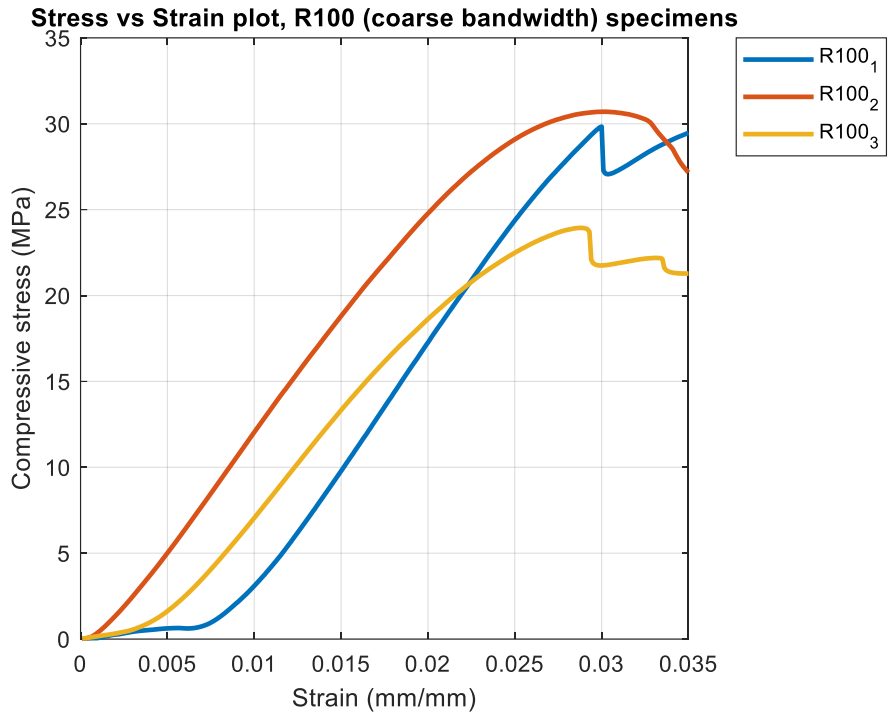

Series R100N

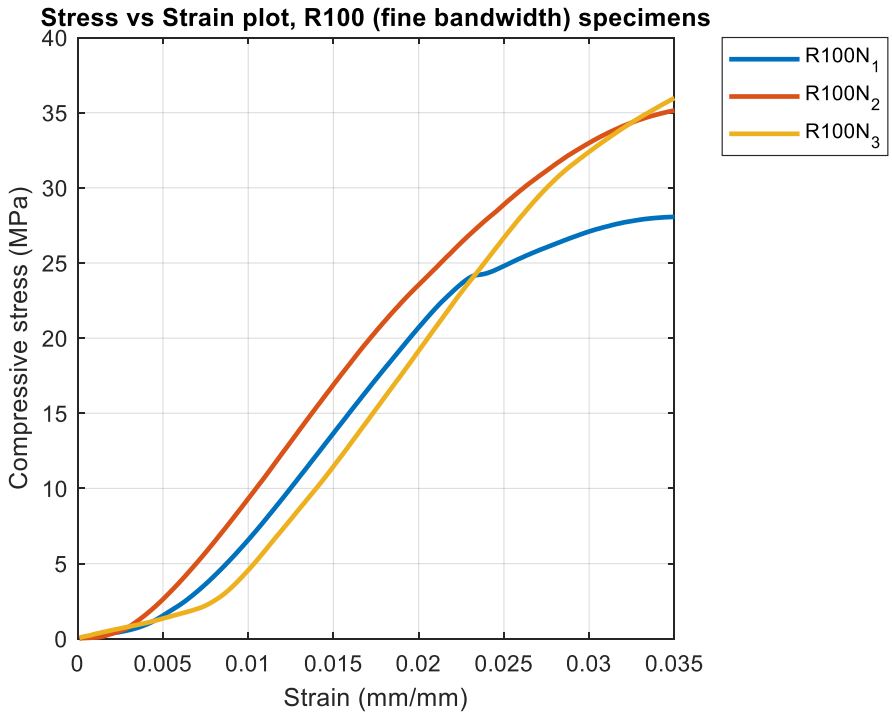

Comparison: Series R100 v R100N:

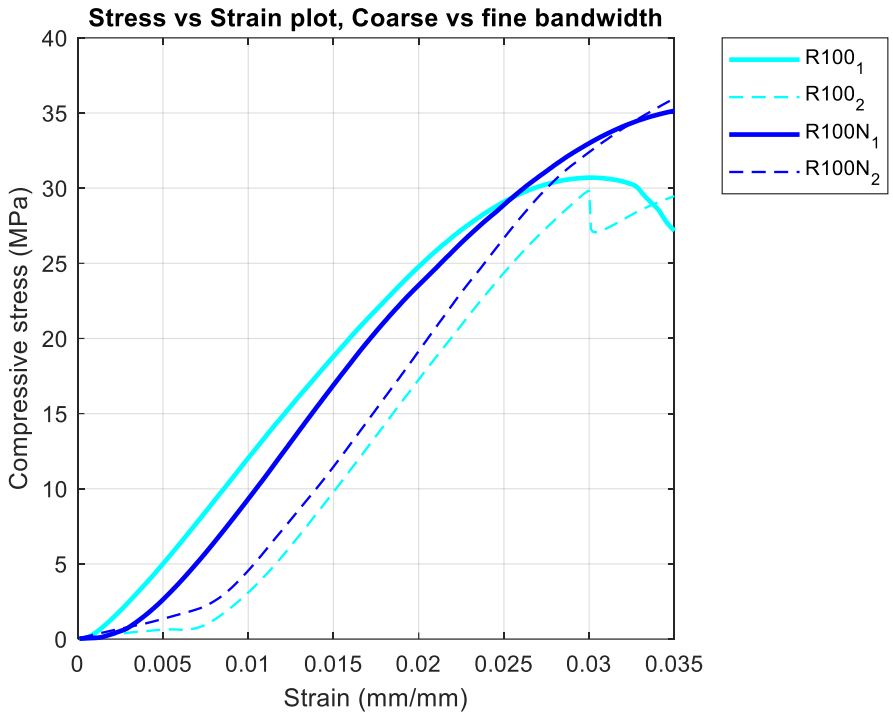

Best performing specimens, all series:

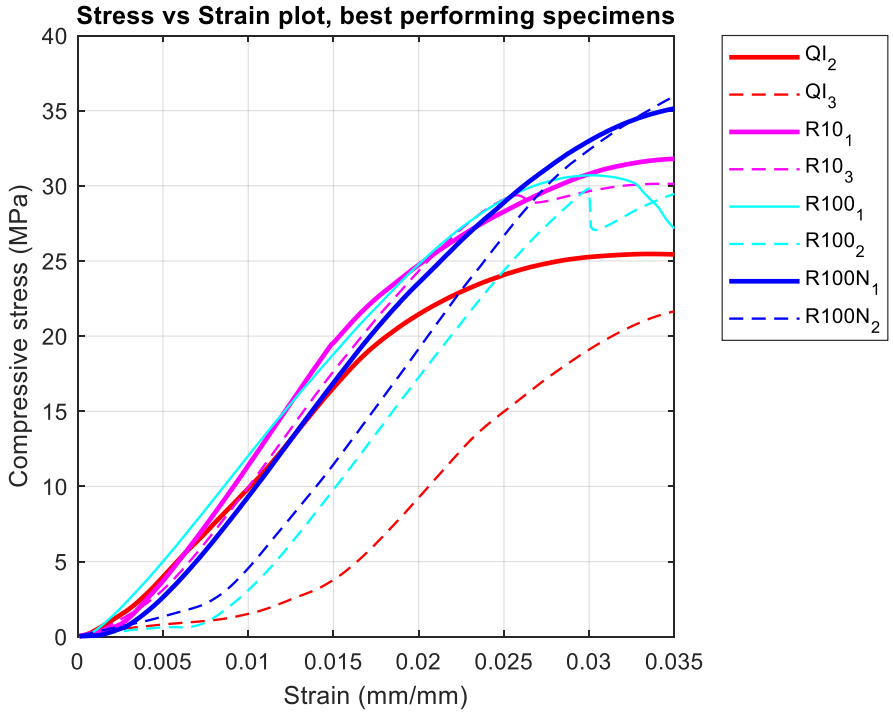

Appendix C – Out of plane displacements for tested specimens

QI_1, onset of buckling at 197.8 N

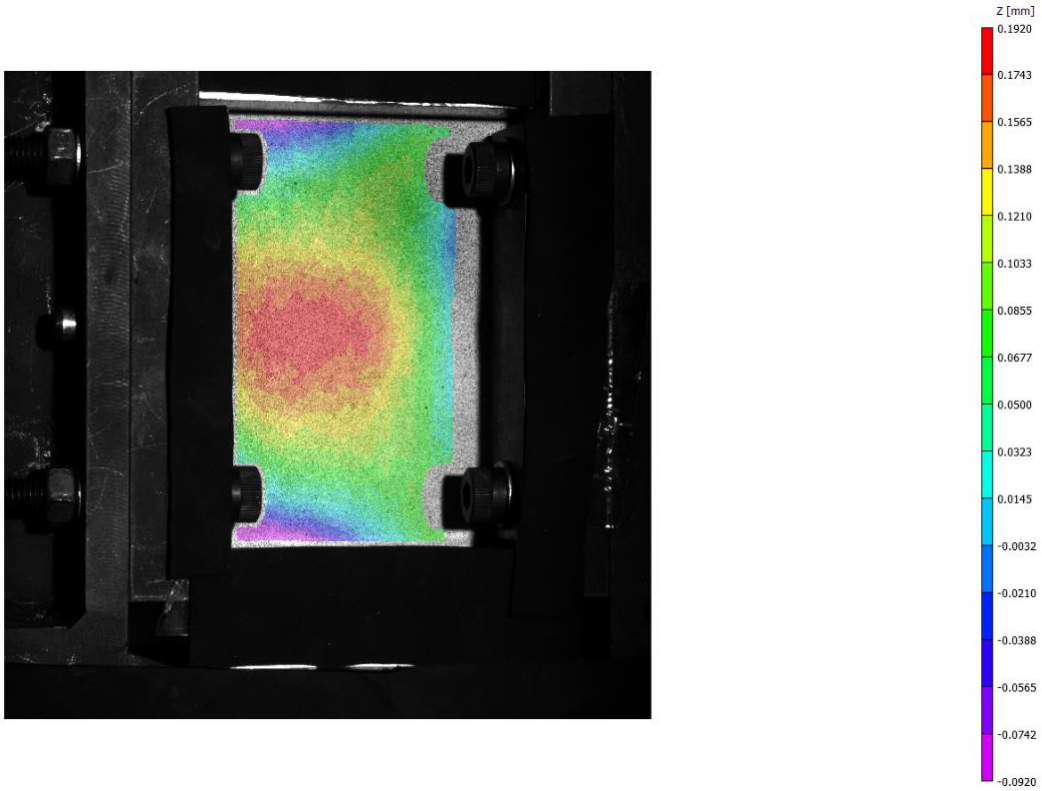

QI_1, mode change at 2329.9 N

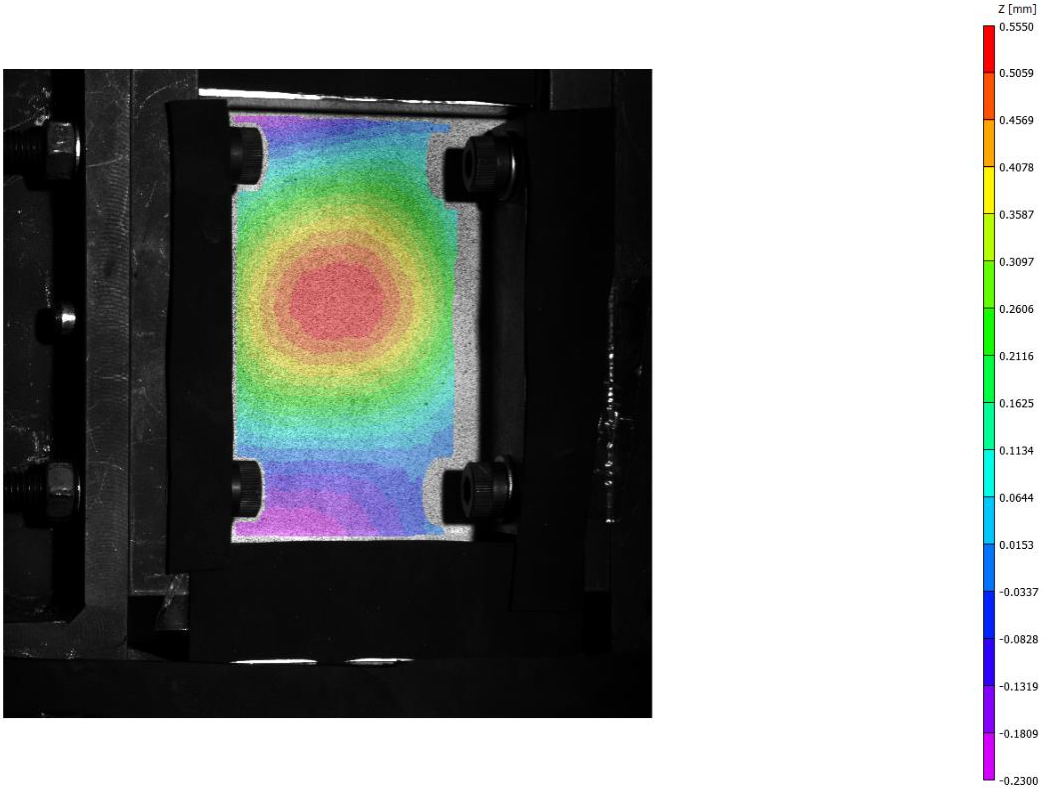

QI_1, end of test at 3688.9 N

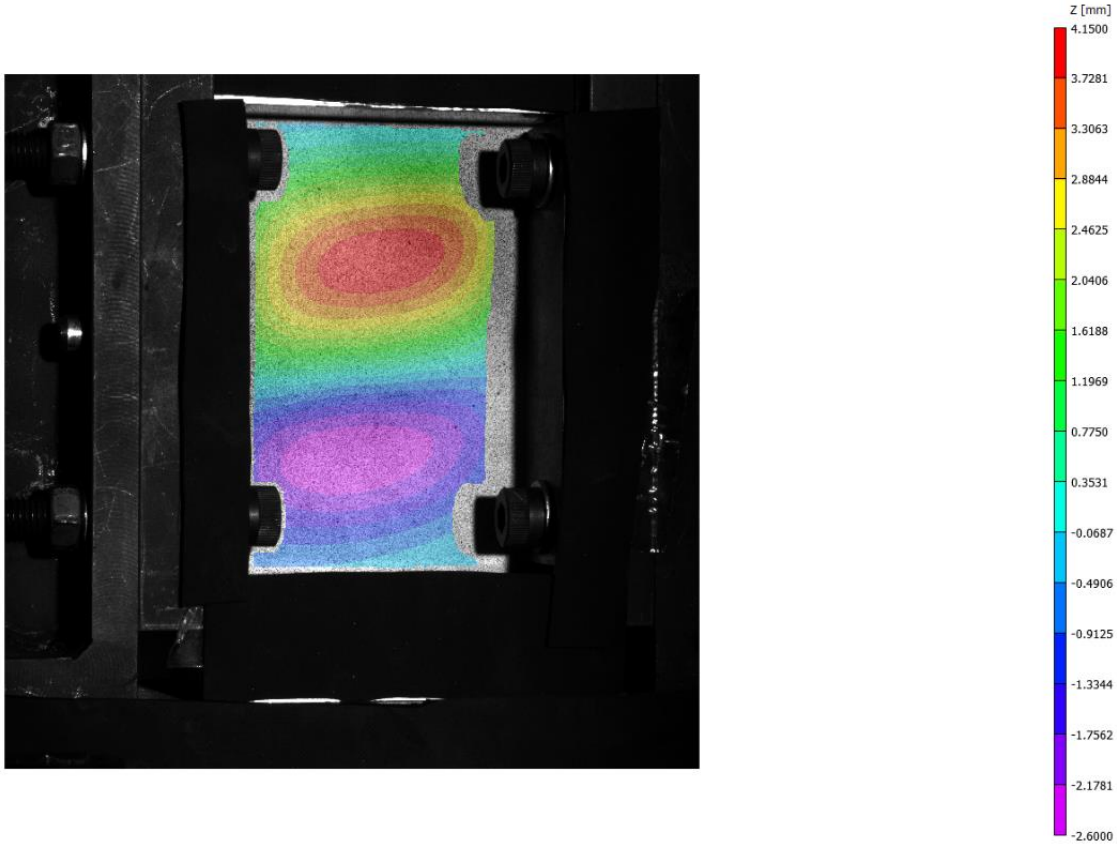

QI_2, onset of buckling 167.3 N

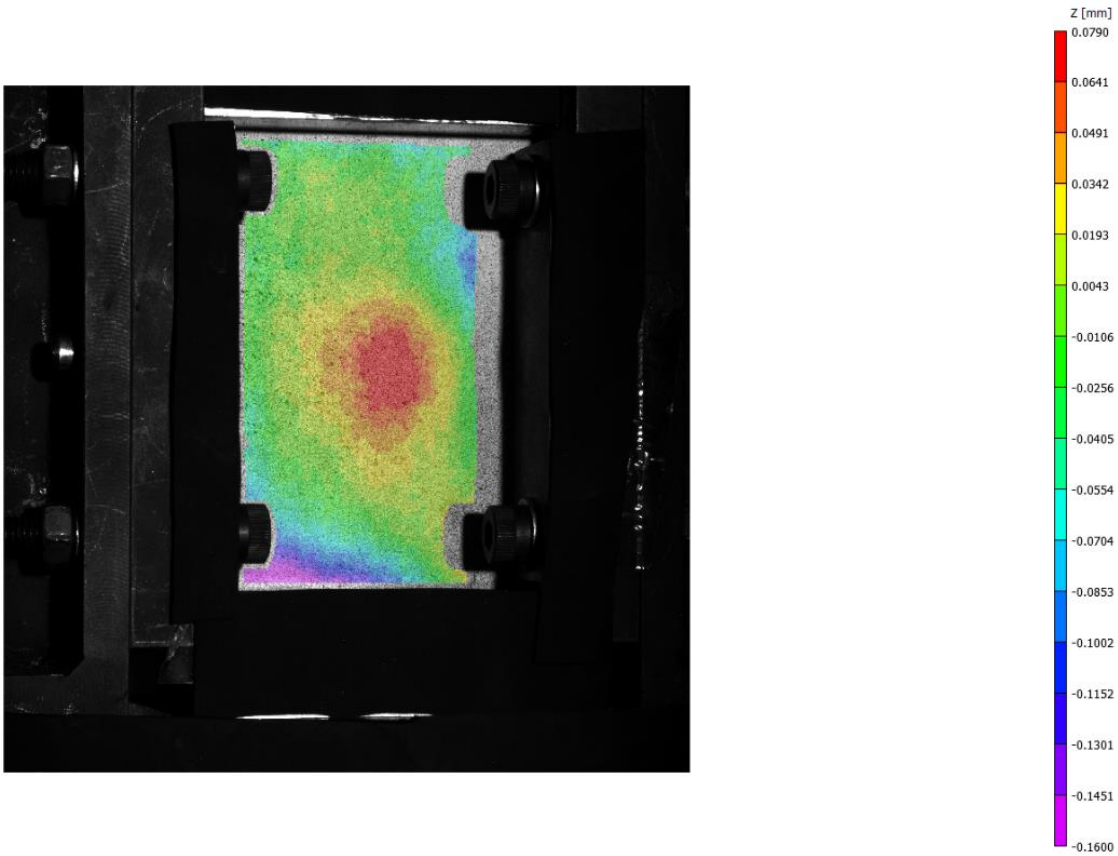

QI_2, mode change at 1512.2 N

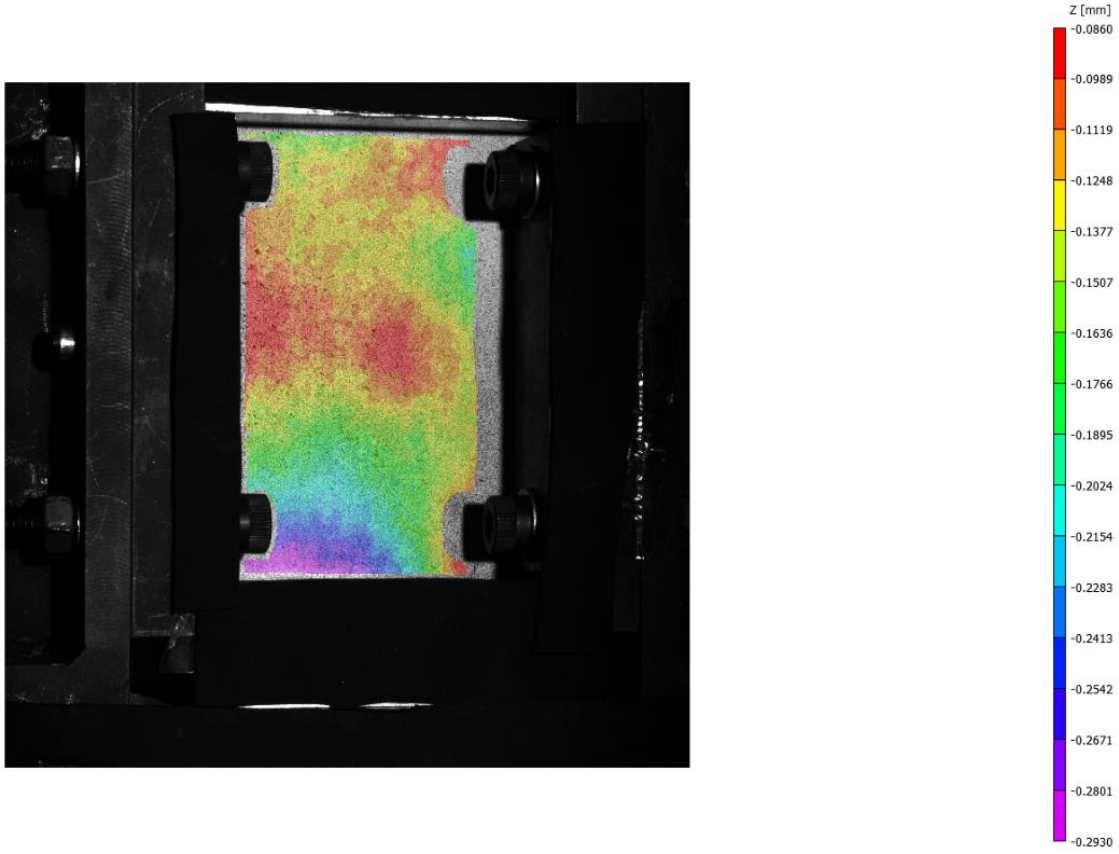

QI_2, end of test at 4143.1 N

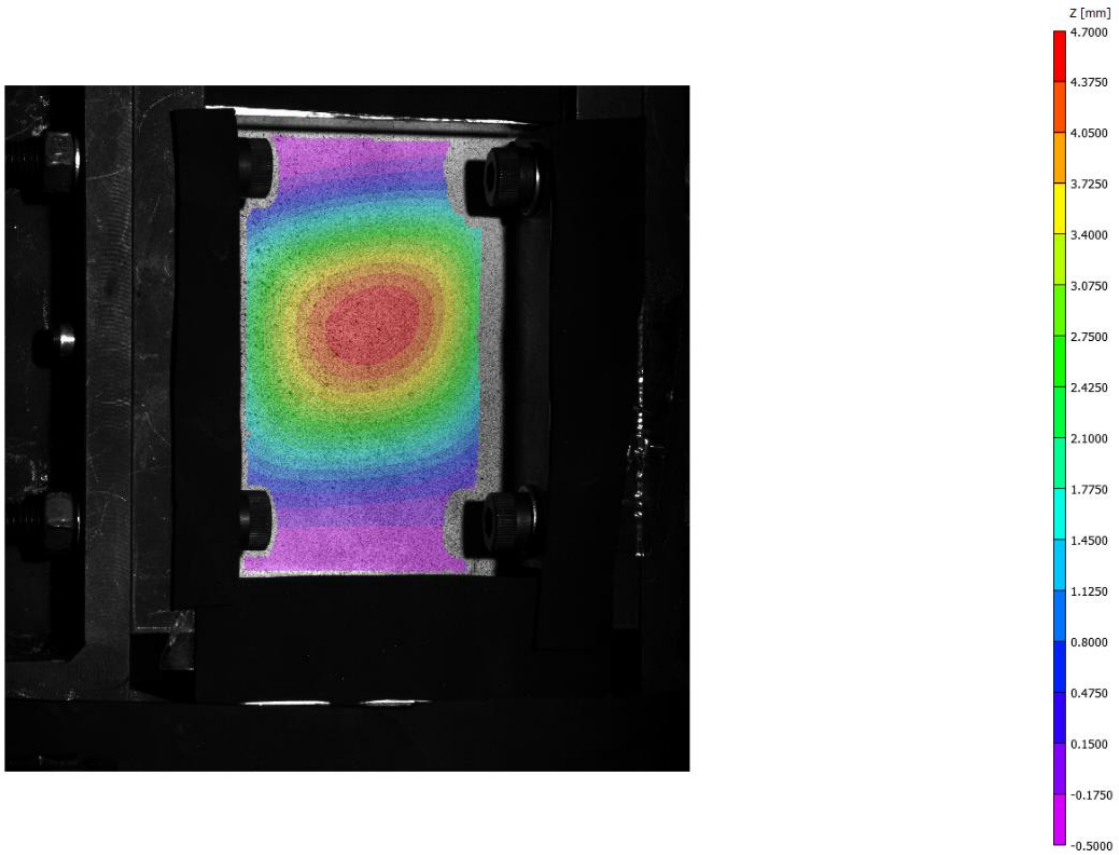

QI_3, end of test at 4517.1 N

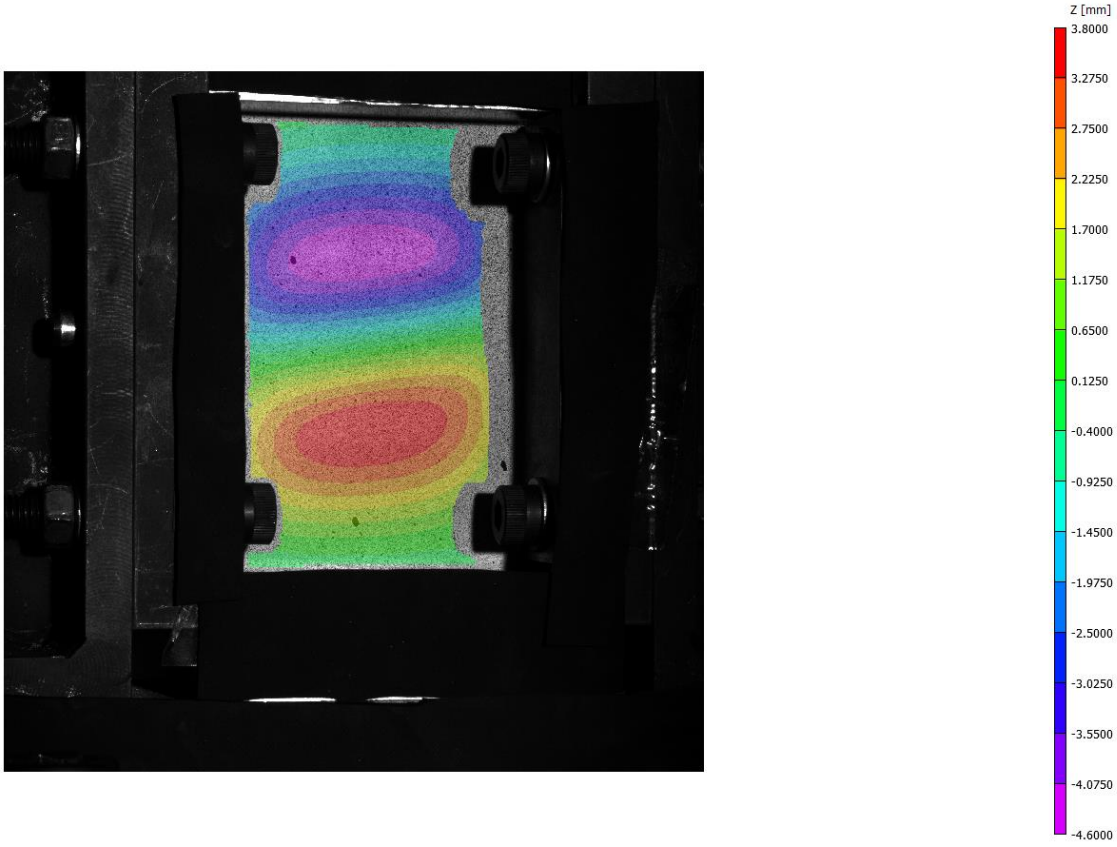

R10_1, onset of buckling 1215.1 N

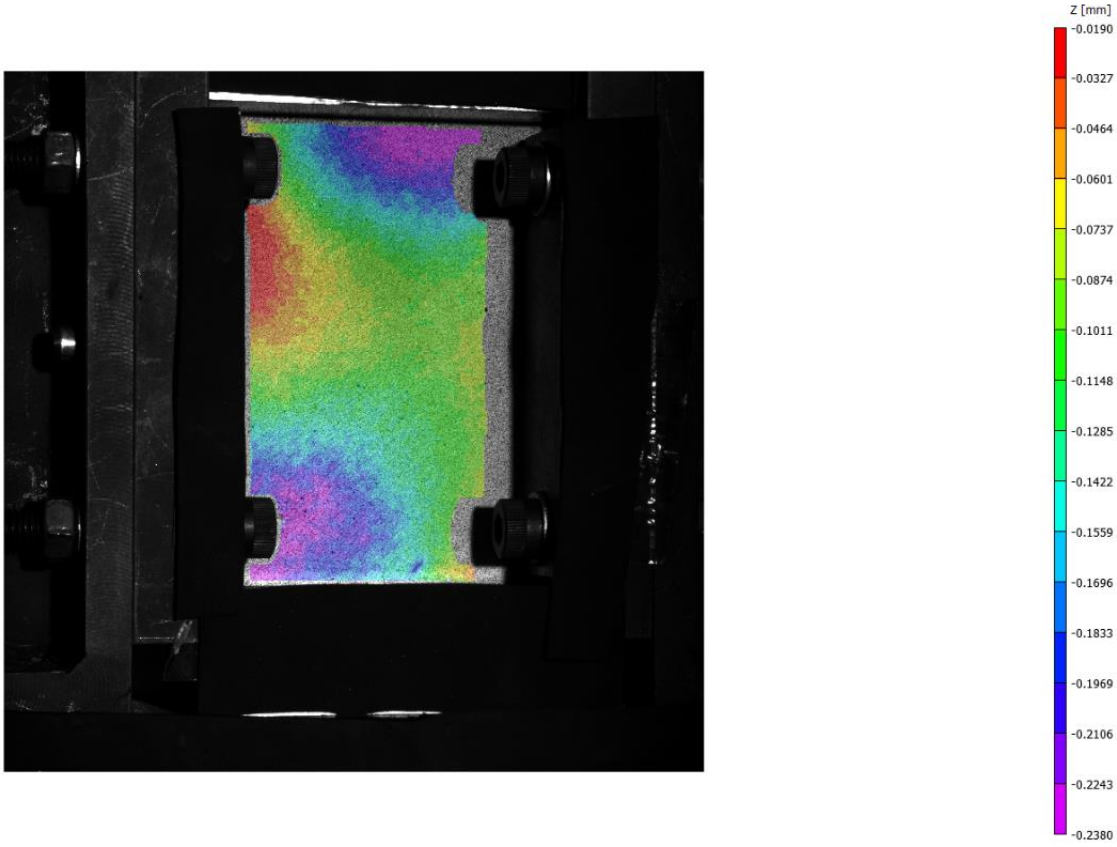

R10_1, mode change at 5365.4 N

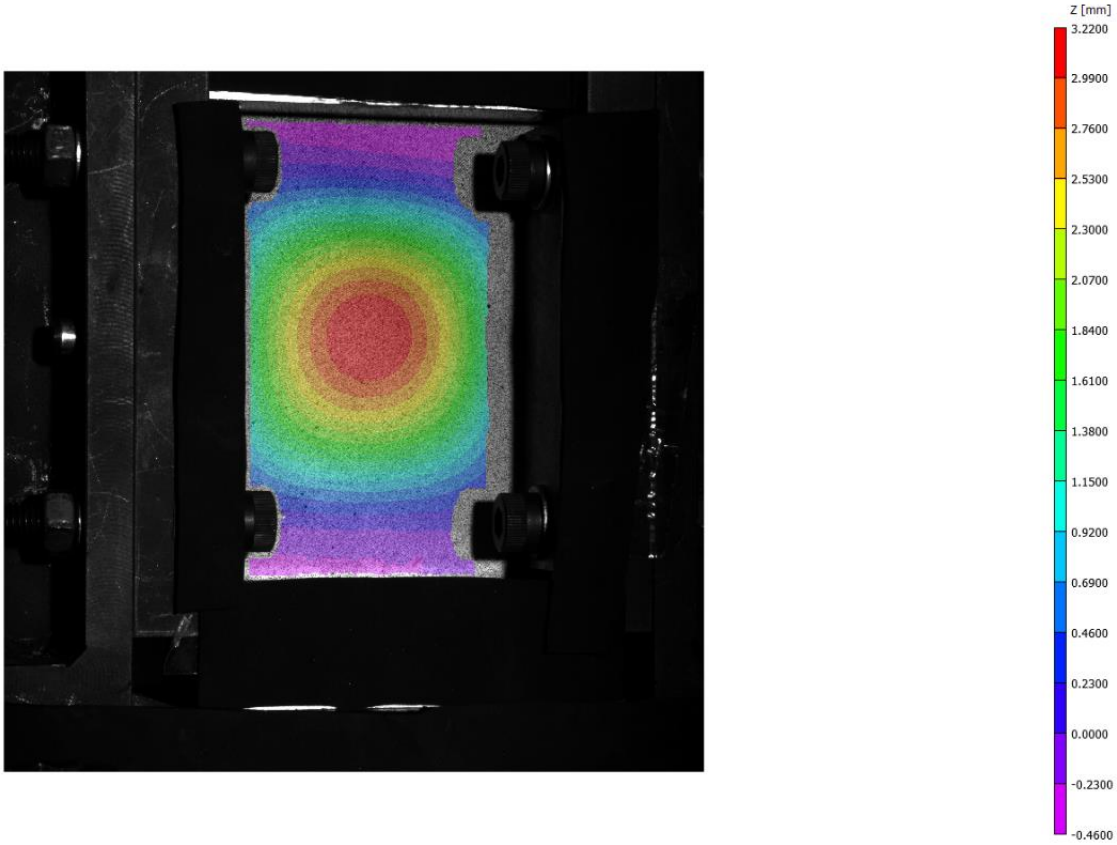

R10_1, end of test 5830.5 N

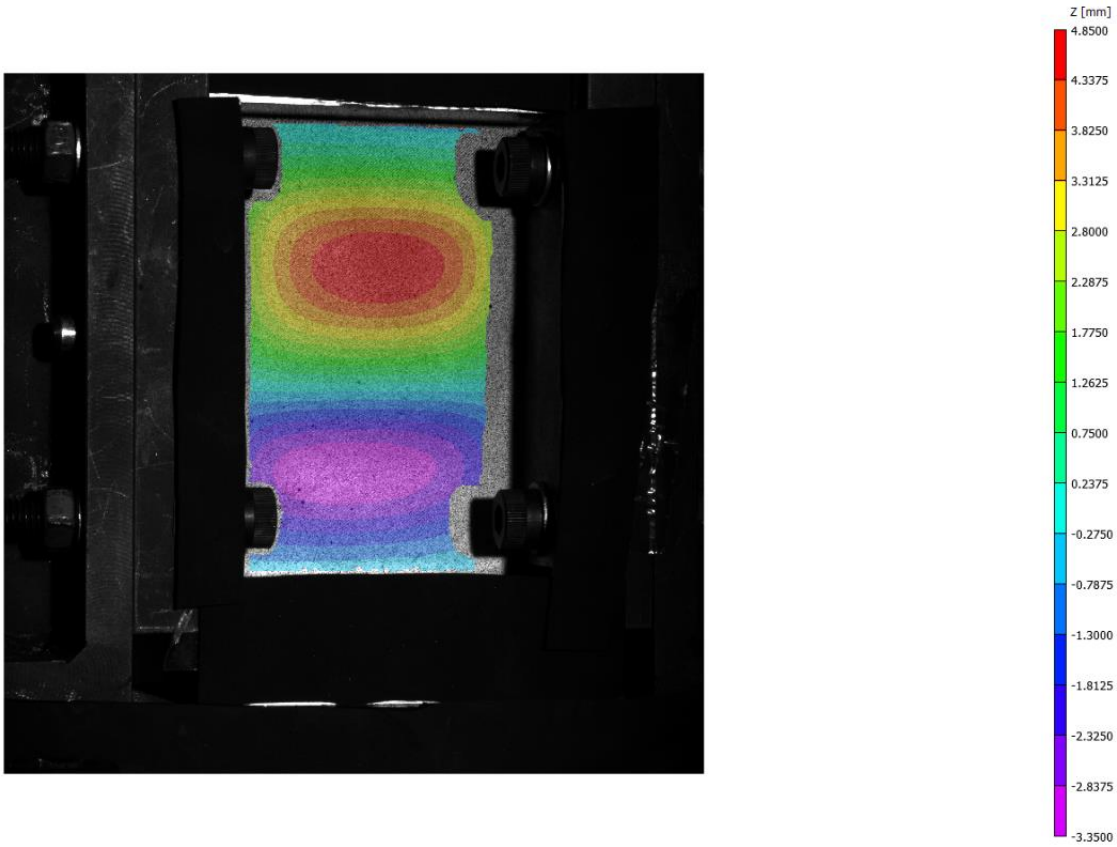

R10_2, end of test at 4994.8

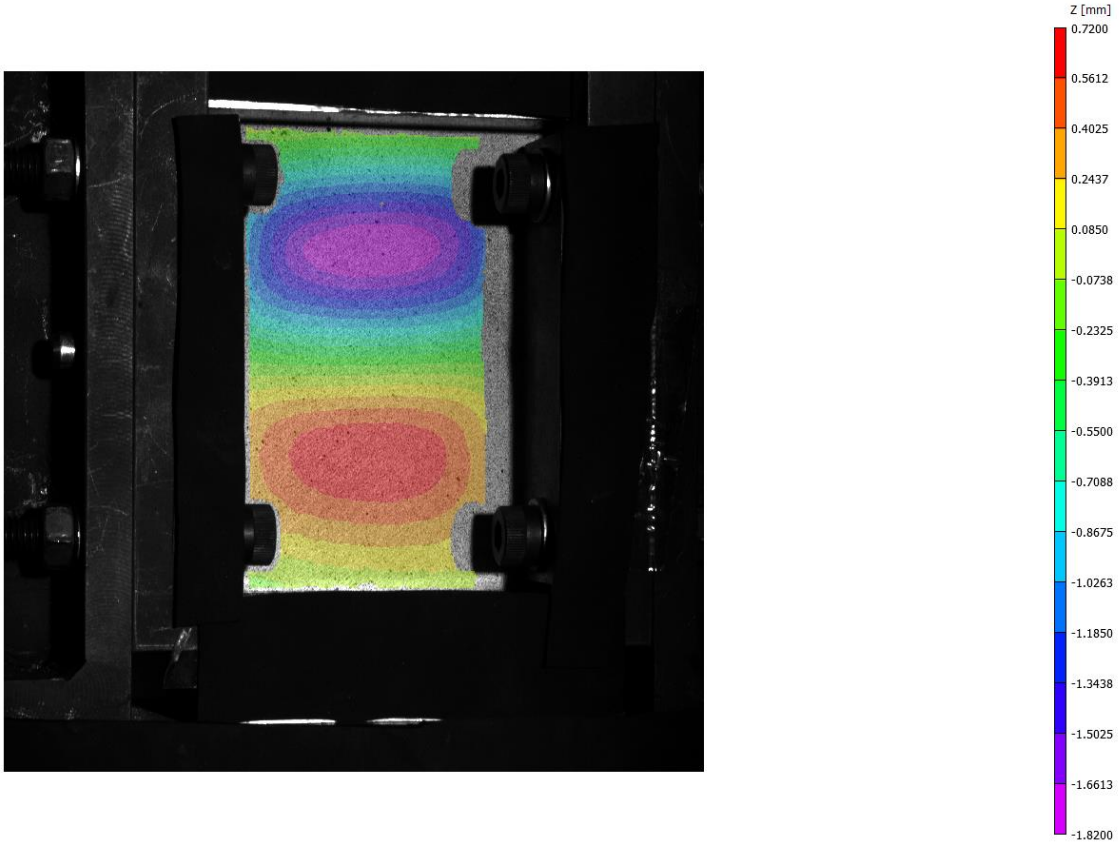

R10_3, onset of buckling at 1296.5 N

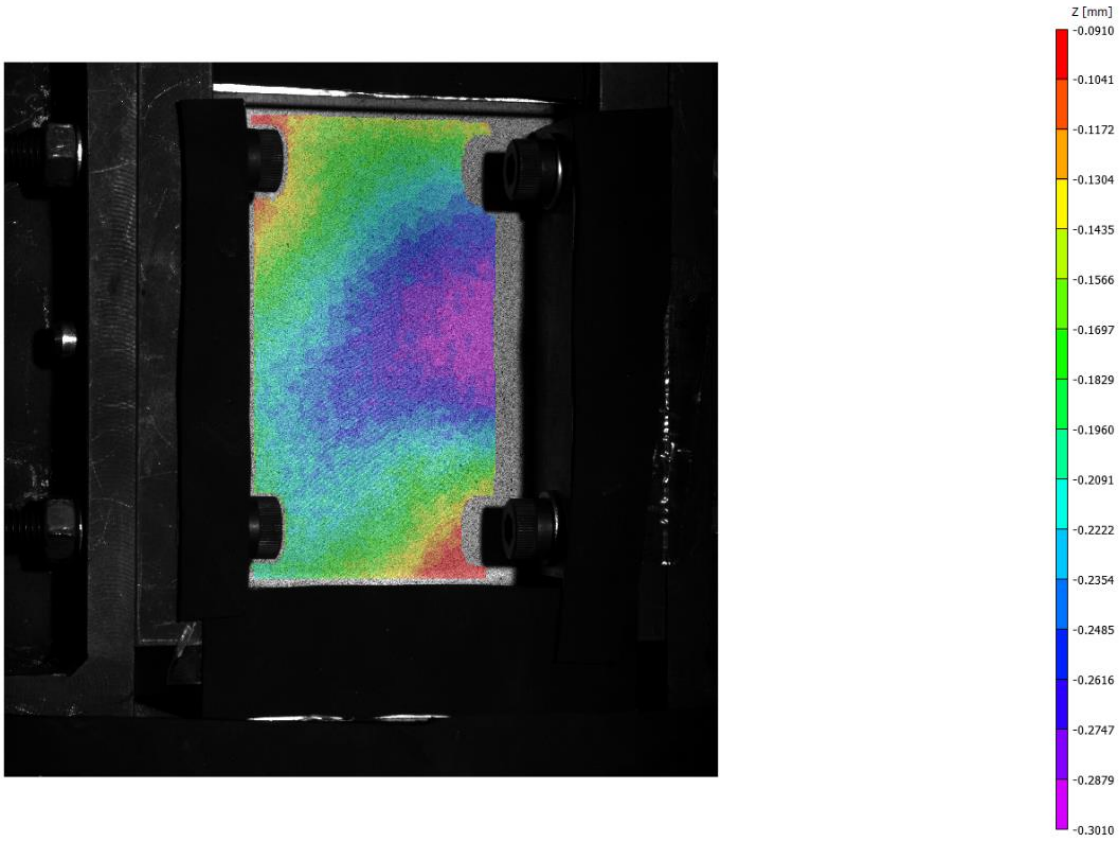

R10_3, mode change at 3656.4 N

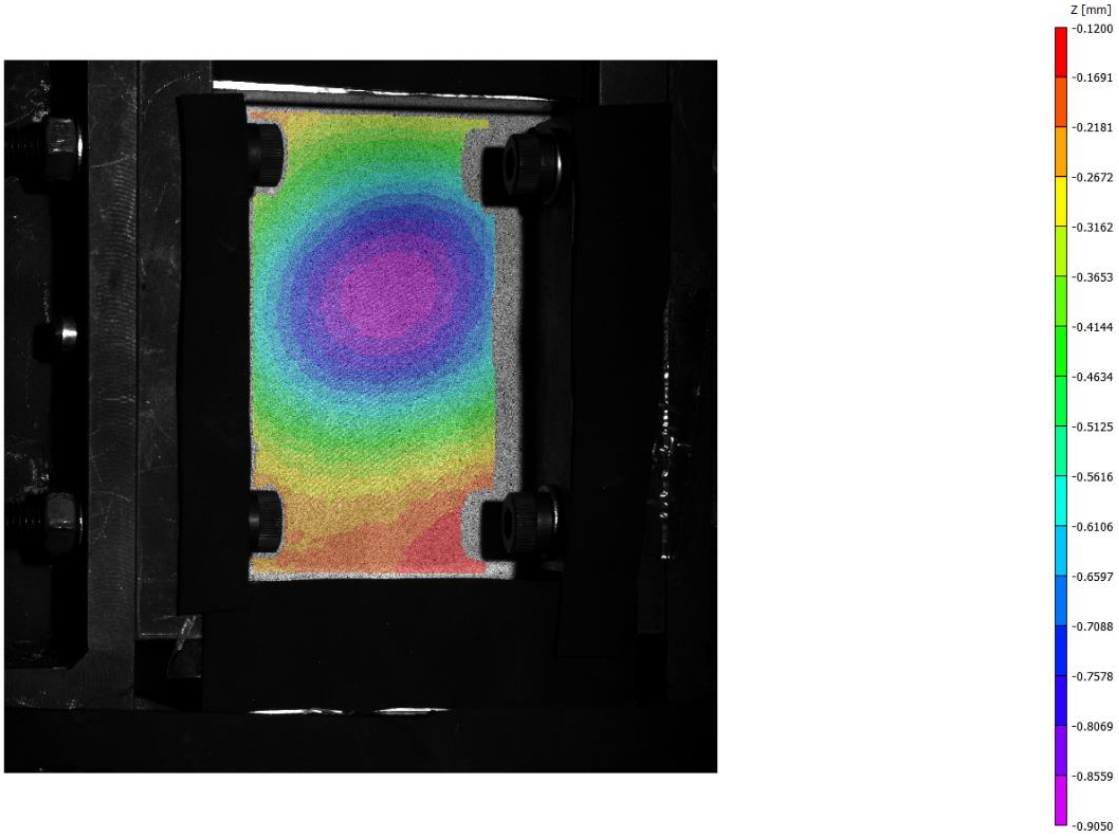

R10_3, end of test at 6089.6 N

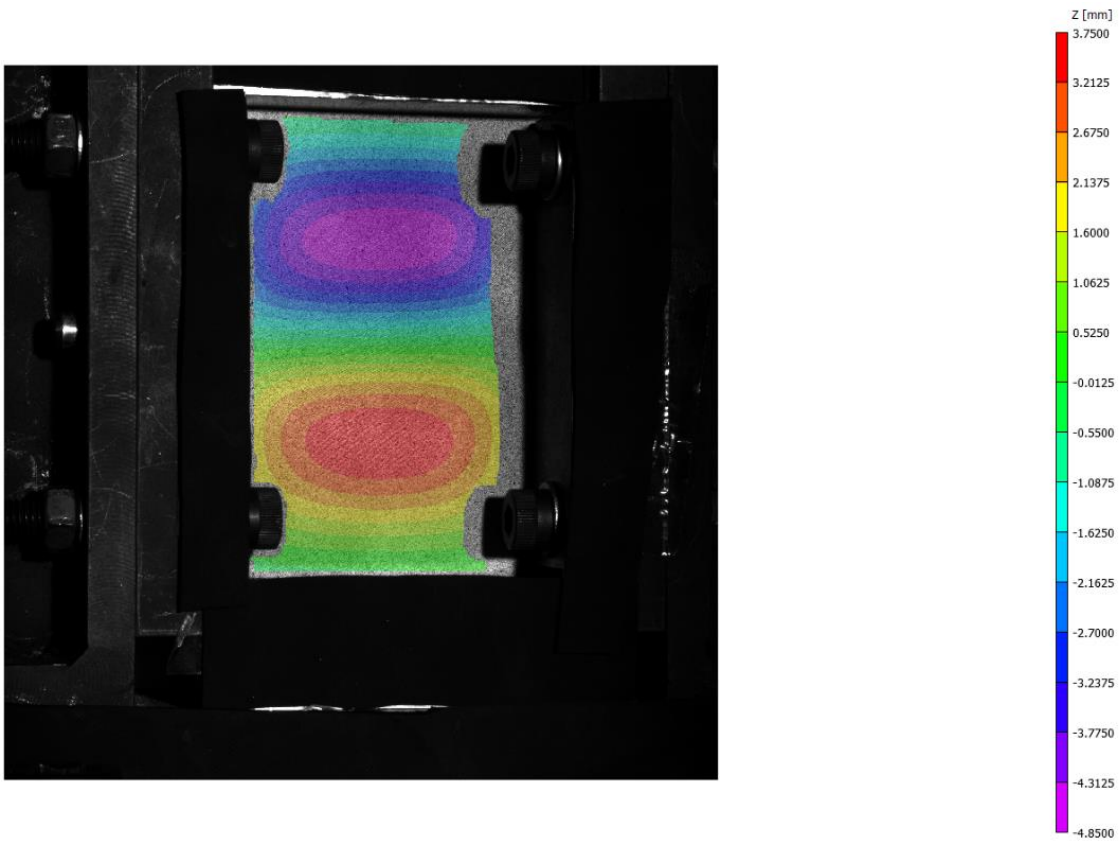

R100N_1, onset of buckling at 401.3 N

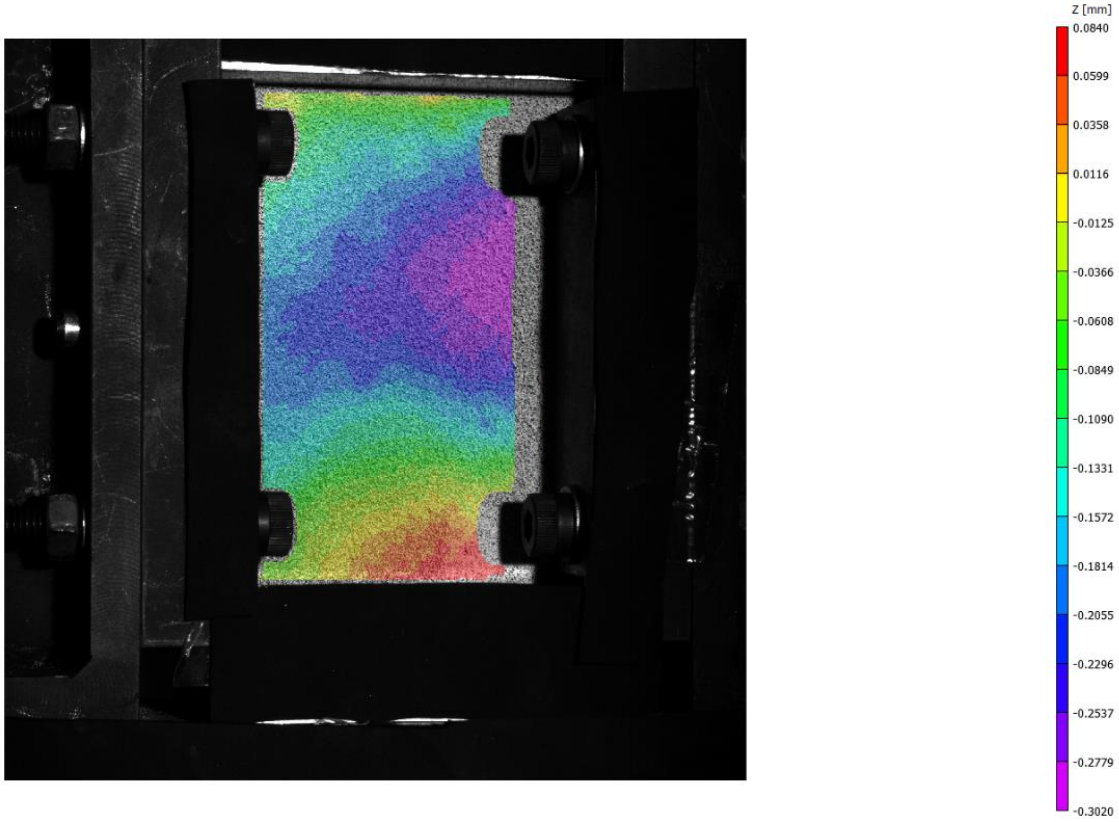

R100N_1, mode change 4282.0 N

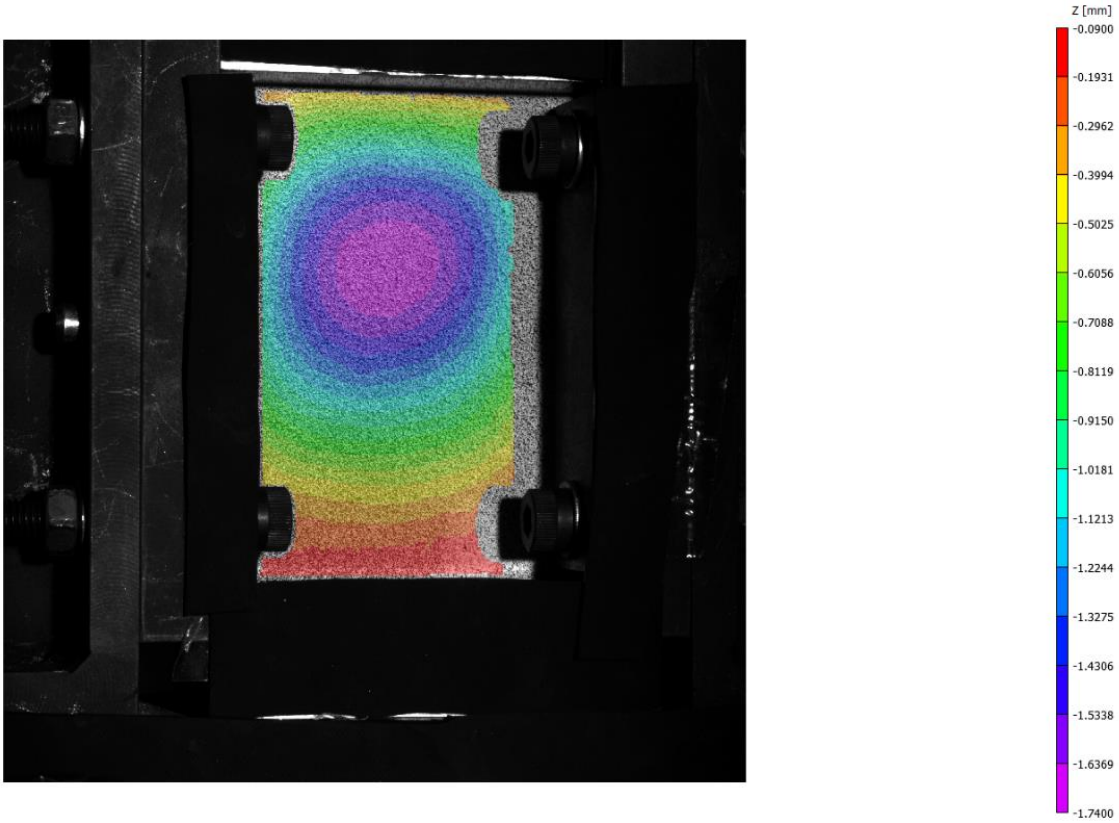

R100N_1, end of test at 5492.5 N

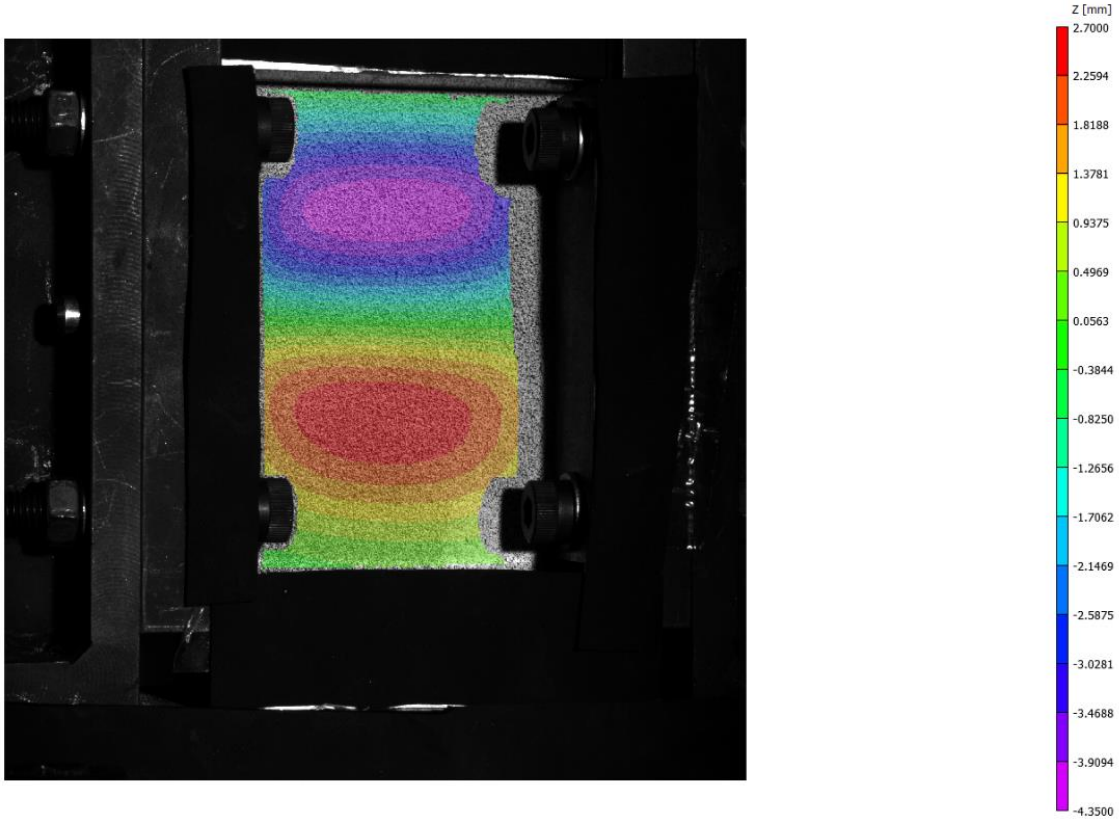

R100N_2, onset of buckling at 1372.7 N

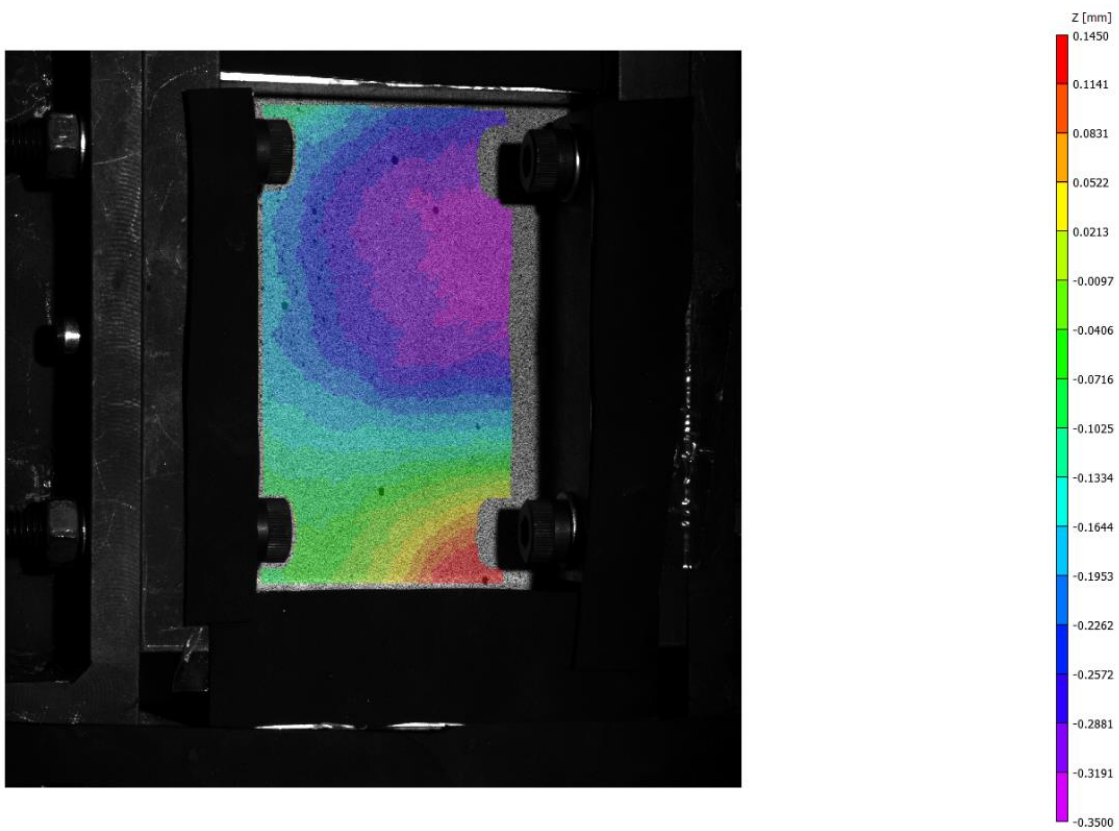

R100_2, end of test at 6871.1 N

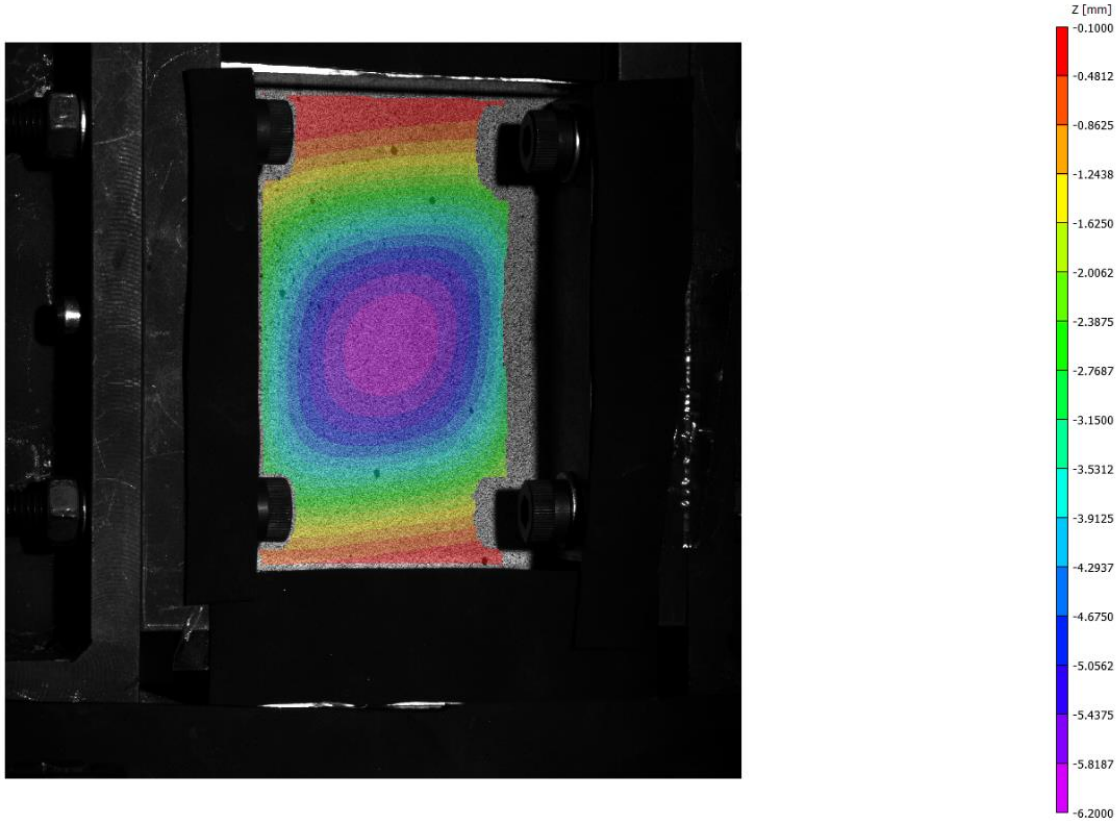

References

[1] R. Hsissou, R. Seghiri, Z. Benzekri, M. Hilali, M. Rafik, and A. Elharfi, “Polymer composite materials: A comprehensive review,” *Compos. Struct.*, vol. 262, p. 113640, Apr. 2021, doi: 10.1016/J.COMPSTRUCT.2021.113640.

[2] G. D. Shaffer, “An Archaeomagnetic Study of a Wattle and Daub Building Collapse,” *J. F. Archaeol.*, vol. 20, no. 1, p. 59, 1993, doi: 10.2307/530354.

[3] S. S. Godara, A. Yadav, B. Goswami, and R. S. Rana, “Review on history and characterization of polymer composite materials,” *Mater. Today Proc.*, vol. 44, pp. 2674–2677, Jan. 2021, doi: 10.1016/J.MATPR.2020.12.680.

[4] R. S. Pierce and B. G. Falzon, “Simulating Resin Infusion through Textile Reinforcement Materials for the Manufacture of Complex Composite Structures,” *Engineering*, vol. 3, no. 5, pp. 596–607, 2017, doi: 10.1016/J.ENG.2017.04.006.

[5] R. Bernatas, S. Dagreou, A. Despax-Ferreres, and A. Barasinski, “Recycling of fiber reinforced composites with a focus on thermoplastic composites,” *Clean. Eng. Technol.*, vol. 5, p. 100272, Dec. 2021, doi: 10.1016/J.CLET.2021.100272.

[6] S. W. Beckwith, “Designing with Composites: Suggested ‘Best Practices’ Rules,” *SAMPE J.*, vol. 45, no. 1, p. 17, 2009.

[7] C. Jareteg *et al.*, “Geometry Assurance Integrating Process Variation with Simulation of Spring-In for Composite Parts and Assemblies,” *J. Comput. Inf. Sci. Eng.*, vol. 16, no. 3, 2016, doi: 10.1115/1.4033726.

[8] A. W. Blom, C. S. Lopes, P. J. Kromwijk, Z. Gürdal, and P. P. Camanho, “A theoretical model to study the influence of tow-drop areas on the stiffness and strength of variable-stiffness laminates,” *J. Compos. Mater.*, vol. 43, no. 5, pp. 403–425, 2009, doi: 10.1177/0021998308097675.

[9] A. Brasington, C. Sacco, J. Halbritter, R. Wehbe, and R. Harik, “Automated fiber placement: A review of history, current technologies, and future paths forward,” *Compos. Part C Open Access*, vol. 6, p. 100182, Oct. 2021, doi: 10.1016/J.JCOMC.2021.100182.

[10] N. Bakhshi, “Process-Induced Defects during Tow Steering in Automated Fiber Placement: Experiment, Modeling and Simulation,” 2018.

[11] B. C. Kim, K. Potter, and P. M. Weaver, “Continuous tow shearing for manufacturing variable angle tow composites,” *Compos. Part A Appl. Sci. Manuf.*, vol. 43, no. 8, pp. 1347–1356, 2012, doi: 10.1016/j.compositesa.2012.02.024.

[12] E. Oromiehie, B. G. Prusty, P. Compston, and G. Rajan, “Automated fibre placement based composite structures: Review on the defects, impacts and inspections techniques,” *Compos. Struct.*, vol. 224, no. May, p. 110987, 2019, doi: 10.1016/j.compstruct.2019.110987.

[13] B. F. Tatting and Z. Gürdal, “Design and Manufacture Tow Placed Plates of Elastically Tailored,” 2002.

[14] D. C. Jegley, B. F. Tatting, and Z. Gürdal, “Optimization of elastically tailored tow-placed plates with holes,” *44th AIAA/ASME/ASCE/AHS/ASC Struct. Struct. Dyn. Mater. Conf.*, no. February, 2003, doi: 10.2514/6.2003-1420.

[15] B. Sobhani Aragh, E. Borzabadi Farahani, B. X. Xu, H. Ghasemnejad, and W. J. Mansur, “Manufacturable insight into modelling and design considerations in fibre-steered composite laminates: State of the art and perspective,” *Comput. Methods Appl. Mech. Eng.*, vol. 379, p.

113752, Jun. 2021, doi: 10.1016/J.CMA.2021.113752.

[16] M. Selezneva and L. Lessard, “Characterization of mechanical properties of randomly oriented strand thermoplastic composites,” *J. Compos. Mater.*, vol. 50, no. 20, pp. 2833–2851, 2016, doi: 10.1177/0021998315613129.

[17] H. Fernandes, H. Zhang, C. Ibarra-Castanedo, and X. Maldague, “Fiber orientation assessment on randomly-oriented strand composites by means of infrared thermography,” *Compos. Sci. Technol.*, vol. 121, no. November, pp. 25–33, 2015, doi: 10.1016/j.compscitech.2015.10.015.

[18] O. Meyer, “Kurzfaser-Preform-Technologie zur kraftflussgerechten Herstellung von Faserverbundbauteilen,” *Diss. Fak. Luft- und Raumfahrttechnik und Geodäsie der Univ. Stuttgart*, p. 193, 2008, doi: http://dx.doi.org/10.18419/opus-3764.

[19] R. Kussmaul, J. G. Jónasson, M. Zogg, and P. Ermanni, “A novel computational framework for structural optimization with patched laminates,” *Struct. Multidiscip. Optim.*, vol. 60, no. 5, pp. 2073–2091, 2019, doi: 10.1007/s00158-019-02311-w.

[20] Cevotec GmbH, “The process at the example of SAMBA Pro,” 2014. https://www.cevotec.com/en/fpp-technology/ (accessed Aug. 20, 2021).

[21] V. Mecnika, M. Hoerr, I. Krievins, S. Jockenhoevel, and T. Gries, “Technical Embroidery for Smart Textiles: Review,” *Mater. Sci. Text. Cloth. Technol.*, vol. 9, p. 56, Mar. 2015, doi: 10.7250/MSTCT.2014.009.

[22] B. C. Kim, K. Hazra, P. Weaver, and K. Potter, “Limitations of fibre placement techniques for variable angle tow composites and their process-induced defects,” 2011.

[23] “General Motors | Generative Design in Car Manufacturing | Autodesk.” https://www.autodesk.com/customer-stories/general-motors-generative-design (accessed Aug. 24, 2021).

[24] H. Benaroya, S. Indyk, and S. Mottaghi, “Advanced systems concept for autonomous construction and self-repair of lunar surface ISRU structures,” *Moon Prospect. Energy Mater. Resour.*, vol. 9783642279690, pp. 641–660, Jul. 2012, doi: 10.1007/978-3-642-27969-0_27.

[25] “United States Patent: 4665492.” https://patft.uspto.gov/netacgi/nph-Parser?Sect1=PTO1&Sect2=HITOFF&d=PALL&p=1&u=%2Fnetahtml%2FPTO%2Fsrchnum.htm&r=1&f=G&l=50&s1=4665492.PN.&OS=PN/4665492&RS=PN/4665492 (accessed Aug. 26, 2021).

[26] “United States Patent: 5134569.” https://patft.uspto.gov/netacgi/nph-Parser?Sect1=PTO1&Sect2=HITOFF&d=PALL&p=1&u=%2Fnetahtml%2FPTO%2Fsrchnum.htm&r=1&f=G&l=50&s1=5134569.PN.&OS=PN/5134569&RS=PN/5134569 (accessed Aug. 26, 2021).

[27] “United States Patent: 5546313.” https://patft.uspto.gov/netacgi/nph-Parser?Sect1=PTO1&Sect2=HITOFF&d=PALL&p=1&u=%2Fnetahtml%2FPTO%2Fsrchnum.htm&r=1&f=G&l=50&s1=5546313.PN.&OS=PN/5546313&RS=PN/5546313 (accessed Aug. 26, 2021).

[28] “United States Patent: 4575330.” https://patft.uspto.gov/netacgi/nph-Parser?Sect1=PTO1&Sect2=HITOFF&d=PALL&p=1&u=%2Fnetahtml%2FPTO%2Fsrchnum.htm&r=1&f=G&l=50&s1=4575330.PN.&OS=PN/4575330&RS=PN/4575330 (accessed Aug. 26, 2021).

[29] “United States Patent: 4938816.” https://patft.uspto.gov/netacgi/nph-

Parser?Sect1=PTO1&Sect2=HITOFF&d=PALL&p=1&u=%2Fnetahtml%2FPTO%2Fsrchnum.htm&r=1&f=G&l=50&s1=4,938,816.PN.&OS=PN/4,938,816&RS=PN/4,938,816 (accessed Aug. 26, 2021).

[30] "United States Patent: 5121329." https://patft.uspto.gov/netacgi/nph-Parser?Sect1=PTO1&Sect2=HITOFF&d=PALL&p=1&u=%2Fnetahtml%2FPTO%2Fsrchnum.htm&r=1&f=G&l=50&s1=5121329.PN.&OS=PN/5121329&RS=PN/5121329 (accessed Aug. 26, 2021).

[31] "United States Patent: 5204055." https://patft.uspto.gov/netacgi/nph-Parser?Sect1=PTO1&Sect2=HITOFF&d=PALL&p=1&u=%2Fnetahtml%2FPTO%2Fsrchnum.htm&r=1&f=G&l=50&s1=5204055.PN.&OS=PN/5204055&RS=PN/5204055 (accessed Aug. 26, 2021).

[32] A. Jadhav and V. S. Jadhav, "A review on 3D printing: An additive manufacturing technology," *Mater. Today Proc.*, Mar. 2022, doi: 10.1016/J.MATPR.2022.02.558.

[33] "Material extrusion - FDM | Make." https://make.3dexperience.3ds.com/processes/material-extrusion (accessed Aug. 24, 2021).

[34] L. W. Chang, S. S. Yau, and T. W. Chou, "Notched strength of woven fabric composites with moulded-in holes," *Composites*, vol. 18, no. 3, pp. 233–241, 1987, doi: 10.1016/0010-4361(87)90413-7.

[35] M. W. Hyer and H. H. Lee, "Innovative design of composite structures: The use of curvilinear fiber format to improve buckling resistance of composite plates with central circular holes," 1990.

[36] M. W. Hyer, R. J. Rust, W. A. Waters, and M. P. Nemeth, "Innovative Design of Composite Structures: Design, Manufacturing, and Testing of Plates Utilitzing Curvilinear Fiber Trajectories," 1994.

[37] P. J. Crothers, K. Drechsler, D. Feltin, I. Herszberg, and T. Kruckenberg, "Tailored fibre placement to minimise stress concentrations," *Compos. Part A Appl. Sci. Manuf.*, vol. 28, no. 7, pp. 619–625, Jan. 1997, doi: 10.1016/S1359-835X(97)00022-5.

[38] Z. GUERDAL and R. OLMEDO, "Composite laminates with spatially varying fiber orientations - 'Variable stiffness panel concept,'" Apr. 1992, doi: 10.2514/6.1992-2472.

[39] R. Olmedo and Z. Gurdal, "Buckling response of laminates with spatially varying fiber orientations," *Collect. Tech. Pap. - AIAA/ASME Struct. Struct. Dyn. Mater. Conf.*, no. pt 4, pp. 2261–2269, 1993, doi: 10.2514/6.1993-1567.

[40] C. S. Lopes, Z. Gürdal, and P. P. Camanho, "Variable-stiffness composite panels: Buckling and first-ply failure improvements over straight-fibre laminates," *Comput. Struct.*, vol. 86, no. 9, pp. 897–907, 2008, doi: 10.1016/j.compstruc.2007.04.016.

[41] C. S. Lopes, Z. Gürdal, and P. P. Camanho, "Tailoring for strength of composite steered-fibre panels with cutouts," *Compos. Part A Appl. Sci. Manuf.*, vol. 41, no. 12, pp. 1760–1767, Dec. 2010, doi: 10.1016/J.COMPOSITESA.2010.08.011.

[42] D. Peeters, "Design Optimisation of Practical Variable Stiffness and Thickness Laminates," Delft University of Technology, 2017.

[43] D. C. Jegley, B. F. Tatting, and Z. Gürdal, "Tow-steered panels with holes subjected to compression or shear loading," *Collect. Tech. Pap. - AIAA/ASME/ASCE/AHS/ASC Struct. Struct. Dyn. Mater. Conf.*, vol. 5, pp. 3453–3466, 2005, doi: 10.2514/6.2005-2081.

[44] H. Ghiasi, K. Fayazbakhsh, D. Pasini, and L. Lessard, “Optimum stacking sequence design of composite materials Part II: Variable stiffness design,” *Compos. Struct.*, vol. 93, no. 1, pp. 1–13, 2010, doi: 10.1016/j.compstruct.2010.06.001.

[45] S. T. Ijsselmuiden, *Optimal design of variable stiffness composite structures using lamination parameters*. 2011.

[46] D. M. J. Peeters, F. X. Irisarri, C. Groenendijk, and R. Růžek, “Optimal design, manufacturing and testing of non-conventional laminates,” *Compos. Struct.*, vol. 210, no. October 2018, pp. 29–40, 2019, doi: 10.1016/j.compstruct.2018.10.062.

[47] M. P. Bendsøe and N. Kikuchi, “Generating optimal topologies in structural design using a homogenization method,” *Comput. Methods Appl. Mech. Eng.*, vol. 71, no. 2, pp. 197–224, Nov. 1988, doi: 10.1016/0045-7825(88)90086-2.

[48] Y. M. Xie and G. P. Steven, “A simple evolutionary procedure for structural optimization,” *Comput. Struct.*, vol. 49, no. 5, pp. 885–896, Dec. 1993, doi: 10.1016/0045-7949(93)90035-C.

[49] M. Y. Wang, X. Wang, and D. Guo, “A level set method for structural topology optimization,” *Comput. Methods Appl. Mech. Eng.*, vol. 192, no. 1–2, pp. 227–246, Jan. 2003, doi: 10.1016/S0045-7825(02)00559-5.

[50] O. Sigmund, “A 99 line topology optimization code written in Matlab,” *Struct. Multidiscip. Optim. 2001 212*, vol. 21, no. 2, pp. 120–127, Feb. 2014, doi: 10.1007/S001580050176.

[51] J. Wu, O. Sigmund, and J. P. Groen, “Topology optimization of multi-scale structures: a review,” *Struct. Multidiscip. Optim. 2021 633*, vol. 63, no. 3, pp. 1455–1480, Mar. 2021, doi: 10.1007/S00158-021-02881-8.

[52] S. Waghmare, S. Shelare, K. Aglawe, and P. Khope, “A mini review on fibre reinforced polymer composites,” *Mater. Today Proc.*, vol. 54, pp. 682–689, Jan. 2022, doi: 10.1016/J.MATPR.2021.10.379.

[53] J. Li, Y. Durandet, X. Huang, G. Sun, and D. Ruan, “Additively manufactured fiber-reinforced composites: A review of mechanical behavior and opportunities,” *J. Mater. Sci. Technol.*, vol. 119, pp. 219–244, Aug. 2022, doi: 10.1016/J.JMST.2021.11.063.

[54] T. Wang, N. Li, G. Link, J. Jelonnek, J. Fleischer, and D. Kupzik, “Load-dependent Path Planning Method for 3D Printing of Continuous Fiber Reinforced Plastics,” *Compos. Part A*, p. 106181, 2020, doi: 10.1016/j.compositesa.2020.106181.

[55] H. Yu, K. D. Potter, and M. R. Wisnom, “A novel manufacturing method for aligned discontinuous fibre composites (High Performance-Discontinuous Fibre method),” *Compos. Part A Appl. Sci. Manuf.*, vol. 65, pp. 175–185, Oct. 2014, doi: 10.1016/J.COMPOSITESA.2014.06.005.

[56] T. Shafighfard, T. A. Cender, and E. Demir, “Additive manufacturing of compliance optimized variable stiffness composites through short fiber alignment along curvilinear paths,” *Addit. Manuf.*, vol. 37, p. 101728, Jan. 2021, doi: 10.1016/J.ADDMA.2020.101728.

[57] “Image Processing Toolbox Documentation - MathWorks Benelux.” https://nl.mathworks.com/help/images/index.html?s_tid=CRUX_lftnav (accessed Jun. 01, 2022).

[58] S. G. Advani and C. L. Tucker, “The Use of Tensors to Describe and Predict Fiber Orientation in Short Fiber Composites,” *J. Rheol. (N. Y. N. Y).*, vol. 31, no. 8, pp. 751–784, 1987, doi: 10.1122/1.549945.

[59] S. G. Advani and C. L. Tucker, “Closure approximations for three-dimensional structure tensors,” *J. Rheol. (N. Y. N. Y).*, vol. 34, no. 3, pp. 367–386, 1990, doi: 10.1122/1.550133.

[60] “tianyikillua/fiberpy: Computational methods for fiber-reinforced composites.” https://github.com/tianyikillua/fiberpy (accessed Jun. 01, 2022).

[61] D. M. J. Peeters, S. Hesse, and M. M. Abdalla, “Stacking sequence optimisation of variable stiffness laminates with manufacturing constraints,” *Compos. Struct.*, vol. 125, pp. 596–604, 2015, doi: 10.1016/j.compstruct.2015.02.044.

[62] D. M. J. Peeters, G. G. Lozano, and M. M. Abdalla, “Effect of steering limit constraints on the performance of variable stiffness laminates,” *Comput. Struct.*, vol. 196, pp. 94–111, 2018, doi: 10.1016/j.compstruc.2017.11.002.

[63] T. Rahman, S. T. Ijsselmuiden, M. M. Abdalla, and E. L. Jansen, “POSTBUCKLING ANALYSIS OF VARIABLE STIFFNESS COMPOSITE PLATES USING A FINITE ELEMENT-BASED PERTURBATION METHOD,” *http://dx.doi.org/10.1142/S0219455411004324*, vol. 11, no. 4, pp. 735–753, Nov. 2011, doi: 10.1142/S0219455411004324.

[64] A. Mebarki, P. Alliez, and O. Devillers, “Farthest Point Seeding for Placement of Streamlines,” *IEEE Trans. Vis. Comput. Graph.*, no. 1.

[65] “gcode viewer - online gcode viewer and analyzer in your browser!” https://gcode.ws/ (accessed May 20, 2022).

[66] B. Gharehpapagh, M. Dolen, and U. Yaman, “Investigation of variable bead widths in FFF process,” *Procedia Manuf.*, vol. 38, no. 2019, pp. 52–59, 2019, doi: 10.1016/j.promfg.2020.01.007.

[67] R. Löffler and M. Koch, “Innovative Extruder Concept for Fast and Efficient Additive Manufacturing,” *IFAC-PapersOnLine*, vol. 52, no. 10, pp. 242–247, 2019, doi: 10.1016/j.ifacol.2019.10.071.

[68] A. N. Dickson, H. M. Abourayana, and D. P. Dowling, “3D Printing of Fibre-Reinforced Thermoplastic Composites Using Fused Filament Fabrication—A Review,” *Polym. 2020, Vol. 12, Page 2188*, vol. 12, no. 10, p. 2188, Sep. 2020, doi: 10.3390/POLYM12102188.

[69] P. Zhuo, S. Li, I. A. Ashcroft, and A. I. Jones, “Material extrusion additive manufacturing of continuous fibre reinforced polymer matrix composites: A review and outlook,” *Compos. Part B Eng.*, vol. 224, p. 109143, Nov. 2021, doi: 10.1016/J.COMPOSITESB.2021.109143.

[70] S. Gantenbein, K. Masania, W. Woigk, J. P. W. Sesseg, T. A. Tervoort, and A. R. Studart, “Three-dimensional printing of hierarchical liquid-crystal-polymer structures,” *Nat. 2018 5617722*, vol. 561, no. 7722, pp. 226–230, Sep. 2018, doi: 10.1038/s41586-018-0474-7.